ENDOGENOUS DNA DAMAGE DRIVES CELLULAR SENESCENCE AND PROMOTES AGING

by

Siobhán Gregg

B.S., State University of NY at Binghamton, 2006

Submitted to the Graduate Faculty of

The School of Medicine in partial fulfillment

of the requirements for the degree of

Doctor of Philosophy

University of Pittsburgh

2011

UNIVERSITY OF PITTSBURGH

SCHOOL OF MEDICINE

This thesis was presented

by

Siobhán Gregg

It was defended on

November 4, 2011

and approved by

Paul D. Robbins, Professor, Microbiology and Molecular Genetics

Donna Beer Stolz, Associate Professor, Cell Biology and Physiology

Bennett Van Houten, Professor, Pharmacology and Chemical Biology

Simon C. Watkins, Professor, Cell Biology and Physiology

Thesis Advisor: Laura J. Niedernhofer, Associate Professor, Microbiology and Molecular Genetics

ENDOGENOUS DNA DAMAGE DRIVES CELLULAR SENESCENCE AND PROMOTES AGING

Siobhán Gregg, B.S.

University of Pittsburgh, 2011

Global populations are shifting, and the number of individuals over the age of 60 is rapidly increasing. People of advanced age (>60 years old) are at risk for several chronic degenerative diseases. In order to improve the quality of life for the elderly living with age-associated diseases, and to minimize medical costs associated with an aging global population, it is critical to understand the molecular mechanisms that underlie aging.

Aging is characterized as the loss of tissue function and the decreased ability to maintain homeostasis, which leads to an increased risk of morbidity and mortality. The time-dependent accumulation of damage to cellular macromolecules is hypothesized to contribute to age-related decline. However, there is no consensus about the type(s) of damage that drive aging. There is evidence to support the hypothesis that DNA damage plays a causative role in aging. This includes mice and humans with defective DNA repair that exhibit symptoms of accelerated aging. Additionally, DNA damage can induce cellular senescence, and senescent cells are thought to contribute to age-associated functional decline. However, direct causal relationships between senescence and aging, and DNA damage and aging have yet to be established.

The overall goal of this thesis was to address these gaps in knowledge. This required the testing of two hypotheses. First, that the accelerated aging seen as a consequence of defects in DNA repair is similar to normal aging at the molecular, cellular and whole tissue level. Second, that spontaneous DNA damage that occurs in cells is sufficient to drive cellular senescence. To test these hypotheses, I employed a genetic approach, utilizing mice and primary cells that were engineered to be defective in the DNA repair endonuclease, ERCC1-XPF. Hence, mice and cells with reduced expression of ERCC1-XPF accumulate a variety of DNA lesions compared to wild type mice and cells. This thesis is divided into two main sections, which take an *in vivo* and *in vitro* approach to testing the hypothesis that endogenous DNA damage can promote aging.

TABLE OF CONTENTS

LIST OF TABLES

LIST OF FIGURES

PREFACE

Graduate school has been a very fulfilling journey, and I owe everything to some very special individuals. First and foremost, I would like to acknowledge my parents, for their love, support, and sacrifices over the years. I know for certain that without you both, I would not have made it here. I am very grateful to my brothers, Eoin and Brendan. Both of you are extraordinary role models, and I love you very much. Thank you to my grandmother and grandfather, who have taught, guided and supported me from day one. I feel very lucky to have grandparents like you.

To Sean, you deserve enormous thanks for your unwavering support. You always knew how to make me laugh. I could not have done this without you by my side.

Thank you to all my lab mates, especially Andria Robinson, Nikhil Bhagwat, and Chelsea Feldman. You started out as co-workers and became friends. You offered endless amounts of experimental support, guidance, and laughs. Thank you for believing in me.

Finally, there is not enough space here to express my appreciation for my mentor, Laura Niedernhofer. You are a great example of a focused, outgoing, and extraordinarily intelligent scientist, and I will always strive to be more like you. Over the past five years, you taught me invaluable lessons, both in science and life, and did it with incredible patience and kindness. Graduate school has its peaks and valleys but you were always there to steer me through the tough times, and to celebrate with me during the great times. Thank you!

1.0 INTRODUCTION

The 21st century has brought a global demographic shift, such that the number of individuals over the age of 60 is increasing rapidly in developed and non-developed nations. In 1950, there were approximately 205 million persons over age 60 globally. By 2050 that number is predicted to reach 2 billion[1]. Old age is the greatest risk factor for numerous chronic degenerative diseases, including cardiovascular disease, arthritis, cataracts, osteoporosis, type 2 diabetes, and neurodegenerative disorders such as Alzheimer's disease and Parkinson's disease. Eighty percent of individuals over the age of 65 have at least one chronic disease and >50% have two or more. In the United States alone, the direct medical costs associated with these diseases total nearly 1 trillion dollars annually (Table 1). In order to improve the quality of life for the elderly, and to minimize the economic burden from the medical care of the aged population, it is critical to identify the molecular mechanisms that underlie aging.

Table 1. Prevalence of age-related diseases in the United States

DISEASE	TOTAL # OF AFFECTED INDIVIDUALS IN THE U.S.	% OF PEOPLE AGED 65+ THAT ARE AFFECTED	U.S. ANNUAL HEALTH CARE COSTS (DIRECT)	REFERENCES
Cardiovascular disease	83 million	43%	$444 billion	[2]
Cancer (all types)	11.7 million	2.2%	$103 billion	[3]
Osteoarthritis	26.9 million	33.6%	$15 billion	[4]
Ocular disorders (cataracts, glaucoma)	24.3 million	21.8%	$51.4 billion	[5, 6]
Osteoporosis	10 million	30%	$13.7-20.3 billion	[7, 8]
Type 2 Diabetes	26 million	27%	$116 billion	[9]
Alzheimer's disease	5.4 million	13%	$183 billion	[10]
Parkinson's disease	1 million	1%	$5.6 billion	[11]
TOTAL			**$931.7-938.3 billion**	

Aging is characterized by the loss of tissue function and the decreased ability to maintain homeostasis. This leads to an impaired ability to respond to stress and a dramatically increased risk of morbidity and mortality[12]. Time-dependent accumulation of damage to cellular macromolecules and organelles is thought to contribute to aging. However, there is no consensus about the type(s) of damage that drive aging. There is evidence to support the hypothesis that DNA damage is one type of damage that plays a role in aging. This includes the fact that defects in the repair of DNA damage leads to accelerated aging in humans and mice[13, 14]. Additionally, DNA damage can induce cellular senescence[15]. The number of senescent cells is increased in aged humans, primates, and rodents compared to young organisms[16-18]. Furthermore, senescent cells are localized at sites of age-associated pathologies, suggesting that senescent cells contribute to age-associated functional decline[19]. However, direct causal relationships between senescence and aging, and DNA damage and aging have yet to be established.

The overall goal of my thesis was to address these gaps in knowledge. This required the testing of two hypotheses. First, that the accelerated aging seen as a consequence of defects in DNA repair is similar to normal aging at the molecular, cellular and whole tissue level. Second that DNA damage that occurs spontaneously in cells is sufficient to drive cellular senescence. To test these hypotheses, I employed a genetic approach, utilizing mice and primary cells that were engineered to be defective in DNA repair, in order to specifically focus on the physiological effect of unrepaired, endogenous DNA damage. ERCC1-XPF is an endonuclease involved in nucleotide excision repair of bulky, helix-distorting monoadducts, the repair of DNA interstrand crosslinks, and the repair of a subset of double-strand breaks. Hence, mice and cells with reduced expression of ERCC1-XPF accumulate increased levels of a variety of

spontaneous, endogenous DNA lesions. This thesis is divided into three main sections, which take an *in vivo* and *in vitro* approach to testing the hypothesis that endogenous DNA damage can promote aging.

In the first chapter, I examine the role of physiological role of ERCC1-XPF in specific DNA repair pathways, and the consequences of deficiency of ERCC1-XPF in humans and mice. The second chapter examines the effect of spontaneous, endogenous DNA damage *in vivo*. The approach I took was to systematically compare the time-dependent molecular, structural and functional changes that occur in the liver of DNA repair deficient *Ercc1*$^{-/\Delta}$ mice, which accumulate DNA damage more rapidly than DNA repair proficient organisms, to the changes that occur in liver with aging in wild-type mice. In the third chapter, I examine the effect of spontaneous, endogenous DNA damage on primary cells *in vitro*. Physiological levels of DNA damage were sufficient to drive cellular senescence *in vitro* and *in vivo*. Furthermore, *in vivo*, we discovered a highly significant correlation between the molecular, cellular and functional changes in the liver of young adult ERCC1-deficient mice and old wild-type mice, providing strong evidence that DNA damage does promote aging. An unexpected finding was that, ERCC1-deficient cells exhibit profound mitochondrial dysfunction, which may reinforce the senescent state through increased production of reactive oxygen species.

1.1 PHYSIOLOGICAL ROLES OF ERCC1-XPF

Chapter 1 is adapted, with copyright permission, from Elsevier Limited, from a published review article. **Gregg, SQ, Robinson, AR, and Niedernhofer LJ. (2011) Physiological consequences of defects in ERCC1-XPF DNA repair endonuclease.** ***DNA Repair*** **10(7): 781-791**

The ERCC1-XPF complex is a structure-specific endonuclease involved in the repair of damaged DNA. ERCC1-XPF performs a critical incision step in nucleotide excision repair (NER), and is also involved in the repair of DNA interstrand crosslinks (ICLs) and some double-strand breaks (DSBs) [20-26]. A fraction of ERCC1-XPF is localized at telomeres, where it is implicated in recombination of telomeric sequences and loss of telomeric overhangs at deprotected chromosome ends [27, 28]. Deficiency of either ERCC1 or XPF in humans results in a variety of conditions, which include the skin cancer-prone disease xeroderma pigmentosum (XP), a progeroid syndrome of accelerated aging, or cerebro-oculo-facio-skeletal syndrome (COFS) [29, 30]. These diseases are extremely rare in the general population and therefore mice with low levels of either ERCC1 or XPF have been generated and studied extensively. These murine models clearly illustrate the importance of DNA repair in preventing aging-related tissue degeneration.

1.1.1 Nucleotide excision repair (NER)

Ultraviolet light damages DNA, resulting in a myriad of lesions, most predominantly cyclobutane pyrimidine dimers (CPDs) and (6-4) photoproducts [31]. NER is the only mechanism by which these photodimers can be removed from DNA in human cells, and ERCC1-

XPF functions as the nuclease that incises the damaged strand 5' to the adduct [32-35]. This incision creates a 3' end that is used as a primer by the replication machinery to replace the excised nucleotides. XPF contains the catalytic activity with its conserved nuclease domain, and ERCC1 is required for binding to DNA [36-40]. Defects in the proteins required for NER can result in xeroderma pigmentosum (XP), trichothiodystrophy (TTD), and Cockayne Syndrome (CS), highlighting the importance of DNA repair in preventing UV-induced skin cancer and developmental abnormalities. XP is a disease characterized by extreme photosensitivity and a 10,000-fold increased risk of cutaneous and ocular neoplasms [41]. Cells from all of the XP complementation groups (XP-A to XP-G, and XP-V) are hypersensitive to UV radiation [29, 42-45]. ERCC1-XPF deficient cells are distinct from other XP patient-derived cells because of their extreme sensitivity to chemicals that induce DNA ICLs [26, 46-48]. Another critical piece of evidence indicating that ERCC1-XPF has functions distinct from NER is that ERCC1 and XPF knockout mice exhibit a much more severe phenotype than XPA null mice, which are completely deficient in NER [26, 49-52].

1.1.2 Interstrand crosslink repair (ICL-R)

The mechanism of DNA ICL repair in mammalian cells is not as well defined as NER. In replicating cells, crosslinking agents lead to DSBs created by endonuclease(s) near the site of stalled replication machinery [53].In the absence of ERCC1-XPF, replication-dependent crosslink-induced DSBs occur, indicating that ERCC1-XPF cannot be solely responsible for creating these DSBs [48]. There is clear evidence that ERCC1-XPF participates in the same mechanism of ICL repair as the Fanconi anemia proteins. In the absence of ERCC1-XPF, FANCD2 is still monoubiquitylated by FANCL, but translocation of FANCD2 to chromatin is

impaired [54]. In addition, when FANCD2 is depleted, replication-dependent incisions of ICLs are dramatically reduced [55].

Recently it was demonstrated that XPF binds SLX4, a related endonuclease, and this interaction is critical for ICL repair [56-59]. Fanconi anemia patients, mice deficient in ERCC1-XPF, and *Slx4(Btbd12)*$^{-/-}$ mice share many spontaneous developmental and degenerative phenotypes, supporting roles for all of these proteins in a common pathway and illustrating the dramatic consequences of failure to repair endogenous ICLs [60, 61]. Recent reports describe the discovery of biallelic mutations in *SLX4* in two patients who exhibited clinical features of Fanconi anemia [62, 63]. Based on evidence that reintroduction of wild-type SLX4 into the patients' cells rescued sensitivity to crosslinking agents, *SLX4* is considered as a new complementation group of Fanconi anemia: FANCP.

1.1.3 Double-strand break repair (DSB-R)

Orthologs of ERCC1-XPF in lower eukaryotes such as *Arabidopsis thaliana, Drosophila melanogaster*, and *Saccharomyces cerevisiae* play a vital role in the repair of DSBs and meiosis [64-67]. The two primary mechanisms of DSB repair are non-homologous end-joining (NHEJ) and homologous recombination (HR). Work in budding yeast has contributed tremendously to defining the role of ERCC1-XPF in DSB repair in mammalian cells. Mutation of *rad10* or *rad1*, the orthologs of *ERCC1* and *XPF* in *S. cerevisiae*, suppresses HR between sequence repeats [68-70]. The function of the RAD10-Rad1 nuclease in HR is to remove non-homologous 3' termini of single-stranded overhangs of broken ends to facilitate single-strand annealing, an error-prone sub-pathway of HR [66, 67, 70, 71]. Like single-strand annealing, there is an error prone sub-pathway of NHEJ that utilizes short stretches of homology to join two broken DNA ends termed

micro-homology mediated end-joining. Rad10-Rad1 also participates in this end-joining pathway in yeast [72]. Yeast Mre11 and Rad1 proteins define a Ku-independent mechanism to repair double-strand breaks lacking overlapping end sequences [72]. Mammalian cells deficient in ERCC1-XPF are modestly sensitive to ionizing radiation (IR), a source of DSBs [22]. Like in yeast, HR and end-joining of DSBs is attenuated in ERCC1-XPF-deficient mammalian cells [23, 73-76]

The ERCC1/XPF endonuclease is required for efficient single-strand annealing and gene conversion in mammalian cells [22, 76]. Therefore, it is proposed that ERCC1-XPF nuclease facilitates both HR and NHEJ pathways (single-strand annealing and microhomology-mediated end-joining) but only if the broken DNA ends contain 3'-overhanging unmatched sequences or that cannot be used to prime DNA synthesis [22].

1.1.4 Role at telomeres

ERCC1-XPF deficiency is linked with accelerated aging, and telomere shortening is associated with aging, therefore it was important to understand if the nuclease impacts telomere length or function [77]. Telomeres in humans with mutations in *XPF*, or *Ercc1* knockout mice, are not shorter than controls [27]. Furthermore, there is no difference in sister chromatid exchange at telomeres in the absence of ERCC1-XPF [78]. However, ERCC1 co-localizes with TRF2 at telomeres [27]. In a TRF2 dominant negative background, ERCC1-XPF deficient cells accumulate telomeric double-minutes. This led to the conclusion that ERCC1-XPF cleaves the G-rich, 3'- overhang, rendering chromosomes vulnerable to end-to-end fusions [27]. Hence the absence of ERCC1-XPF apparently does not have a deleterious impact on telomere length or function. Consistent with that, correction of XP-F cells or overexpression of XPF in normal

human cells leads to telomere shortening [79]. Therefore, accelerated aging associated with ERCC1-XPF deficiency is presumed to arise from cellular senescence and cell death and not as a consequence of telomere-dependent replicative senescence.

1.2 CONSEQUENCES OF DEFICIENCY OF ERCC1-XPF

1.2.1 XPF mutations in humans

Humans with mutations in *XPF* can be classified into two groups based on the clinical manifestations of their disease (see Table 2). The majority of XP-F patients present with mild symptoms of XP, which include sun sensitivity, freckling of the skin, and basal or squamous cell carcinomas typically occurring after the second decade of life. This is in contrast to many XP-A and XP-C patients, in which skin cancer occurs even before 2 yrs of age [80]. The second group of XP-F patients exhibit neurological deterioration in addition to their XP-like symptoms. There has been one published case of a patient with mutations in *XPF* with dramatically accelerated aging [29]. The mutation in *XPF*, its impact on protein expression, function and subcellular localization are all critical determinants in the clinical manifestations [81]. Of note, all XP-F patients carry a missense mutation in at least one allele, and none of these affect the catalytic domain of the protein (Table 2). This has led to speculation that ERCC1-XPF is essential for human life [30]. This is supported by the observation that mice homozygous for null alleles of these genes are not viable except in select genetic backgrounds.

Table 2. Human XPF mutations

Patient Code	Mutation	Amino Acid anges	Age[1] (M or F)	% UDS[2]	UV-S[3]	Neuro[4]	Abnormal pigmentation[5]	Skin Carcinoma[6]	Ref
XP26BR	Base sub 2377 (C→T) Homozygous	Arg799→Trp Arg799→Trp		15		-	+	+	[62]
XP32BR		Arg589→Trp Pro379→Ser	12	10	+ (2X)	-	+	+	[62]
XP23OS	1bp insert 1330 Heterozygous	Lys455→Stop482	45 (F)	10	+ (4X)	-	+	-	[63]
XP126LO	Base sub 2377 (C→T)	Arg799→Trp	22 (F)	45	+	-		-	[13,67]
XP7NE		Pro379→Ser Silent	28	25	+ (2X)	-	+		[73]
XP25KO			8 (F)	12	+ (3X)	-	+	-	[66]
XP27KO			11 (F)	12	+ (2.5X)	-	+	-	[68]
XP28KO			8 (F)	12	+ (3X)	-	+	-	[68]
XP38KO			44 (F)	20-25	+ (2.3X)	-	+	-	[69]
XP46KO			61 (F)	12	+ (2.8X)	-	+	-	[66]
XP90TO			42 (M)	12	+ (3X)	-	+	+ (42)	[70]
XP92TO			40 (F)	12	+ (3X)	-	+	+ (41)	[70]
XP29MA			24 (M)	>5	+ (6X)	-	+	-	[71]
XP30MA			29 (M)	>5	+ (6X)	-	+	-	[71]
XP42RO	Base sub 2377 (C→T) Homozygous	Arg799→Trp	62 (M)	22	+ (2X)	+ (47)	+	+ (27)	[76]
XP24BR	Base sub 2377 (C→T) Homozygous	Arg799→Trp Arg799→Trp	29	5	+ (3X)	+	+	+	[73]
XP24KY	10bp deletion (1575) Base sub 2377 (C→T)	Val536→Stop533 Arg799→Trp	48 (M)	7	+ (3X)	+	+	-	[74]
XP62RO	Base sub 2377 (C→T) Homozygous	Arg799→Trp Arg799→Trp		20	+ (2X)	+ (late onset)			[62]
AS871		Arg589→Trp Deletion of Exon 3		15	+ (2X)	+			[62]
XP51RO	Base sub 458 (G→C) Homozygous	Arg153→Pro	15 (M)	>5	+ (10X)	+ (6)		-	[10]
XP48DC	Base sub 2377 (C→T) Heterozygous	Arg799→Trp				+			[129]
CO14TA	Base sub 2377 (C→T) Heterozygous	Arg799→Trp				+			[129]
CO107TA	Base sub 2377 (C→T) Heterozygous	Arg799→Trp				+			[129]
XP202DC	Nonsense Splice mutation in ERCC1	Lys226→STOP IVS6-26G→A	15			+		-	[129]
165TOR		Glu158→STOP Phe231→Leu	congenital	15	+ (5X)	+	-	-	[11]

1. Age of patient at time of diagnosis and patient's gender. 2. Unscheduled DNA synthesis as a percentage compared to control cells 3. Fold increase in UV sensitivity of patient fibroblasts compared to control cells 4. Presence (+) or absence (-) of neurodegenerative symptoms. 5. Presence (+) or absence (-) of abnormal pigmentation including freckling, blistering, epidermal atrophy and keratoses. 6. Presence (+) or absence (-) of skin carcinomas (basal cell and squamous cell carinomas). Blue region indicates XP-F patients without symptoms of neurodegeneration; pink region indicates XP-F patients with symptoms of neurodegeneration; green region indicates patients with mutations in ERCC1.

The first XPF-deficient human patient was reported in 1979, several years before the *XPF* gene was identified and cloned [82]. The patient, referred to as XP23OS, was confirmed as XP-F by genetic complementation analysis, and exhibited mild XP symptoms including freckling and photosensitivity. Primary cells from patient XP23OS have only 10% of the normal level of NER as measured by UV-induced unscheduled DNA synthesis (UDS), but only modest sensitivity to UV as measured by clonogenic survival. The discrepancy can be explained by the fact that UDS measures NER that occurs in the first 3 hours following UV irradiation, whereas in a clonogenic survival assay cell growth is measured in the 7-10 days following UV irradiation. Thus XP23OS cells must have low levels of NER, but that is adequate to prevent cell death and replicative senescence given adequate time to repair the genome [83]. Furthermore, host cell reactivation of reporter expression following UV damage was only modestly impaired. These results suggest that although the efficiency of NER was impaired in this patient, the pathway must be intact to explain the relatively mild symptoms in this 45 year-old patient. In the years that followed, several patients with XP group F were described, most of them from Japan, having mild to moderate symptoms, similar to patient XP23OS [84-89]. The majority of XP-F patients had UV sensitivity and freckling of the skin, but severe ocular and neurological symptoms were rare in the XP-F complementation group (see Table 1) [90, 91]. It is important to note that there have been reports of additional XP-F patients that are not included in Table 2 because the mutations have yet to be verified in genomic DNA [92].

The human *XPF* gene was cloned in 1996 with the identification of a human gene homologous to yeast *Rad1* [45, 93]. This cDNA corrected the defect in cells from XP group F patients. Additionally, causative mutations were identified in XP-F patients that corresponded to this gene. Following the cloning of *XPF*, an unusual XP-F patient was described displaying

progressive late-onset neurologic decline [94]. This patient, referred to as XP42RO, had mild ocular photophobia with severe erythema on sun exposure. Basal and squamous cell carcinomas were detected in the second decade of life and by the fourth decade the patient exhibited profound neurodegenerative symptoms including ataxia, cerebral and cerebellar atrophy. The mutation found in XP42RO cells is a C→T transition at nucleotide 2377, which results in a change of the conserved arginine residue at 799 to a tryptophan. The R799W mutation was identified in at least eight other XP-F patients, in six of whom neurodegeneration was reported (see Table 1). Patient XP126LO harbors the R799W mutation but without neurologic symptoms to date. One possible explanation is that neurologic symptoms may not appear until the 4th or 5th decade of life, and this patient was assessed and diagnosed at 22 years of age.

More recently, mutations in *XPF* were linked to a novel progeroid syndrome or disease of accelerated aging (called XFE progeroid syndrome). The patient, referred to XP51RO, had severe photosensitivity, which led investigators to hypothesize that NER was defective, and genetic complementation with XP patient cells revealed that XPF was affected [29]. In addition to sun sensitivity and the classical symptoms of XP, patient XFE had severe symptoms of accelerated aging that affected the neurologic, hepatobiliary, musculoskeletal, and hematopoietic systems. Mutation analysis revealed a G→C transversion at position 458 which resulted in a non-conservative substitution of arginine at residue 153 to proline. The mutation in *XPF* was unexpected because patient XFE had severe symptoms of accelerated aging unlike most other XP-F patients who had mild XP. R153 is located within a conserved helicase motif of XPF which is also a leucine-rich region postulated to be important for protein-protein interactions. Primary fibroblasts from patient XP51RO are highly sensitive to UV and the crosslinking agent mitomycin C. Patient XP51RO had normal early postnatal development, but progeroid

symptoms began to appear in early prepubescence. The symptoms included an old, wizened appearance, loss of subcutaneous fat, liver dysfunction, vision and hearing loss, renal insufficiency, muscle wasting , osteopenia, kyphosis and cerebral atrophy. These symptoms of accelerated aging are strikingly similar to those seen in *Ercc1*$^{-/-}$ and *Xpf*$^{m/m}$ mice (Figure 17).

Very recently a patient with features similar to XP51RO was identified in the UK. The patient has the facial appearance of CS, sun-sensitivity, microcephaly, neurological problems and developmental delay, together with pancytopenia and renal failure. Cellular studies revealed low UDS and assignment to the XP-F group (D. Pilz, D. McGibbon, R. Sarkany, M. Stefanini and A Lehmann, *personal communication*). XP-F patients with early onset and more severe symptoms appear to have mutations that lead to mislocalization of ERCC1-XPF to the cytoplasm, thereby decreasing the cellular capacity for efficient repair of nuclear DNA [81].

1.2.2 ERCC1 mutations in humans

ERCC1 was the first human DNA repair gene cloned [95]. For decades, however, no patients were identified with *ERCC1* mutations; hence the gene does not have the standard XP nomenclature (XP-x) like other NER factors associated with xeroderma pigmentosum. Recently, a single patient was discovered who had mutations in *ERCC1* resulting in severe pre- and postnatal developmental defects [30]. The patient, referred to as 165TOR, had severe skeletal defects at birth, including microcephaly, arthrogryposis and rocker-bottom feet. These abnormalities were seen in conjunction with neurological alterations including cerebellar hypoplasia and blunted cortical gyri. The clinical diagnosis was cerebro-oculo-facio-skeletal syndrome, or COFS syndrome. COFS syndrome was first reported by Lowry in 1971, and further characterized in the Manitoba aboriginal population by Pena and Shokeir in 1974 [96,

97]. COFS syndrome is a rare autosomal recessive disorder in which patients undergo rapid neurologic decline. Symptoms include but are not limited to brain microcephaly and atrophy with calcifications, cataracts, optic atrophy, progressive joint contractures, and severe postnatal growth failure [98]. Patients with COFS syndrome are reported to have mutations in genes encoding DNA repair proteins *ERCC6/CSB*, *ERCC5/XPG* and *ERCC2/XPD* [99, 100].

Two mutations were found in the coding region of *ERCC1* in patient 165TOR. The maternal allele harbors a C→T transition that converts Gln158 into an amber translational stop codon. The result is a truncated polypeptide that lacks the entire C-terminal domain, essential for binding XPF [101]. The paternal allele has a C→G transversion, resulting in the conversion of Phe231 to leucine. This amino acid falls within the C-terminal tandem helix-hairpin-helix domain of ERCC1, critical for binding XPF, and is conserved in invertebrates and mammals [101]. *ERCC1* mRNA levels were normal in this patient, although the protein levels of ERCC1 and XPF in the nucleus were reduced 4-5-fold. The truncated protein was not detectable by immunoblot. Accordingly, fibroblasts from patient 165TOR had 15% of the normal level of NER, representing a modest defect, suggesting that the missense mutation affects stability of ERCC1-XPF and/or its nuclear localization, but not enzymatic activity.

Unexpectedly, the expression of ERCC1-XPF in 165TOR cells is reduced but comparable to a patient with mild XP-F. Several hypotheses have been proposed to explain this incongruity, the simplest being that ERCC1 and XPF play distinct roles *in vivo*. Evidence against this hypothesis includes the fact that $Ercc1^{-/-}$ and $Xpf^{m/m}$ mice have apparently identical phenotypes [49, 52]. Additionally, ERCC1 and XPF are required to stabilize one another *in vivo* [32, 101]. It is important to note that COFS is also caused by mutations in the TFIIH subunit XPD and the NER endonuclease XPG that stabilizes TFIIH [98, 102-104]. ERCC1-XPF and the

other members of the NER machinery have been demonstrated to play a role in regulating transcription that has been suggested to be independent of their role in DNA repair [105]. Therefore, the clinical severity of patient 165TOR may be due to a transcriptional transcription-coupled nucleotide excision repair defect during development. It is also possible that 165TOR was genetically replete of functional ERCC1-XPF during development, but selective pressure led to partial reversion of the cellular phenotype postnatally. Reversion with mosaicism has been reported in many genome instability disorders including Fanconi anemia, Werner and Bloom syndromes, and observed for ERCC1-XPF deficient cells chronically exposed to crosslinking agents [60, 106-108]. In addition, there are undoubtedly modifier genes that affect the severity of symptoms caused by mutations in ERCC1 or XPF as illustrated by the fact that *Ercc1*$^{-/-}$ mice are not viable in inbred C57Bl/6 or FVB/n inbred backgrounds but are born with Mendelian frequency in an f1 mixed background [29]. Finally, little is known about regulation of ERCC1-XPF expression, which could be tissue-specific and therefore contribute to heterogeneous phenotypes. Identifying modifier genes, identifying regulators of nuclease expression and modeling additional patient mutations in mice will be essential for deciphering genotype:phenotype correlations. A second patient with mutations in ERCC1 was briefly described recently [129]. The patient had a nonsense mutation affect amino acid 226, which lies early in the helix-hairpin-helix domain necessary for binding XPF. The second allele contains a splicing mutation (IVS6-G→A). The patient displayed neurologic symptoms beginning at age 15 years and died by the age of 37. Neurodegeneration was progressive and severe resulting in dementia and cortical atrophy. The symptoms are very similar to XPF patients with neurologic involvement (Table 1) supporting the conclusion that ERCC1 and XPF function exclusively as a complex *in vivo*.

1.3 MOUSE MODELS OF ERCC1-XPF DEFICIENCY

1.3.1 ERCC1 knockout mice

To understand the biological significance of ERCC1, the gene was knocked-out in the mouse by two independent laboratories [43, 49]. The two knockout alleles were created by interrupting different exons. McWhir *et al* created the first knockout mouse model by disrupting exon 5 of *Ercc1* leading to a truncated transcript missing the last four exons, which contain the XPF interaction domain [32, 36, 49]. The second knockout strain was generated by inserting a *neomycin* resistance cassette into exon 7 of *Ercc1* [43]. The result was a truncation in the helix-hairpin-helix motif required for interaction with XPF [101]. *Ercc1* mRNA was not detected in these mice [43]. The former strain is born with Mendelian frequency; the latter is sub-Mendelian, likely due to differences in the genetic background [43, 49]. Deletion of ERCC1 is lethal in a fully inbred genetic background, indicating that there are modifier genes that influence the severity of the phenotype [29]. In both knockout strains, postnatal growth is severely retarded and the mice die at approximately 3 weeks of age when they weigh only about 20% compared to their normal littermates [43, 49]. The median lifespan of *Ercc1*$^{-/-}$ mice in an f1 mixed genetic background of 50:50 C57BL/6:FVB/n is 21 days and the maximum lifespan 28 days [29]. The *Ercc1*$^{-/-}$ mice spontaneously develop symptoms characteristic of progressive neurodegeneration, including dystonia, trembling and ataxia [29].

The hematopoietic system of *Ercc1*$^{-/-}$ mice develops normally [109]. However, by the end of life, *Ercc1*$^{-/-}$ mice are leukopenic and thrombocytopenic, and there is extensive adipose transformation of the bone marrow, hallmark features of normal aging in mice [109]. Proliferation of multi-potent and lineage-committed progenitors from *Ercc1*$^{-/-}$ mice is profoundly

impaired [109]. Collectively, these data suggest that ERCC1-deficient mice undergo rapid turnover of hematopoietic cells leading to premature exhaustion of stem cell reserves. In addition, bone marrow progenitors from *Ercc1*$^{-/-}$ mice are exquisitely sensitive to crosslinking agents, similar to murine models of Fanconi anemia [109, 110] .

The liver of *Ercc1*$^{-/-}$ mice is prominently affected, with hepatocellular polyploidy, aneuploidy and G2 arrest [49, 111, 112]. The structural changes correlate with impaired liver function as demonstrated by significantly increased liver enzymes in the serum [49]. *Ercc1*$^{-/-}$ mice develop kyphosis, sarcopenia, dystonia and ataxia, indicative of musculoskeletal and nervous system defects [29]. There is a suppression of the somatotroph, lactotroph and thyrotroph hormonal axes in the *Ercc1*$^{-/-}$ mice, which explains their growth delay and diminutive size [29]. Many of the degenerative and endocrine abnormalities are similar to what occurs with old age in mice [113, 114]. To further investigate the relationship of DNA repair deficiency to normal aging, genome-wide expression changes in *Ercc1*$^{-/-}$ mice relative to wild-type littermates was compared to changes that occur with natural aging (differences in gene expression between old wild-type and young wild-type mice). There is a highly significant overlap between these two profiles whether comparing gene-by-gene or by comparing over-represented biological pathways [29]. This provided some of the early support for the notion that DNA damage may contribute to aging.

1.3.2 XPF mutant mice

Tian *et al* recreated the *XPF* mutation in patient XP23OS in the mouse [52]. The patient had a single base insertion after nucleotide 1330 leading to a frameshift mutation after Lysine 455 and a stop codon 38 residues later [92]. This leads to truncation of XPF upstream of the catalytic

domain and its ERCC1-interaction domain [36]. The clinical phenotype of the patient was mild, having reached her 4th decade without neurodegeneration or skin cancer [92]. In keeping with this, the level and length of the *XPF* transcript in XP23OS cells are comparable to normal cells, illustrating that the patient must have a 2nd *XPF* allele. To further emphasize this, a mouse homozygous for the frameshift mutation has undetectable levels of *Xpf* mRNA and a severe phenotype identical to that of ERCC1 null mice [52]. The *Xpf*$^{m/m}$ mice develop normally and are born with Mendelian frequency. However, postnatal growth is delayed such that by 2 wks of age the *Xpf*$^{m/m}$ mice are approximately 25% the size of littermates, and die by 3 wks of age. Hepatocellular polyploidy was prominent, as in the *Ercc1*$^{-/-}$ mice [52]. The phenotypic parallels between ERCC1 and XPF null mice strongly suggest that the proteins function exclusively as a complex.

Importantly, ERCC1 and XPF-deficient mice appear to have a normal complement of mature and immature B cells [52, 115, 116]. This provides definitive evidence that ERCC1-XPF is not essential for NHEJ, the DSB repair pathway required for class switch recombination (CSR) [117]. However, *ex vivo* CSR is mildly attenuated in splenocytes isolated from *Ercc1*$^{-/-}$ mice and the mutation pattern in the switch region of the immunoglobulin locus is significantly different from that of normal littermate mice, suggesting that ERCC1-XPF may contribute to DNA end-processing of DSBs at the Ig locus [116]. Consistent with this, ERCC1-deficient mice are hypersensitive to IR, which induces DNA DSBs [22].

1.3.3 Liver corrected *Ercc1*$^{-/-}$ mice

To investigate the cause of death in *Ercc1*$^{-/-}$ mice, Selfridge *et al* crossed the mice with a transgenic strain expressing ERCC1 specifically in the liver, using transthyretin (TTR) regulatory sequences to control ERCC1 expression [118]. The resulting mice (*Ercc1*$^{-/-}$ + TG) have dramatically improved growth, reaching 58% of normal body weight for their age. Furthermore, their lifespan is significantly increased, with a median survival of ~75 days. Hepatocellular polyploidy and abnormal liver functions are largely corrected by expression of ERCC1 in the liver. Interestingly, by 7 wks of age, the transgenic mice begin to display evidence of renal dysfunction (significantly elevated serum creatinine and proteinuria) and renal histopathology (glomerulosclerosis, hyaline casts, renal tubular epithelial anisokaryosis, karyomegaly, hyperchormasia, pyknosis and keryorrhexis) [118, 119]. These data suggest that *Ercc1*$^{-/-}$ mice die of liver failure and that hepatocytes and renal cells are the most vulnerable to loss of ERCC1-XPF-dependent DNA repair.

Since the *Ercc1*$^{-/-}$ + TG mice live longer than *Ercc1*$^{-/-}$ mice, they are a practical system for identifying other tissues affected by ERCC1-deficiency. Performance of *Ercc1*$^{-/-}$ + TG mice on an opto-kinetic response test to measure visual acuity is impaired by 4 wks and worsens with age [119]. Structural abnormalities of the eye were not detected, indicating that loss of vision is not due to a developmental defect [119]. Also, there is no evidence for retinal degeneration typical of CSB mice, another NER-defective mutant strain [120].

Like *Ercc1*$^{-/-}$, symptoms associated with neurodegeneration were observed in *Ercc1*$^{-/-}$ + TG mice. The *Ercc1*$^{-/-}$ + TG mice displayed dystonia and ataxia indicative of a cerebellar defect. While mild atrophy of the neocortex and cerebellum were observed, there were no abnormalities or loss of Purkinje cells to explain these phenotypes. Also, there were no signs of degeneration at

the neuromuscular junctions. Therefore these symptoms were attributed to uraemic encephalopathy, caused by kidney failure [119].

Male and female *Ercc1*$^{-/-}$ + TG mice were found to be infertile [121]. Testes of these mice were approximately 50% the normal size at puberty and contained significantly less spermatocytes. Spermatogenesis is not arrested at a particular stage, as expected for a meiotic defect, but instead there is abundant apoptosis in these rapidly dividing cells [121, 122]. This leads to a resulting 97% reduction in the sperm count [122]. Ovaries from adult *Ercc1*$^{-/-}$ + TG mice showed a reduced number of oocytes and an absence of primary follicles [121].

1.3.4 ERCC1 mutant mice

To further probe the DNA repair function of ERCC1 *in vivo*, a premature stop codon was engineered at position 292 of *mErcc1* [43]. This results in a C-terminal deletion of 7 amino acids of the murine protein, including a phenylalanine residue at position 293, thought to be essential for binding to XPF [101]. Thus the prediction was that this mutation would ablate DNA repair function without compromising the protein stability [32]. Unlike either of the null alleles, normal levels of the mutant *Ercc1* transcript are detected in the tissues from the mutant mice [43]. Homozygous *Ercc1*^{*292} (also referred to as *Ercc1*$^{\Delta/\Delta}$) mice live up to 6 months, which is 6X longer than ERCC1 null mice. Similar to the *Ercc1*$^{-/-}$ mice, the *Ercc1*^{*292} mice are infertile and their skin is atrophic and lacks subcutaneous fat [43]. The spleen of *Ercc1*^{*292} mice contains increased ferritin and hemosiderin deposits, indicative of a high turnover of erythrocytes. The kidney exhibits dilated renal tubules with hyaline casts. Nuclear polyploidy is common in the liver and kidney. Thus virtually all of the phenotypes of *Ercc1*$^{-/-}$ mice are recapitulated in this longer-lived mutant strain. Primary mouse embryonic fibroblasts (MEFs) from the *Ercc1*$^{-/-}$ mice

are modestly more sensitive to the crosslinking agent mitomycin C than MEFs from *Ercc1*^{*292} mice, suggesting that their increased longevity is due to increased DNA repair capacity [43]. Despite this, topical application of the tumor initiator DMBA to *Ercc1*^{*292} mice, leads to acute toxicity rather than carcinogenesis, illustrating a dramatic difference from other NER-deficient mice [43].

1.3.5 ERCC1 hypomorphic mice

Combination of one null and one mutant *Ercc1* allele yields mice (*Ercc1*$^{-/*292}$; *Ercc1*$^{-/\Delta}$ or *Ercc1*$^{d/-}$) that are born with Mendelian frequency and have an even greater maximal lifespan of 7 months in an f1 background of 50:50 C57Bl/6J:FVB/n [123]. *Ercc1*$^{-/\Delta}$ mice are runted compared to their wild-type littermates [124]. However, they develop normally until sexual maturity, at which point they began to exhibit signs of rapid aging [125]. They live 24-30 weeks while progressively developing dystonia, tremors, kyphosis and ataxia [124].

The *Ercc1*$^{-/\Delta}$ mice were crossed with a transgenic lacZ reporter strain to measure the mutation frequency *in vivo* [123]. The mutation frequency is modestly elevated in the liver of 5-6 month old *Ercc1*$^{-/\Delta}$ mice compared to normal littermates. Interestingly, the mutations are primarily chromosomal rearrangements characteristic of old wild-type mice rather than point mutations characteristic of NER-deficient mice [123]. This observation extends the parallels between the progeroid *Ercc1*$^{-/\Delta}$ mice and aged normal mice.

Ercc1$^{-/\Delta}$ mice are hypersensitive to IR [22]. Even though these mice are hypomorphic for ERCC1-XPF, they were equally as sensitive to IR as DNA-PKcs knockout mice [126]. IR causes persistent γ-H2AX foci in ERCC1-deficient cells and mice, supporting a role for ERCC1-XPF in the repair of DSBs. The involvement of ERCC1-XPF in DSB repair is presumably a Ku-

independent pathway since *Ercc1*$^{-/-}$ *Ku86*$^{-/-}$ mice are not viable [22]. *Ercc1*$^{-/-}$ MEFs have normal levels of spontaneous and mitomycin C-induced sister chromatid exchanges, illustrating that ERCC1-XPF is not essential for homologous recombination [75, 127]. In contrast, DSBs with 3' overhangs cause large deletions in *Ercc1*$^{-/-}$ cells [22, 75]. These genetic and *in vitro* data support a role for ERCC1-XPF in processing a subset of DSBs (those with 3' overhangs) and a role in the alternative end-joining pathway of DSB repair [128].

Ercc1$^{-/-}$, *Ercc1*$^{-/-}$ + TG, and *Ercc1*$^{-/\Delta}$ mice all develop progressive dystonia, tremors and ataxia, highly suggestive of neurodegeneration [29, 119, 124]. The former strains display cerebellar hypoplasia, similar to the ERCC1 patient 165TOR, but this could not be completely dissected from developmental abnormalities, due to their young age [29, 30, 119]. Evidence for degenerative processes in the central nervous system is quite clear in *Ercc1*$^{-/\Delta}$ mice [124]. De Waard *et al* found profound astrocytosis and microgliosis in the spinal cord of 4 month old *Ercc1*$^{-/\Delta}$ mice, compared to normal littermates and 1 month old mutant animals. This is accompanied by a significant reduction in the number of motor neurons in the ventral horn of the spinal cord and a concomitant denervation of the skeletal muscle. There is an approximately 50% reduction in neurons from 4-8 wks of life, and then again from 8-16 wks of life in the *Ercc1*$^{-/\Delta}$ mice. It is also evident that the pre-synaptic motor nerve terminals have degenerated in the aged *Ercc1*$^{-/\Delta}$ mice with characteristics similar to those seen in amyotrophic lateral sclerosis and aging motor neurons [124].

Genome-wide expression profiling of *Ercc1*$^{-/\Delta}$ mice revealed a highly significant correlation with the transcriptome of numerous long-lived models, including Ames and Snell dwarf mice and/or calorically restricted mice [113]. In addition, there is a significant correlation with the transcriptome of old wild-type mice. This indicates that *Ercc1*$^{-/\Delta}$ mice look biologically

"old", but also that the failure to repair DNA damage in these mice triggers activation of a stress response that is transcriptionally regulated and promotes longevity. Schumacher *et al* showed that this same stress response is also triggered by nutritional deprivation and is mediated through suppression of GH-IGF1 signaling as evidenced by the significant correlation with Ames and Snell dwarf mice. All of these mice displayed suppression of the somatotroph axis, oxidative metabolism and peroxisomal biogenesis coupled with an upregulation of antioxidants, DNA damage and apoptosis [113].

This was further supported by analysis of metabolites in the serum and urine of *Ercc1*$^{-/\Delta}$ mice [125]. There is no difference between *Ercc1*$^{-/\Delta}$ mice and normal littermates at 8 and 12 weeks of age. However by 16 weeks, there are significant differences, which become further amplified by 20 weeks of age. Collectively, these data support the conclusion that *Ercc1*$^{-/\Delta}$ mice develop normally into adulthood, but then undergo degenerative changes. Several of the metabolic changes mimic those that occur with caloric restriction, including increased HDL, decreased LDL and VLDL, and ketosis. However, a number of metabolic changes in the *Ercc1*$^{-/\Delta}$ mice are also consistent with degeneration, such as increased glucose, citrate and succinate in the urine indicative of kidney dysfunction, and metabolic alkalosis indicative of liver dysfunction [125]. These observations are consistent with the model that DNA damage accumulates in *Ercc1*$^{-/\Delta}$ mice leading to metabolic reprogramming in response to stress [113]. This may be beneficial, but in the long-run is insufficient to sustain the organism in the face of continued DNA damage [29].

Remarkably, *Ercc1*$^{-/\Delta}$ mice spontaneously develop numerous diseases associated with old age in humans (Table 3). This includes osteoporosis and intervertebral disc degeneration [129]. There is progressive attrition of disc extracellular proteoglycans with age, leading to loss of disc

height and its cushioning function [130, 131]. Similar changes were observed in discs of 5 month old *Ercc1*$^{-/\Delta}$ mice and exacerbated in mice treated with genotoxic chemotherapeutic agents [129]. These observations support the conclusion that DNA damage, if not repaired, can promote common aging-related degenerative diseases, even in post-mitotic tissues.

.

	Ercc1$^{-/-}$	*Ercc1*$^{-/\Delta}$	XFE	Human aging	Ref.
Maximum Lifespan	4 weeks	28 weeks	16 years	120 years	[76]
Loss of subcutaneous fat	+	+	+	+	[100]
Atrophic epidermis	+	+	+	+	[99]
Hearing loss	+	+	+	+	[76]
Visual impairment	+	+	+	+	[76]
Tremors	+	+	+	+	[101]
Ataxia	+	+	+	+	[101]
Cerebral atrophy	+	+	+	+	[102]
Hypertension	?	?	+	+	[76]
Renal acidosis	+	+	+	+	[103]
Bone marrow degeneration	+	+	+	+	[100]
Osteoporosis	+	+	+	+	[76]
Kyphosis	+	+	+	+	[102]
Dystonia	+	+	+	-	[10, 86]
Sarcopenia	+	+	+	+	[76]
Frailty	+	+	+	+	[76]
Urinary Incontinence	?	+	+	+	[76]
Disc degeneration	+	+	?	+	[104]

Table 3. DNA repair deficiency parallels natural aging

Symptoms observed in *Ercc1*$^{-/-}$ mice, *Ercc1*$^{-/\Delta}$ mice, and patient XP51RO who had a progeroid syndrome (or disease of accelerated aging) due to a homozygous mutation in *XPF*, and which the ERCC1 mice model. Also indicated are whether or not the same symptoms associated with old age in humans of human aging and (+) or (-) indicates presence or absence in the *Ercc1*$^{-/-}$ mice, *Ercc1*$^{-/\Delta}$ mice, or progeroid patient XP51RO.

1.3.6 Tissue specific deletion of ERCC1

Tissue-specific deletion of a gene is a powerful tool for dissecting a complex phenotype, such as that of the ERCC1-deficient mice, allowing for dissection of whether a particular symptom or pathology is a direct consequence of a deletion of a gene or merely a secondary consequence (*e.g.*, is neurodegeneration due to loss of ERCC1 in neurons or uraemic encephalopathy due to loss of ERCC1 in the kidneys?). Tissue specific knockout of protein expression occurs if the gene of interest (or an exon vital to its function) is flanked (floxed) by recombination signals (loxP or FRT) and mice expressing the two copies of the floxed allele are crossed with transgenic mice expressing recombinase (CRE or FLP, respectively) under a tissue specific promoter [132]. Another important attribute of this approach is that it is possible to distinguish developmental from degenerative changes by selecting promoters that are active only postnatally.

A floxed allele of *Ercc1* was generated by inserting loxP sites in intron 2 and 5, such that Cre recombinase excises exons 3-5 of the *Ercc1* locus [133]. Mice harboring two floxed alleles of *Ercc1* were crossed with transgenic mice expressing Cre-recombinase under a tyrosinase promoter [134]. The goal was to knockout expression of ERCC1 in melanocytes to generate a murine melanoma model. Unexpectedly, the mice die by 6 months of age due to severe colonic obstruction. Tyrosinase is expressed in all neural crest cell-derived lineages, including parasympathetic neurons that innervate the gastrointestinal tract and are required for colonic peristalsis. Knocking-out ERCC1 expression in neural crest cells causes p53 activation and apoptosis of ganglion cells in the mesenteric plexus. Denervation of the bowel explains the colonic obstruction and demonstrates that ERCC1-XPF dependent DNA repair is critical for protecting neurons from degeneration [134]. This provides strong evidence that the neurological

symptoms observed in ERCC1-deficient mice are due, at least in part, to loss of functional neurons rather than a defect in supportive glial cells.

ERCC1 was also knocked-out specifically in the skin to create a model of UV-induced skin cancer. *Ercc1*$^{flox/-}$ mice were crossed with transgenic mice expressing Cre recombinase under the keratin 5 (K5) promoter, which is only expressed in the basal layer of the epidermis [133]. To facilitate UV carcinogenesis studies, these mice were produced in an albino, hairless background. Deletion of *Ercc1* in the skin leads to a 20-fold reduction in the minimal erythemal dose in response to UV-B irradiation, leading to dramatic, but transient hyperplasia [133]. Furthermore the mice develop significantly more skin tumors, early, and at a lower dose of UVB than normal controls. The cumulative dose of UV-B required to induce tumors in half of the ERCC1-deficient mice was 37X lower than normal controls in a chronic exposure study [133]. The mice also developed actinic keratosis and squamous cell carcinomas. Thus this tissue-specific knockout strain offers an accurate and rapid (tumors within 8 weeks) model of UV-induced skin cancer, which may be useful in the study of XP. Subsequently, these mice have been used to test topical treatments that protect against UV-induced skin cancer [135].

1.3.7 Double mutant mice

TRF1 and TRF2 are sheltrin proteins required to protect telomeres at chromosomal ends [136]. Overexpression of either protein leads to a dominant negative effect exemplified by telomere shortening, loss of telomeric 3' G-rich overhangs and end fusions [28, 137]. Overexpression of TRF2 in the skin of mice by putting the cDNA under control of the keratin 5 promoter (K5TRF2), leads to skin atrophy, hyperpigmentation and increased skin cancer in sun-exposed areas. These results demonstrate that dysregulation of telomeres promotes UV-induced skin

cancer [28]. Skin and keratinocytes isolated from either K5TRF1 or K5TRF2 mice contain telomeric defects, which were rescued by knocking-out *Xpf* [28, 137]. This strongly supports the previous observation that the absence of ERCC1-XPF does not negatively impact telomere length or function, but instead has an unexpected beneficial effect [27].

1.4 SUMMARY

There is tremendous variability between patients with mutations in ERCC1 or XPF, ranging from mild cutaneous symptoms to severe neurodegeneration. ERCC1 patient 165TOR had severe developmental abnormalities that are not normally seen in XP-F patients. These differences cannot be fully predicted by the patients' mutations or the level of residual NER (UDS) in patient fibroblasts. Clearly, further work is needed to decipher how expression and activity of ERCC1-XPF is regulated. This in turn is likely to yield better methods for predicting the physiological consequences of a particular mutation [138]. The studies in mice have been crucial for a number of reasons. First, the identical phenotypes of *Ercc1*$^{-/-}$ and *Xpf*$^{m/m}$ mice, which are null for XPF, provide the strongest possible evidence that ERCC1 and XPF must function exclusively as a heterodimer. Second, the unexpected premature aging phenotypes of the ERCC1 mutant mice led to the discovery of a new rare genetic disease (XFE progeroid syndrome) and contributed to the body of evidence that DNA damage is one type of cellular damage that promotes aging-related degenerative changes (e.g., neurodegeneration). Third, it is clear that the severity of symptoms, associated with ERCC1-XPF deficiency, are somehow linked to variable levels of expression or activity. This implies that functional single nucleotide polymorphisms in either gene may be important for predicting risk of cancer or degenerative diseases. Fourth,

Ercc1 mutant mice are unique amongst the NER-deficient mutant strains because they spontaneously develop neurodegeneration, which may be used to screen therapies for treating XP, CS and TTD patients. Finally, tissue-specific ERCC1 knockout strains will be crucial for identifying which tissues and cell types are most vulnerable to DNA damage and are responsible for triggering systemic stress responses.

2.0 THE LIVER RESPONSE TO ENDOGENOUS DNA DAMAGE

Chapter 2 is adapted, with copyright permission, from John Wiley and Sons, from a published article in *Hepatology*. **Gregg, SQ, Gutierrez, V, Robinson, AR, Woodell, T, Nakao, A, Ross, MA, Michalopoulos, GK, Rigatti, L, Rothermel, CE, Kamileri, I, Garinis, G, Stolz, DB, and Niedernhofer LJ. (2011) A mouse model of accelerated liver aging due to a defect in DNA repair.** ***Hepatology [epub ahead of print]*** Please note figure numbers have changed.

The liver changes with age leading to an impaired ability to respond to hepatic insults and increased incidence of liver disease in the elderly. Therefore, there is critical need for rapid model systems to study aging-related liver changes. One potential opportunity is murine models of human progerias, or diseases of accelerated aging. *Ercc1*$^{-/\Delta}$ mice model a rare human progeroid syndrome caused by inherited defects in DNA repair. To determine if hepatic changes that occur with normal aging occur prematurely in *Ercc1*$^{-/\Delta}$ mice, we systematically compared liver from 5 month-old, progeroid *Ercc1*$^{-/\Delta}$ mice to old (24-36 month) wild-type (WT) mice. Both displayed areas of necrosis, foci of hepatocellular degeneration and acute inflammation. Loss of hepatic architecture, fibrosis, steatosis, pseudocapillarization, and anisokaryosis were more dramatic in *Ercc1*$^{-/\Delta}$ mice than in old WT mice. Liver enzymes were significantly elevated in serum of *Ercc1*$^{-/\Delta}$ mice and old WT mice, while albumin was reduced, demonstrating liver damage and dysfunction. The regenerative capacity of *Ercc1*$^{-/\Delta}$ liver following partial

hepatectomy was significantly reduced. There was evidence of increased oxidative damage in *Ercc1*$^{-/\Delta}$ and old WT liver, including lipofuscin, lipid hydroperoxides and acrolein as well as increased hepatocellular senescence. There was a highly significant correlation in genome-wide transcriptional changes between old WT and 16 but not 5 week-old *Ercc1*$^{-/\Delta}$ mice emphasizing that the *Ercc1*$^{-/\Delta}$ mice acquire an aging profile in early adulthood. Conclusion: There are strong functional, regulatory and histopathological parallels between accelerated aging driven by a DNA repair defect and normal aging. This supports a role for DNA damage in driving aging and validates a murine model for rapidly testing hypotheses about causes and treatment for aging-related hepatic changes.

2.1 INTRODUCTION

Aging is characterized by the progressive loss of homeostatic reserve in all tissues leading to a decreased ability to respond to stress, functional decline and dramatically increased risk of morbidity and mortality[12]. Chronic liver disease and cirrhosis are the twelfth leading cause of death in the United States, with 25,192 (1.1%) deaths each year[139]. Mortality due to liver disease is not limited to the United States, as the World Health Organization (WHO) estimates that 20 million individuals have cirrhosis and/or liver cancer worldwide, and that 1-2 million die annually as a result of liver failure. Many liver diseases are more prevalent in the elderly, including alcohol-induced cirrhosis, viral hepatitis-induced cirrhosis, diabetic-associated chronic liver disease, hepatocellular carcinoma and biliary cirrhosis[140, 141], illustrating that aged liver is less able to cope with a variety of stressors.

Although there are no definitive biomarkers of aged liver, there are several hallmark structural changes. The volume of the liver decreases with age[142]. This decrease is gender-specific, with an average decrease of 6.5% in males and 14.3% in females[143]. Hepatocytes are quiescent cells, until stimulated to proliferate following injury or surgical resection[144]. The capacity for hepatocyte regeneration following partial hepatectomy decreases with age[145]. During the aging process, the nuclear size and shape of hepatocytes becomes altered[112]. Nuclear invaginations and larger nuclei are commonly associated with age in liver samples[146]. Nuclear polyploidy of hepatocytes increases with age, rising from 7-10% in young mice to approximately 30% in old mice[112]. Finally, lipofuscin, insoluble oxidized proteins, accumulates in the cytoplasm of hepatocytes[147, 148].

Liver sinusoidal endothelial cells (LSEC) line the hepatic microvasculature, express little to no basement membrane, and exhibit numerous fenestrations necessary for filtering lipopoteins from the portal blood supply. A reduction in the number of these pores combined with the thickening of the endothelium, called pseudocapillarization, is commonly seen in aged livers[149], as is non-alcoholic fatty liver disease or steatosis[150]. The underlying cause for fatty liver disease is not known, but some possibilities include diabetes mellitus, oxidative stress, mitochondrial dysfunction and metabolic and hormonal imbalances[151]. All of these age-related liver changes in humans are recapitulated in the mouse[152-156].

Aging research is challenging because of the incredible variability in humans. Mice offer an attractive alternative because genetic and environmental variables can be controlled. Nevertheless, the time and expense required to generate and maintain mice >3 years of age is daunting. One approach to overcome this is to use mouse models of accelerated aging, or human progerias. Werner syndrome, Cockayne syndrome, XFE progeroid syndrome and

trichothiodystrophy are examples of human diseases of accelerated aging[157]. A common thread linking these disorders is that they all result from mutations in genes that are involved in genome maintenance. These observations strongly suggest that DNA damage can promote age-related degenerative changes.

ERCC1-XPF is a structure-specific endonuclease involved in the repair of several types of DNA lesions including interstrand crosslinks, double-strand breaks, and bulky, helix-distorting lesions[22, 48]. ERCC1 and XPF are obligate binding partners and stabilize one another *in vivo*[29]. Mutations in *XPF* that cause reduced expression of ERCC1-XPF cause a progeroid syndrome characterized by dramatically accelerated aging of most organ systems[29]. *Ercc1*$^{-/-}$ and *Xpf*$^{-/-}$ mice have an identical phenotype to one another and mimic the human progeroid syndrome[49, 52]. These mice die in the 4th week of life with aging-like degenerative changes, including osteoporosis, neurodegeneration, bone marrow hypoplasia, epidermal atrophy, sarcopenia, and liver and kidney dysfunction[29, 109]. Liver dysfunction is life-limiting in *Ercc1*$^{-/-}$ mice[118]. Mice with reduced but not ablated ERCC1-XPF expression live longer than *Ercc1*$^{-/-}$ mice (30 weeks vs. 4 weeks maxiumum lifespan)[124, 158] The *Ercc1*$^{-/\Delta}$ mice are healthy into adulthood (8 weeks) then begin to show numerous progressive symptoms associated with aging[158]. The aim of this study was to systematically compare the liver of 4-5 month-old *Ercc1*$^{-/\Delta}$ mice to that of old WT mice (2+ yrs old) to determine if the progeroid mice offer an accurate model of natural aging that could be used to accelerate research on the biology of aging-related liver changes and therapeutic interventions to extend healthspan

2.2 MATERIALS AND METHODS

Animal Care and Experimentation

Experiments involving mice were approved by the University of Pittsburgh Institutional Animal Care and Use Committee and in accordance with the NIH guidelines for humane care of animals. Ercc1$^{-/\Delta}$ mice were bred and genotyped as previously described[22]. All mice used in this study were in an f1 mixed genetic background (FVB/n:C57Bl/6).

Histological analyses

6-7 and 20-24 week old WT and *Ercc1*$^{-/\Delta}$ mice, along with aged (26-36 month) WT mice were sacrificed by CO_2 inhalation, and excised livers were fixed with 10% formalin and embedded in paraffin. Tissue sections (6μm) were cut and stained with hematoxylin and eosin (H&E) to detect changes in liver architecture and Masson's trichrome to detect fibrosis, using standard procedures. Alternatively liver specimens were cryopreserved by fixation in 10% formalin for 2-4 hours, followed by incubation in 30% sucrose at 4°C overnight. Tissues were embedded in OCT and flash frozen prior to sectioning on a Microm cryostat.

Liver Perfusion and Processing for Ultrastructural Analysis

For scanning and transmission electron microscopy, the liver of euthanized animals was cleared of blood by perfusion with phosphate-buffered saline (PBS) at 3mL/min through the inferior vena cava as previously described[159]. Samples of liver were fixed with glutaraldehyde and processed also as described previously[160]. TEM images were captured with the JEOL JEM 1011 microscope and SEM images were taken with the JEOL JSM 6330F microscope (JEOL

Ltd, Peabody, MA). Porosity was determined using MetaMorph imaging software. Fenestrations were manually predetermined and porosity expressed as percent of measured total sinusoid area.

Immunofluorescence Analyses

Staining for acrolein was performed on deparaffinized liver sections from 20 wk-old WT, *Ercc1*$^{-/\Delta}$ mice and aged (24-36 mth-old) WT mice. Paraffin embedded tissue sections were subjected to heat induced-epitope retrieval by incubation in sodium citrate buffer (10mM, pH 6.0) for 10 min in a microwave, followed by 30 min cool-down. Sections were permeabilized with PBS-Tween (0.05%) and incubated with rabbit polyclonal to acrolein (1:500, ab37110, Abcam, Cambridge, MA), CD31 (1:500, 550274, BD Pharmingen, San Diego, CA), F4/80 (1:500, 552958, BD Pharmingen, San Diego, CA), α-SMA (1:500, #6198, Sigma, St. Louis, MO), and Desmin (1:250, ab15200, Abcam, Cambridge, MA) overnight at 4°C. The secondary antibody, Alexa Fluor 594 goat anti-rabbit IgG (1:1000, A11012, Molecular Probes, Eugene, OR), was allowed to incubate for 60 min in the dark. Nuclei were stained with Vectashield with DAPI mounting medium (Vector Laboratories, Inc., Burlingame, CA). Ten random images per sample were acquired using an Olympus BX51 fluorescent microscope. Acrolein fluorescence intensity was quantified using the Axio Vision imaging software (Carl Zeiss, Gottingen, Germany). Average fluorescence intensity is shown ± S.E.M. All p-values reported were derived using a standard Student's *t* test with a two-tailed distribution. Differences were considered significant at the 95% confidence interval ($p < 0.05$).

Immunohistochemical analyses

Immunohistochemistry for Ki67 (rat anti-mouse Ki67 (TEC-3), Dako Cytomation, Carpinteria, CA) was performed on deparaffinized liver sections from 10 wk-old WT and *Ercc1*$^{-/\Delta}$ mice that had undergone partial hepatectomy surgery. Endogenous peroxidase activity was blocked with

3% hydrogen peroxide. Tissue sections were subjected to heat induced-epitope retrieval by incubation in sodium citrate buffer (10mM, pH 6.0) for 30 min in a decloaker, followed by 30 min cool-down. Blocking was done with 5% rabbit serum for 20 min. Primary antibody was applied for 1 hour. Secondary antibody was applied for 30 minutes, followed by the label antibody (ABC Elite, Vector Laboratories, Burlingame, CA) for 30 min. DAB chromagen (Dako Cytomation, Carpinteria, CA) was applied for 6 min, followed by 2 rinse steps in distilled water. Hematoxylin was used as a counterstain. Brightfield images were collected using an Olympus BX51 fluorescent microscope, and Ki67 positive cells were quantified from 5 random fields of view from each of 4 mice per group. Mean percentages were plotted ± S.E.M.; asterisk indicates $p<0.05$ as calculated with the Student's *t* test with a two-tailed distribution.

Detection of Lipids

Slides with frozen liver tissue were warmed to room temperature, fixed in 2% PFA for 10 min, rinsed with PBS, and incubated with LipidTox Red Neutral Lipid Stain (Invitrogen, Foster City, CA) for 30 min at room temperature. Tissues were rinsed in PBS and nuclei were counterstained with Hoechst dye for 1 min. Hoechst dye was rinsed off with 3 PBS washes and tissue was covered using gelvatol mounting medium. Image acquisition was done on an Olympus BX51 fluorescent microscope.

Detection of Lipofuscin

Intracellular lipofuscin was observed by fluorescence microscopy. 6μM liver cryosections were fixed in 4% PFA for 10 min, rinsed with PBS and the nuclei stained with Vectashield and DAPI mounting medium (Vector Laboratories, Inc., Burlingame, CA). Green autofluorescent granules were detected at an excitation wavelength of 488 nm. Five random images per mouse (n=5 animals per age group) were acquired using an Olympus BX51 fluorescent microscope. For

quantification, the lipofuscin fluorescence intensity was analyzed using the AxioVision imaging software (Carl Zeiss, Gottingen, Germany). All data shown are mean ± S.E.M. P-values were calculated using a standard Student's *t* test with a two-tailed distribution.

Lipid peroxidation measurement

Lipid hydroperoxides were measured in fresh tissue homogenates using the Hydroperoxide Assay kit (#705003, Cayman Chemicals, Ann Arbor, MI) according to the manufacturer's instructions. Liver specimens were sonicated on ice in 1 ml of HPLC-grade water and used immediately after collection.

Partial Hepatectomy

One-third partial hepatectomy (PHx) was performed as previously described[161]. Mice were anesthetized using ketamine/xylazine, and a midline incision was made so that the median lobe of the liver could be excised. A knot was tied above the excised lobe, and double-layered sutures were used to close the wound. Mice were warmed and monitored hourly for 12 hours post-PHx. Mice were sacrificed 48 hours post-PHx, and tissues were preserved in 2% PFA and frozen in 2-methylbutane for immunohistochemistry.

Liver Function Analyses

Blood was collected by heart puncture from 6 animals per group and placed in plasma separator tubes coated with lithium heparin (BD Microtainer, Franklin Lakes, NJ). The samples were separated following the manufacturer's instructions. The plasma was sent to Antech Diagnostics (Pittsburgh, PA) for measurement of liver function tests (AST, ALT, Cholesterol, and Albumin). The average values were plotted ± S.E.M.; significance was calculated using the Student's two tailed *t*-test; *p* values less than 0.05 were considered significant.

SA-β-Galactosidase Assay

SA-β-galactosidase (SA-β-gal) staining was performed as previously described [16] on 6μM frozen liver sections from 20 week-old WT, 20 week-old *Ercc1*$^{-/\Delta}$, and 26 month-old WT. Sections were fixed with 2% PFA and 0.25% glutaraldehyde for 5 min at room temperature, washed 3 times with PBS, and incubated overnight at 37°C, 20% CO_2 in the SA-β gal staining solution.

Immunoblotting

Flash frozen liver tissue was weighed and sonicated in NETT buffer (100mM NaCl, 50mM Tris pH 7.5, 5mM EDTA pH 8.0, 0.5% Triton-X) with Protease Inhibitor Cocktail Set III (Calbiochem, Gibbstown, NJ). For immunodetection of p16 and laminin, 50μg of total protein from each liver sample was boiled in 4X loading buffer [0.25mol/L Tris-HCl (pH 8.5), 8% SDS, 1.6mmol/L EDTA, 0.1mol/L DTT, 0.04% bromophenol blue, 40% glycerol] and separated by SDS-PAGE on a 4-20% Mini-PROTEAN gradient gel (Bio-Rad, Hercules, CA), and transferred to nitrocellulose membrane. Rabbit anti-p16 (clone M-156, Santa Cruz Biotechnology, Santa Cruz, CA), rabbit anti-laminin (1:2500, a gift from Simon Watkins) and rabbit anti-tubulin (1:1000, ab4074, Abcam, Cambridge, MA), followed by an AP-conjugated anti-rabbit IgG secondary antibody (1:1000, S-373, Promega, Madison, WI). Blots were developed in the presence of Western Blue® Stabilized Substrate for Alkaline Phosphatase (Promega, Madison, WI) and imaged using the Alpha Innotech Red (Santa Clara, CA) gel imaging system. Densitometry was calculated using the spot density software on the Alpha Innotech Red gel imaging system.

Quantitation of nuclear size

Frozen liver sections were fixed with 2% paraformaldehyde and coverslips attached with VectaShield mounting medium with DAPI (H-1500, Vector Labs, Burlingame, CA). Ten

random images per sample (n=3 mice per group) were acquired using an Olympus BX51 fluorescent microscope. Nuclear size was measured using MetaMorph imaging software to set an inclusive threshold to select for hepatocyte nuclei. Greater than five hundred nuclei were analyzed for each experimental group. Average nuclear size is shown ± S.E.M. p-values were derived using a standard Student's *t* test with a two-tailed distribution.

Microarray hybridizations

Standard procedures were used to obtain total RNA (Qiagen, Valencia, CA) from the liver of 5- and 16-week old *Ercc1*$^{-/\Delta}$ mice and WT littermate controls (6 mice per group). Synthesis of double-strand cDNA and biotin-labeled cRNA was performed using the GeneChip Expression 3'-Amplification IVT Labeling kit according to the manufacturer's instructions (Affymetrix, Santa Clara, CA). Fragmented cRNA preparations were hybridized to full mouse genome oligonucleotide arrays (Affymetrix, mouse 430 V2.0 arrays), using Affymetrix hybridization Oven 640, washed, and subsequently scanned on a GeneChip Scanner 3000 (Affymetrix, Santa Clara, CA). Initial data extraction and normalization within each array was performed by means of the GCOS software (Affymetrix, Santa Clara, CA). Expression intensities were log transformed and normalized within and between arrays with the quantile normalization method using the R open statistical package (http://www.r-project.org/).

Microarray data analysis

Two-tail, pair-wise analysis or a two-way analysis of variance was used to extract the statistically significant data from each group of mice by means of the Spotfire Decision Site software package 7.2 v10.0 (Spotfire Inc., Somerville, MA). The criteria for significance were set at $p \leq 0.05$ and a $\geq \pm 1.2$-fold change in gene expression. We used the bivariate correlation procedure to compute Spearman's rho coefficient, a non-parametric measure of correlation that

assesses how well an arbitrary monotonic function describes the relationship between two variables without making any assumptions about the frequency distribution of the variables by means of the statistical package SPSS 12.0.1. By scoring for qualitative rather than quantitative similarities, this approach disregards variations in the magnitude of gene expression that might originate from, for example, differences in genetic background, sex or animal housing conditions.

Quantitative Real Time PCR Evaluation

Total RNA was isolated from the liver of 5 and 16-week old Ercc1$^{-/\Delta}$ and WT mice, and 130 week-old WT mice using a Total RNA isolation kit (Qiagen, Valencia, CA) as described by the manufacturer. Quantitative PCR (Q-PCR) was performed with a DNA Engine Opticon device according to the instructions of the manufacturer (MJ Research). Primer pair designed to generate intron-spanning products of 180-210bp are available upon request. The generation of specific PCR products was confirmed by melting curve analysis and gel electrophoresis (using Roche Agarose MS for analyzing small PCR products). Each primer pair was tested with a logarithmic dilution of a cDNA mix to generate a linear standard curve (crossing point (CP) plotted versus log of template concentration), which was used to calculate the primer pair efficiency ($E = 10^{(-1/slope)}$). Hypoxanthine guanine phosphoribosyltransferase1 (*Hprt-1*) mRNA was used as an external standard. For data analysis, the second derivative maximum method was applied: ($E_{1\text{gene of interest}}$ $^{\Delta CP\ (cDNA\ of\ wt\ mice\ -\ cDNA\ of\ Ercc1\text{-}/\Delta)\ gene\ of\ interest}$)/ ($E_{hprt\text{-}1}$ $^{\Delta CP\ (cDNA\ wt\ mice\text{-}\ cDNA\ of\ Ercc1\text{-}/\Delta)\ hprt\text{-}1}$).

2.3 RESULTS

2.3.1 Histopathological changes in *Ercc1*$^{-/\Delta}$ liver mimic normal aging

To investigate structural changes in the liver of progeroid *Ercc1*$^{-/\Delta}$ mice we compared liver tissue of 20-24 week-old *Ercc1*$^{-/\Delta}$ mice to wild-type (WT) littermates and to 26-34 month old WT mice. The relative liver/body weight of *Ercc1*$^{-/\Delta}$ mice was not significantly different from littermate controls at any age[158]. The architecture of the *Ercc1*$^{-/\Delta}$ liver was irregular, with mild to moderate variation in lobular size (Figure 1A). Pathologic changes detected in both *Ercc1*$^{-/\Delta}$ mice and old WT mice include multifocal degeneration, necrosis and neutrophilic inflammation, a diffuse increase in sinusoidal lining cells, and karyomegaly, with intranuclear inclusions (Figure 1 and 2). None of these changes were detected in young adult (20-24 week-old) WT mice. The only abnormalities detected in juvenile (7 wk-old) *Ercc1*$^{-/\Delta}$ mice were mild anisokaryosis and intranuclear inclusions. Liver from aged WT mice, like humans, displays mild portal fibrosis (Figure 1B) and increased neutral lipid accumulation (Figure 1C). Similar changes were detected in 20-24 wk-old *Ercc1*$^{-/\Delta}$ mice, but not age-matched WT mice or 7 wk-old *Ercc1*$^{-/\Delta}$ mice. This demonstrates that the *Ercc1*$^{-/\Delta}$ mice undergo progressive degenerative processes, rather than having developmental liver abnormalities.

Stellate cells are pericytes that reside between hepatocytes and endothelial cells lining the sinusoids in the extracellular space of Disse. Stellate cells store fat and when activated produce extracellular matrix proteins, contributing to fibrosis. With aging in humans, stellate cell number, but not activity is reported to increase[162]. Stellate cells also increase in number in 3 year-old WT mice and progeroid *Ercc1*$^{-/\Delta}$ mice, as measured by desmin and α-smooth muscle actin (SMA) staining, markers of stellate cells and their activation, respectively (Figure 1D). Kupffer

cells, resident liver macrophages, are also reported to increase in number and phagocytic activity with aging in humans [163]. However, we did not detect increased F4/80 immunostaining, a macrophage marker, in liver sections of old WT or progeroid mice (Figure 3).

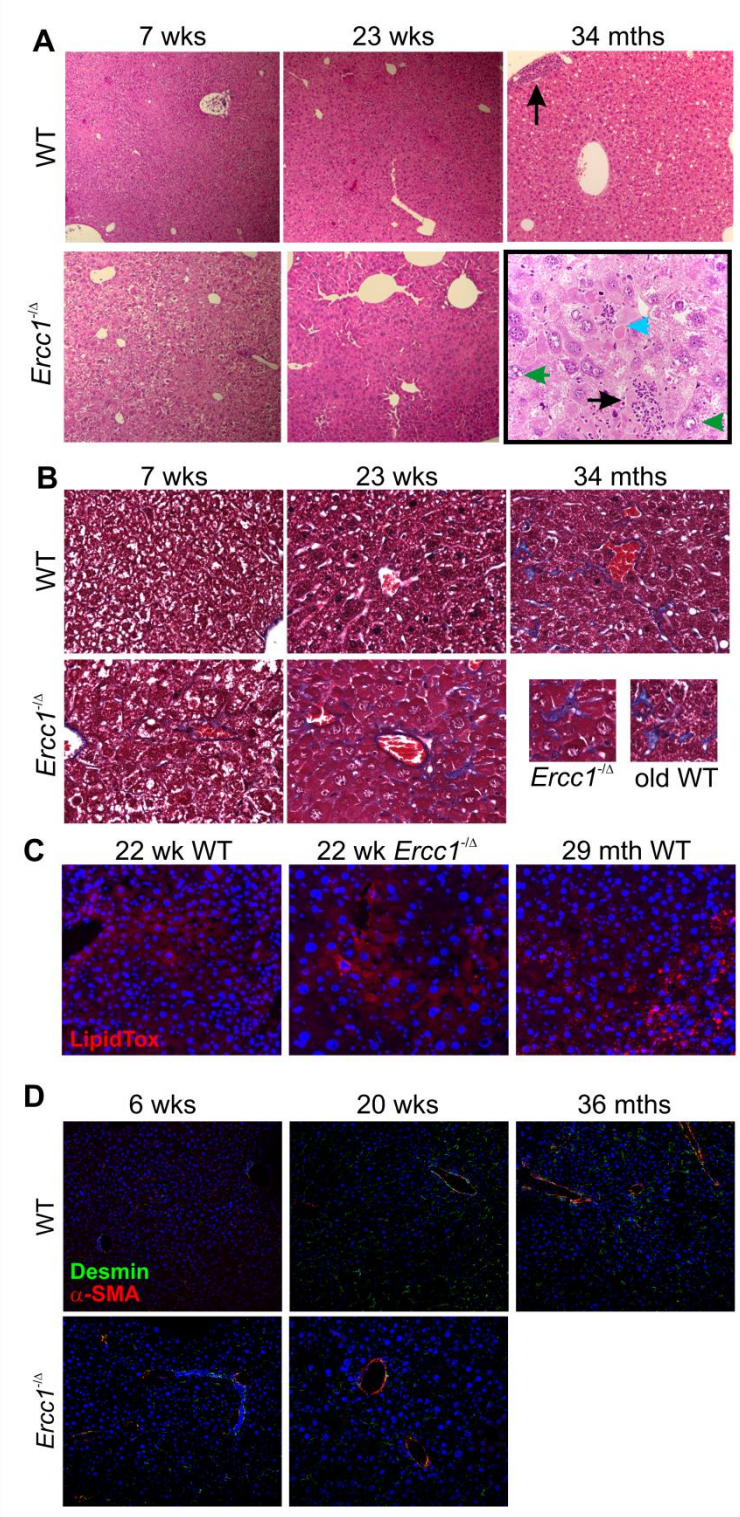

Figure 1. Premature onset of age-related liver pathology in *Ercc1*$^{-/\Delta}$ mice

(A) Hematoxylin and eosin (H&E) stained liver sections from 7 wk, 23 wk, and 34 mth-old WT mice, and *Ercc1*$^{-/\Delta}$ littermates (10X). The bottom right panel is a high magnification (40X) image of *Ercc1*$^{-/\Delta}$ liver (23 wk) illustrating

inflammatory infiltrate (black arrows), abnormal nuclei with inclusion (green arrows) and dead hepatocytes (blue arrows). (B) Masson's trichrome stained liver sections. Insets (40X) in the bottom right panel show perisinusoidal fibrosis in *Ercc1*$^{-/\Delta}$ and old WT liver samples. (C) LipidTOX™ stain of liver sections to detect neutral lipids (20X). (D) Immunofluorescence detection of desmin and α-SMA, markers of hepatic stellate cells and their activation, respectively, in frozen liver sections (20X).

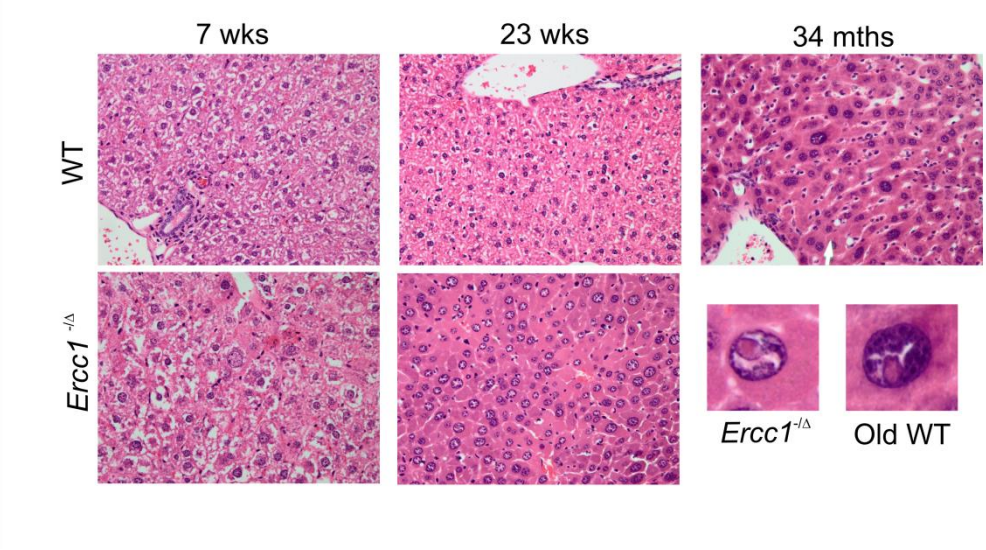

Figure 2. Age-related structural changes in *Ercc1*$^{-/\Delta}$ mouse liver

Hematoxylin and eosin (H&E) stained liver sections from 7 wk, 23 wk, and 34 mth-old WT mice, and *Ercc1*$^{-/\Delta}$ littermates (40X). The bottom right panel illustrates abnormal nuclei seen in 23 wk-old *Ercc1*$^{-/\Delta}$ and old WT mice.

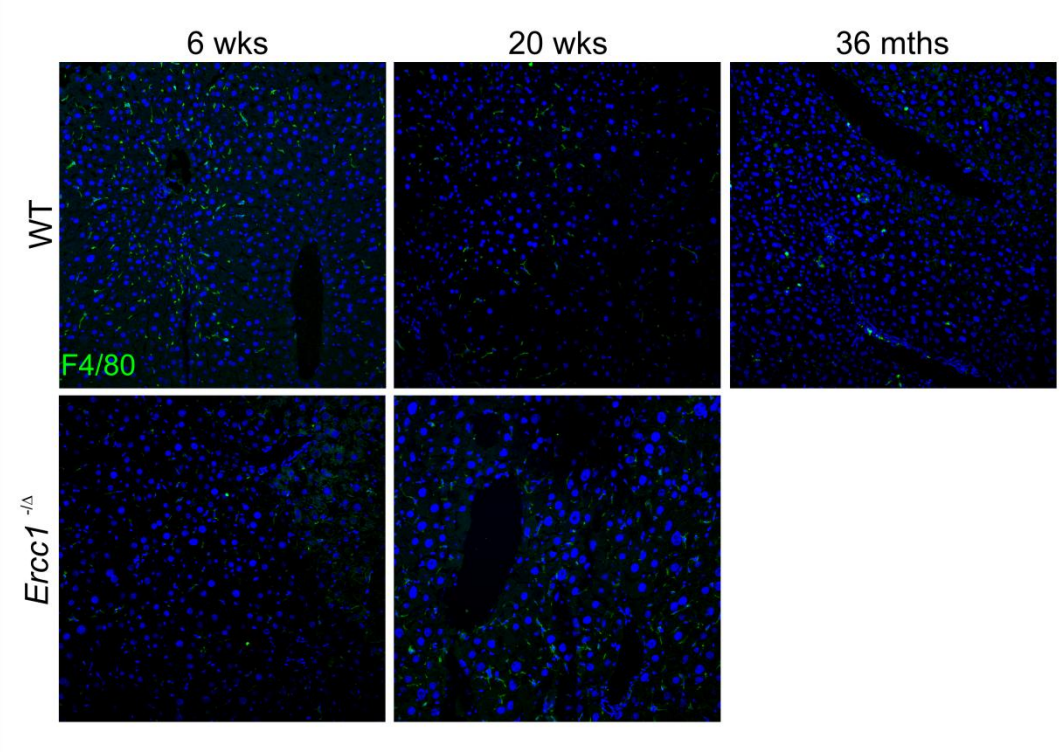

Figure 3. Kupffer cells do not increase in number in *Ercc1*$^{-/\Delta}$ liver

Immunofluorescence detection of F4/80, a marker of Kupffer cells in frozen liver sections (20X).

2.3.2 Ultrastructural changes in progeroid *Ercc1*$^{-/\Delta}$ mouse liver

Age-associated endothelial changes in the liver are prominent and contribute to age-related decline in liver function[164]. Expression of CD31, a marker of endothelium, was dramatically increased in 5 month-old *Ercc1*$^{-/\Delta}$ mice and 2.5 year-old WT mice compared to young adult WT mice (Figure 4A), indicative of pseudocapillarization. Pseudocapillarization encompasses many alterations including thickening of the sinusoidal endothelial cells (LSECs) and increased deposition of basement membrane proteins in the space of Disse[149, 165]. Transmission electron microscopy of liver from old and progeroid mice revealed a thickening of

the basement membrane (Figure 4B). This was confirmed by immunblot detection of the basement membrane protein laminin, which revealed a dramatically increased level of laminin in old WT and 20 week-old *Ercc1*$^{-/\Delta}$ mouse liver compared to young adult WT mice (Figure 4C).

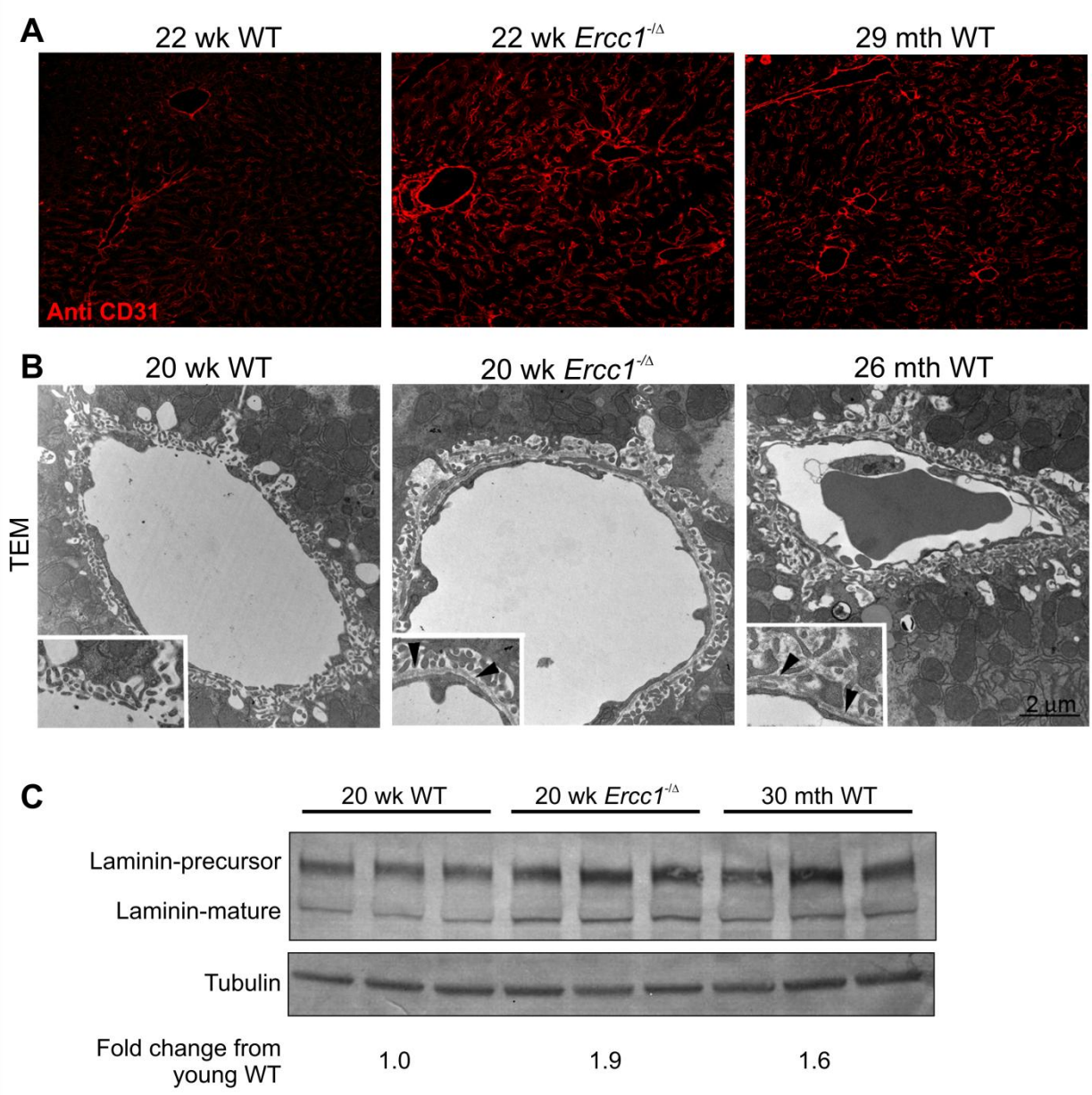

Figure 4. Age-related thickening of the sinusoidal endothelium in *Ercc1*$^{-/\Delta}$ mouse liver

(A) Immunofluorescence detection of CD31, a surface marker of endothelial cells in frozen liver sections (20X). (B) Transmission electron micrographs (TEM; 12,000X) of liver illustrating thickening of the basement membrane

in sinusoids of mutant and old WT mice compared to young WT. Insets show enlargement of a portion of the original image and arrows indicate deposition of basement membrane and pseudocapillarization of the sinusoidal endothelium. (C) Immunoblot to detect the extracellular matrix protein laminin in liver lysates from 20 wk-old *Ercc1*$^{-/\Delta}$ mice, control littermates and old WT (2-3 year) mice (n=3 per group). Densitometry was used for quantification and averages are listed as a ratio compared to 20 week-old WT mice.

With advanced age LSECs also lose their fenestrations, necessary for lipoprotein filtration, endocytosis, and immunological functions[164]. Scanning electron microscopy of murine liver sections revealed a significant reduction in fenestration of the sinusoids in old (26-30 month-old) WT mice compared to young (20 week-old) WT animals (Figure 5A). Micrographs from 20 week-old *Ercc1*$^{-/\Delta}$ mice looked more similar to those from the old WT mice than to their WT littermates, with significantly reduced fenestrations, decreased porosity, and loss of sieve plates (Figure 5A-5B).

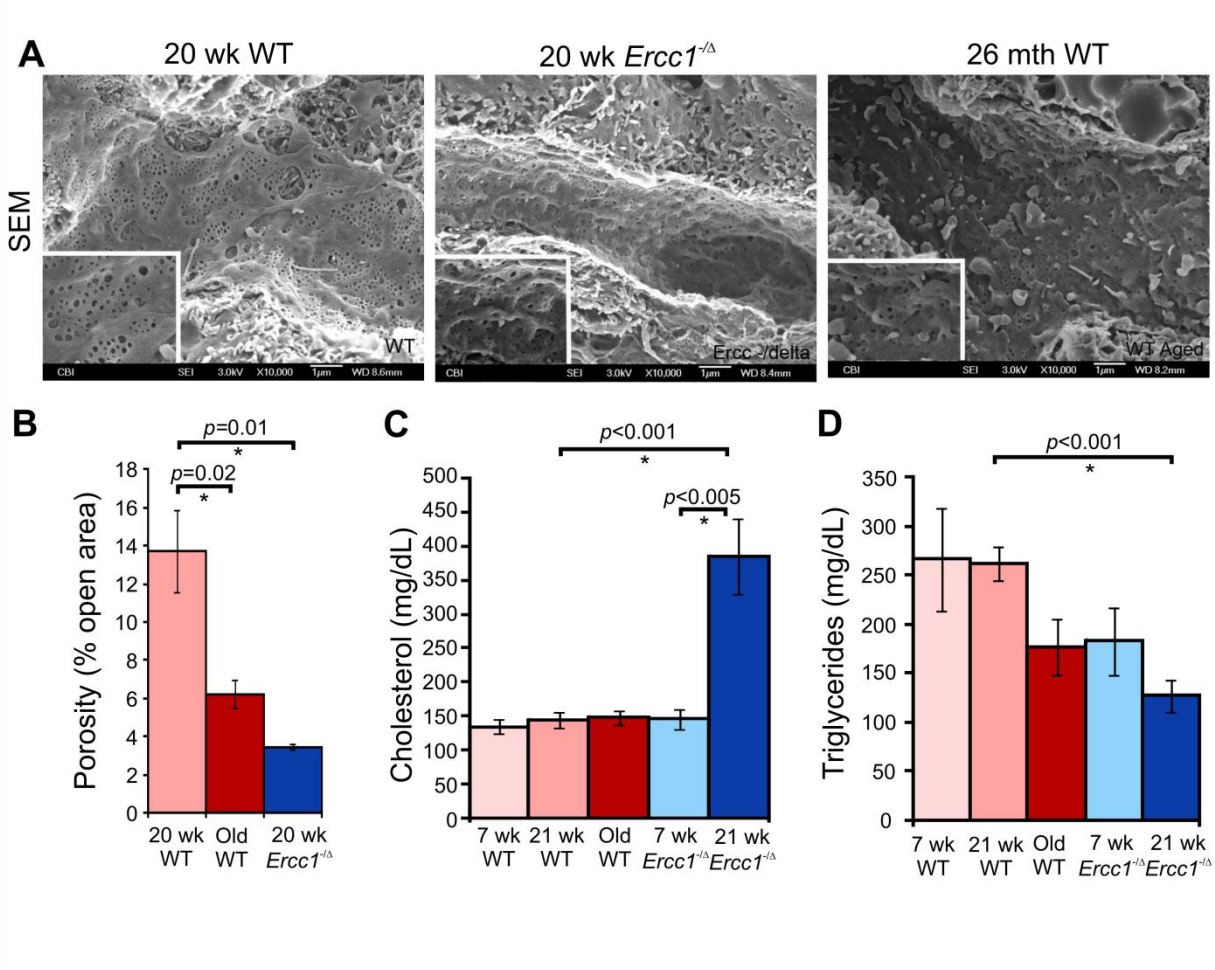

Figure 5. Premature defenestration in *Ercc1*$^{-/\Delta}$ mouse liver

(A) Scanning electron micrograph (10,000X) of liver, illustrating defenestration in sinusoids of mutant and old WT mice. Insets show enlargement of a portion of the original image. (B) Quantification of porosity shown in A. 3 SEM images per mouse (n=3 mice per group) were quantified, and the % open area of the sinusoid is represented ± S.E.M. Asterisks indicate significant differences. (C) Serum cholesterol and (D) triglyceride levels in WT and *Ercc1*$^{-/\Delta}$ mice of various ages. The average ± S.E.M. are plotted (n=6 for 7 wk-old mice, n=9 for 21 wk-old and old WT mice). Asterisks indicate significant differences as calculated by a paired Student's t test.

Age-related LSEC defenestration can lead to impaired hepatic clearance of atherogenic lipoproteins, contributing to hypertriglyceridemia, hypercholesteremia and vascular disease[166, 167]. Therefore we measured serum cholesterol levels in the mice. Cholesterol levels were normal in young (7 wk-old) *Ercc1*$^{-/\Delta}$ mice (Figure 5C). By 21 weeks of age, when defenestration

was apparent, serum cholesterol was significantly elevated in *Ercc1*$^{-/\Delta}$ mice compared to WT littermates. In contrast, serum triglycerides were significantly lower in 21 week-old compared to littermate controls (Figure 5D). Serum lipoproteins were not significantly altered in old WT mice compared to young WT mice.

2.3.3 Functional changes in *Ercc1*$^{-/\Delta}$ mouse liver

Under normal conditions hepatocytes are quiescent cells, but can be stimulated to proliferate in response to parenchymal damage[168]. In an experimental setting, proliferation is induced by partial hepatectomy (PHx), which leads to compensatory hyperplasia. Hepatocyte proliferation in response to PHx is significantly decreased in aged rodents compared to young animals[145]. Thirty-percent of the liver was surgically resected from 10 wk-old WT and *Ercc1*$^{-/\Delta}$ mice. *Ercc1*$^{-/\Delta}$ mice did not survive a standard PHx, which removes 70% of the liver. Thus the surgery was modified to only remove 1 lobe, or 30% of the liver. At 48 hours post-resection, the mice were euthanized and liver tissue collected for analysis. Previous experiments in which WT mice were euthanized every 12 hours post-partial hepatectomy, from 12-72 hours, indicated that 48 hours was the time point at which proliferation was the highest in 10 week-old WT mice (data not shown). Immunohistochemical staining for the proliferation-associated antigen Ki67 revealed a significant decrease in the number of proliferating cells in the liver from *Ercc1*$^{-/\Delta}$ mice compared to WT littermates (Figure 6A). Therefore regenerative capacity of the liver is prematurely reduced in *Ercc1*$^{-/\Delta}$ mice.

To further monitor liver function and integrity, liver function tests were performed on plasma of *Ercc1*$^{-/\Delta}$ and WT mice at multiple ages (Figure 6B). ALT was significantly elevated in

old WT mice compared to young, as previously reported[169]. ALT was also significantly elevated in *Ercc1*$^{-/\Delta}$ mice compared to age-matched WT mice, even at 7 wks of age. ALT levels more than doubled as the *Ercc1*$^{-/\Delta}$ mice aged. AST was also significantly elevated in old WT and 21 wk-old *Ercc1*$^{-/\Delta}$ mice compared to young adult WT mice. Serum albumin is known to decrease with age in humans and rodents[170, 171]. Albumin was significantly reduced in the plasma of 21 wk-old, but not 7 wk-old *Ercc1*$^{-/\Delta}$ mice (Figure 6B). Thus, a very similar pattern of time-dependent changes in liver function tests, indicative of chronic, progressive tissue degeneration and loss of organ function, are observed in *Ercc1*$^{-/\Delta}$ and WT mice. However, the changes are dramatically accelerated in the *Ercc1*$^{-/\Delta}$ mice.

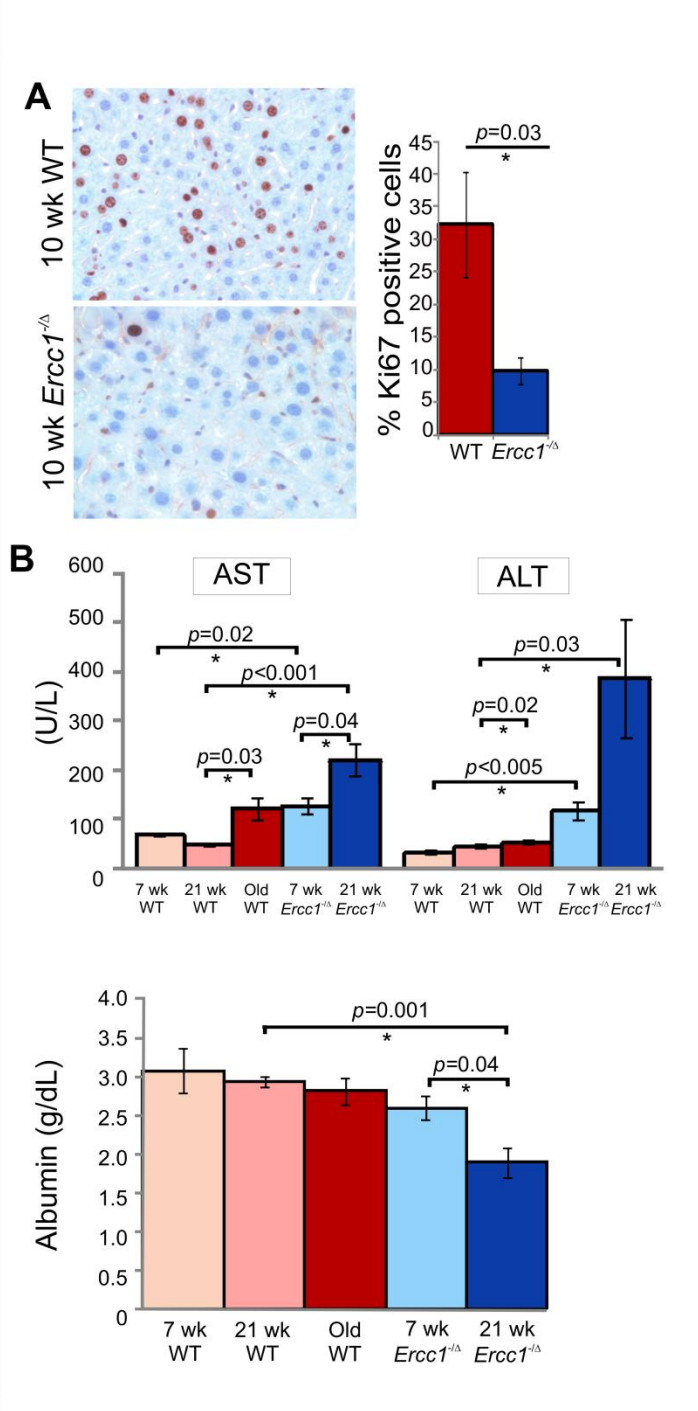

Figure 6. Premature loss of liver function in *Ercc1*$^{-/\Delta}$ mice

(A) Representative liver sections from 10 week-old WT and *Ercc1*$^{-/\Delta}$ mice immunostained for the proliferation marker Ki67 48 hr post-partial hepatectomy. The fraction of proliferating hepatocytes is graphed (5 random fields of view analyzed from n=4 mice per genotype; asterisk indicates p<0.05, Student's two tailed t-test). (B) Serum chemistries reflecting liver function. Plotted are the average ± S.E.M. for 6 mice per age and genotype. WT animals

are graphed in reds; *Ercc1*$^{-/\Delta}$ mice in blues. Darker colors indicate increasing age. AST is aspartate transminase; ALT is alanine transaminase. Asterisks indicate significant differences.

2.3.4 Increased cellular senescence in *Ercc1*$^{-/\Delta}$ and old WT liver

To further investigate the mechanism driving the loss of regenerative capacity in *Ercc1*$^{-/\Delta}$ and old WT mice, we asked if hepatocytes were undergoing cellular senescence. Liver sections were stained to detect senescence-associated β-galactosidase (SA-β gal) activity, a marker of cellular senescence (Figure 7A). SA-β Gal staining was increased in liver of 20 week-old *Ercc1*$^{-/\Delta}$ and old WT mice compared to 20 week-old WT mice. p16^{INK4a} is another established marker of senescent cells[172]. p16^{INK4a} expression was increased 1.4- and 2.0-fold in 20 wk-old *Ercc1*$^{-/\Delta}$ and 2 yr-old WT mice, respectively, compared to young WT mice (Figure 7B). Increased cell size, nuclear size, and the nuclear:cytoplasmic ratio are also associated with cell senescence and old age[173-175]. The nuclear size of hepatocytes was heterogeneous in *Ercc1*$^{-/\Delta}$ and old WT mice compared to 7 and 23 wk-old WT mice (Figure 7C). Hepatocyte nuclei of *Ercc1*$^{-/\Delta}$ mice were significantly larger than that of WT littermates at 7 wks of age, and increased by 21 wks of age (Figure 7C). Nuclear size was also significantly increased in old WT mice compared to young WT mice. Electron micrographs revealed a highly irregular surface area of the hepatocyte nuclei from *Ercc1*$^{-/\Delta}$ and old, but not young, WT mice (Figure 7D).

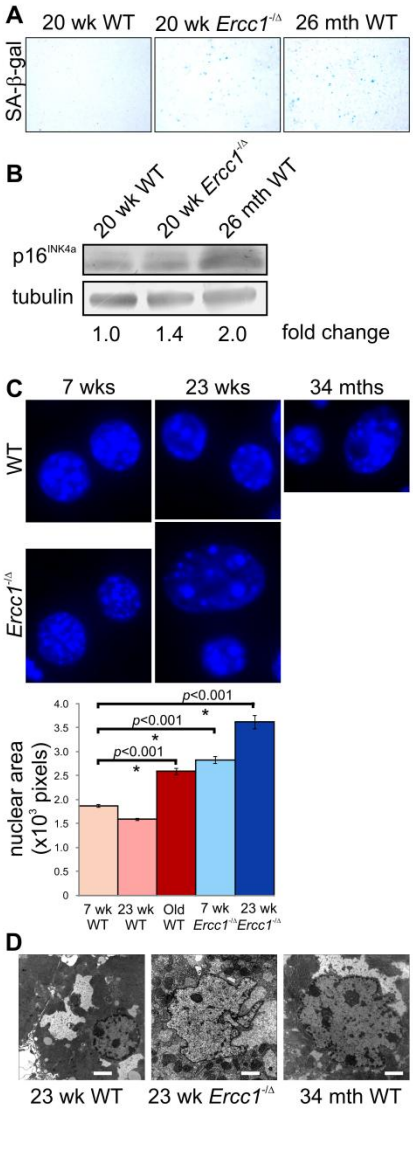

Figure 7. Premature senescence of *Ercc1*$^{-/\Delta}$ mouse liver

(A) Senescence-associated (SA) β-galactosidase histochemical stain on flash frozen liver sections. (B) Immunoblot detection of the senescence marker p16^{INK4a} in liver lysates of a 20 week-old WT mouse and an *Ercc1*$^{-/\Delta}$ littermate, and a 26 month-old WT mouse. Tubulin was used as a loading control to calculate the fold-increase in p16 expression relative to adult WT mice. (C) DAPI staining of hepatocyte nuclei illustrating increased nuclear size and heterogeneity in old WT (34 months) and adult *Ercc1*$^{-/\square}$ mouse liver (1000X). Quantification of nuclear size using Metamorph imaging software and images of DAPI-stained frozen liver sections. Plotted are the average nuclear areas ± S.E.M. calculated from 10 random fields from 5 mice per group. The asterisks indicate significant differences. (D) Transmission electron micrographs of representative hepatocyte nuclei (12,000X).

2.3.5 Increased oxidative damage in *Ercc1*$^{-/\Delta}$ liver

Oxidative stress has been implicated in driving age-dependent cellular senescence[176]. To determine if oxidative stress is elevated in *Ercc1*$^{-/\Delta}$ mice and with old age, we measured lipid peroxidation in liver. The level of lipid hydroperoxides, measured by ELISA, was elevated in the liver of 20 wk-old *Ercc1*$^{-/\Delta}$ mice compared to WT littermates (Figure 8A). A similar elevation was seen in old WT mouse liver compared to young WT. This increase in lipid peroxidation was confirmed by immunodetection of acrolein, a stable product of lipid peroxidation. *Ercc1*$^{-/\Delta}$ and old WT mice had significantly increased acrolein compared to adult WT mice (Figure 8B).

One of the most common markers of aged liver is the cytoplasmic accumulation of lipofuscin, which is highly oxidized lipid material[147]. Lipofuscin granules, which fluoresce at 488nm, were 30-fold elevated in liver of 20 week-old *Ercc1*$^{-/\Delta}$ mice compared to WT littermates (Figure 8C). A similar increase in lipofuscin was observed in old WT mouse liver compared to young WT mice.

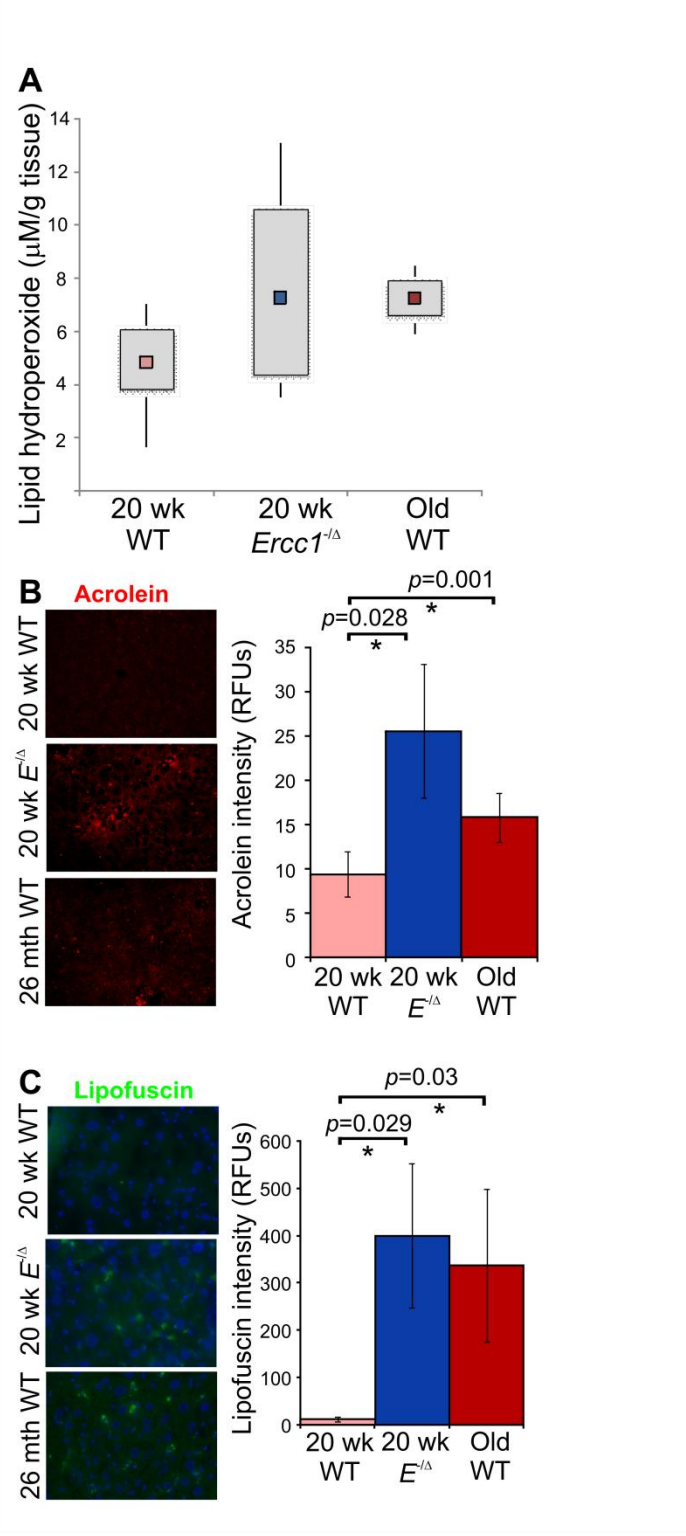

Figure 8. Increased oxidative damage in liver of old and progeroid mice

(A) Immunodetection of lipid hydroperoxides, a by-product of lipid peroxidation, in liver lysates from 20 wk-old WT and *Ercc1*$^{-/\Delta}$ littermate mice vs. old WT mice (26-34 months of age). The box plot represents the mean (in

colored square), along with the 25th and 75th percentile for each group (n=5 mice). Average lipid hydroperoxide levels for groups were as follows: 20 wk WT (4.8μM/g liver), 20 wk *Ercc1*$^{-/\Delta}$ (7.3μM/g liver; p=0.12, one-tailed Student's t-test), and old WT (7.2μM/g liver). (B) Immunofluorescence detection of acrolein, a by-product of lipid peroxidation. The staining intensity was quantified using AxioVision imaging software. Plotted are the averages ± S.E.M. determined from analysis of 10 random fields of liver sections from 2 mice per group. Asterisks indicate significant differences. (C) Representative images illustrating lipofuscin accumulation in 20 week-old WT and *Ercc1*$^{-/\Delta}$ mice and 26-34 month-old WT mouse liver. AxioVision software was used for quantification of 10 random fields measured from 5 mice per group. Plotted is the average fluorescence intensity for each group ± S.E.M. Asterisks indicate significant differences.

2.3.6 Age-related transcriptional changes in *Ercc1*$^{-/\Delta}$ mouse liver

Gene expression changes were measured by microarray in liver of *Ercc1*$^{-/\Delta}$ mice and WT littermates at 5 and 16 weeks of age. Genes that were significantly up or downregulated compared to WT littermates are shown (Figure 9A). There is a progressive downregulation of genes associated with the IGF-1/GH axis and oxidative phosphorylation in *Ercc1*$^{-/\Delta}$ mice as they age compared to WT littermates. Additionally, genes involved in DNA damage, oxidative stress response, cell cycle arrest, and apoptosis were significantly upregulated in 16 week-old *Ercc1*$^{-/\Delta}$ mice compared to WT littermates. qPCR was used to confirm the microarray results (Figure 9B).

The transcriptional changes observed in 16 week-old *Ercc1*$^{-/\Delta}$ mouse liver are comparable to old WT (130 week) mice (Figure 9C). Spearman's r correlation indicates that as *Ercc1*$^{-/\Delta}$ progeroid mice age from 5 weeks to 16 weeks, their gene expression profiles have increasing similarity to old WT mice.

A

Suppression of oxidative metabolism					
code	Gene	5-wks FC	p	16-wks FC	p
1426059_at	Gckr	1.32	0.1353	-1.26	0.0066
1416090_at	Pdhb	-1.03	0.6851	-1.37	0.0001
1419146_a_at	Gck	-1.41	0.2856	-5.41	0.0000
1422577_at	Cs	-1.19	0.0171	-1.38	0.0006
1452206_at	Sucla2	-1.05	0.4352	-1.21	0.0004
1421258_a_at	Pklr	-1.32	0.3211	-2.03	0.0001
1443186_at	Pkm2	-1.52	0.2389	-2.87	0.0282
1455235_x_at	Ldh2	-16.70	0.3382	1.46	0.0328
1419737_a_at	Ldh1	1.12	0.0796	1.20	0.0056
Cell cycle arrest					
1424638_at	Cdkn1a	4.54	0.000	20.43	0.000
1440040_at	Cdk6	-1.13	0.718	1.96	0.019
1416868_at	Cdkn2c	1.25	0.082	1.79	0.000
1422439_a_at	Cdk4	1.28	0.046	1.66	0.001
1455287_at	Cdk6	1.16	0.239	1.54	0.001
1417649_at	Cdkn1c	-1.10	0.793	1.47	0.032
1449229_a_at	Cdkl2	1.05	0.743	1.27	0.007
1451741_a_at	Cdk7	1.44	0.025	1.27	0.013
1423067_at	Cdk5rap3	1.20	0.072	1.20	0.012
Response to DNA damage					
1421430_at	Rad51l1	2.23	0.041	2.43	0.013
1448497_at	Xpb	1.25	0.049	2.31	0.000
1449483_at	Polk	1.42	0.025	2.10	0.001
1417904_at	Dclre1a	2.31	0.001	2.02	0.000
1448520_at	Dclre1b	1.67	0.010	2.00	0.039
1424629_at	Brca1	1.26	0.204	1.98	0.000
1421731_a_at	Fen1	1.61	0.026	1.78	0.002
1443891_at	Rad51l3	-1.10	0.389	1.66	0.008
1416641_at	Lig1	1.60	0.008	1.57	0.001
1417572_at	Mpg	1.03	0.873	1.48	0.041
1417800_at	Parp2	1.57	0.011	1.37	0.027
1416602_a_at	Rad52	1.09	0.467	1.35	0.018
1433999_at	Slk	1.03	0.786	1.28	0.028
1460725_at	Xpa	1.03	0.863	1.28	0.022
1422624_at	Rev1l	-1.02	0.877	1.28	0.041
1416748_a_at	Mre11a	1.04	0.557	1.21	0.042
1437447_s_at	Ercc1	-4.47	0.000	-7.72	0.000

Upregulation of apoptosis					
code	Gene	5-wks FC	p	16-wks FC	p
1450971_at	Gadd45b	-1.80	0.198	3.17	0.012
1419004_s_at	Bcl2a1a	1.47	0.069	3.12	0.025
1437527_x_at	Mcl1	1.38	0.202	2.49	0.000
1449297_at	Casp12	-1.10	0.589	1.99	0.001
1416837_at	Bax	1.32	0.009	1.68	0.000
1415995_at	Casp6	1.42	0.001	1.36	0.017
1449491_at	Card10	-1.27	0.626	1.35	0.005
1450731_s_at	Tnfrsf21	-9.97	0.335	1.34	0.016
1416582_a_at	Bad	-1.08	0.571	1.27	0.047
Suppression of the GH/IGF1 axis and growth stimuli					
1418918_at	Igfbp1	2.36	0.125	4.05	0.008
1434413_at	Igf1	1.18	0.405	-1.22	0.024
1422826_at	Igfals	-1.11	0.657	-1.55	0.002
1452114_s_at	Igfbp5	-5.88	0.314	-1.79	0.017
1417962_s_at	Ghr	-1.28	0.001	-2.02	0.000
1417991_at	Dio1	-1.65	0.062	-14.51	0.000
1444166_at	Thrsp	-1.69	0.179	-1.75	0.007
1460420_a_at	Egfr	-1.31	0.320	-1.87	0.045
1451803_a_at	Vegfb	-2.15	0.079	-1.89	0.000
1419675_at	Ngfb	-1.22	0.107	-1.93	0.004
1450869_at	Fgf1	-1.52	0.001	-2.17	0.000
1438946_at	Pdgfra	-1.14	0.665	-2.19	0.003
Response to (oxidative) stress and detoxification					
1451695_a_at	Gpx4	1.05	0.762	1.55	0.000
1452135_at	Gpx6	-2.49	0.399	4.04	0.000
1456036_x_at	Gsto1	1.48	0.016	1.55	0.007
1416411_at	Gstm2	1.31	0.052	1.80	0.037
1416842_at	Gstm5	-1.58	0.400	1.56	0.001
1417883_at	Gstt2	1.52	0.046	1.31	0.005
1441931_x_at	Gss	-1.37	0.626	2.32	0.000
1428630_x_at	Haghl	1.31	0.379	1.70	0.000
1452592_at	Mgst2	1.66	0.318	3.86	0.045
1448300_at	Mgst3	-1.41	0.490	1.74	0.017
1437014_x_at	Prdx1	1.36	0.038	1.33	0.034
1450748_at	Smpd3	1.01	0.961	4.76	0.001
1416926_at	Trp53inp1	1.20	0.510	1.61	0.001
1416399_a_at	Hmox2	-1.09	0.308	1.23	0.001

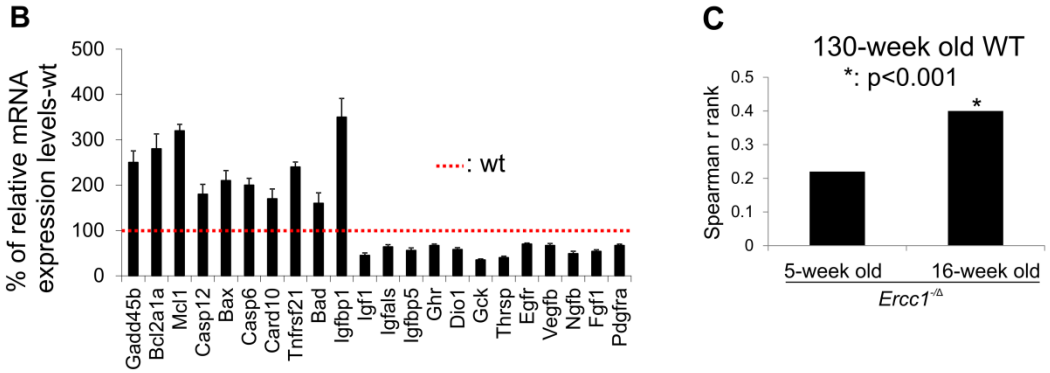

Figure 9. Age-associated transcriptional reprogramming in liver of *Ercc1*$^{-/\Delta}$ mice

(A) Significant gene expression changes (p<0.05, two tailed t-test) in the liver of 5- and 16-week old *Ercc1*$^{-/\Delta}$ mutant livers as compared to littermate control animals. Note the progressive dampening in the expression of genes involved in oxidative metabolism and the GH/IGF1 axis along with the upregulation in the expression of genes involved in cell cycle arrest, DNA damage responses, oxidative stress and detoxification (red color: up-regulated; green color: down-regulated, FC: fold change, wks: weeks). (B) qPCR measuremtn of mRNA levels of a subset of

genes identified to be differentially expressed in the liver of 16-week old *Ercc1*$^{-/\Delta}$ animals compared to wild-type littermates. For each gene, expression levels in the mutant tissue are plotted relative to those of controls (red dotted line). Error bars indicate S.E.M. between replicates ($n \geq 4$). (C) Spearman's r correlation reflecting transcriptome similarities between the 5 or 16 week-old *Ercc1*$^{-/\Delta}$ and the 130 week-old mouse livers where -1.0 is a perfect negative (inverse) correlation, 0.0 is no correlation, and 1.0 is a perfect positive correlation.

2.4 DISCUSSION

The human liver undergoes numerous characteristic structural and functional changes with increasing age[149]. Structural changes include loss of organ volume, nuclear polyploidy, anisokaryosis, and pseuodcapillarization[149, 169, 177]. These changes lead to impaired liver function and loss of regenerative capacity. Not surprisingly, transplanted livers from late-age donors have decreased graft acceptance and function[178, 179]. However, the underlying cause for these changes remains unknown.

Non-human primates have been used to study liver aging, but the commonly used species *Macaca mulatta* and *Macaca nemestrina* can live more than 20 years[180, 181]. Mice are shorter-lived and importantly age-related changes characteristic of aged human liver are recapitulated in mice, including pseudocapillarization, increased polyploidy, decreased hepatocyte number, and increased nuclear size[154-156, 182]. Thus, mice represent an accurate model system for studying age-associated liver changes in humans. However, the 3 year lifespan of mice still represents a substantial barrier to rapid testing of hypotheses about the causes and treatments of liver aging.

Herein we establish that the structural, functional and regulatory changes that occur in the liver of WT mice in their third year of life are recapitulated in the *Ercc1*$^{-/\Delta}$ progeroid mouse strain within their 7-month lifespan. There is a highly significant correlation between the

genome-wide expression profile of 4 month-old *Ercc1*$^{-/\Delta}$ mice and 32 month-old WT mice (Figure 7). Both have elevated LFTs and reduced regenerative capacity, as well as focal necrosis, inflammation, anisokaryosis, and steatosis (Figures 1 and 4). Markers of cellular senescence (SA-βgal and p16) are elevated in livers of progeroid and old mice (Figure 5). This is supported by the strong upregulation of genes associated with cell cycle arrest (Figure 7) and the observation that livers of *Ercc1*$^{-/\Delta}$ mice, like that of old WT mice[183-185] have reduced regenerative capacity following partial hepatectomy (Figure 4). Collectively, these data support the conclusion that age-related decrease of liver function is due to dysfunction of hepatocytes rather than their attrition. Interestingly, there is accumulation of oxidation products (lipofuscin and lipid peroxidation) in the livers of progeroid and old mice (Figure 6), suggesting that oxidative damage may drive hepatocyte dysfunction.

Defenestration and pseudocapillarization, which were significantly elevated in livers of *Ercc1*$^{-/\Delta}$ and old WT mice (Figures 2 and 3), contribute to reduced regenerative capacity[185]. Defenestration is also implicated in dyslipidemia due to impaired clearance of lipoproteins from the blood to hepatocytes[166]. Serum cholesterol was significantly elevated in progeroid *Ercc1*$^{-/\Delta}$ mice compared to littermate controls (Figure 3). In contrast, serum triglycerides were significantly lower in mutant animals compared to WT mice. Despite the fact that the extent of defenestration was similar in progeroid and old WT mice, serum lipid levels were within normal range in the naturally aged mice. Hence the dyslipidemia in the *Ercc1*$^{-/\Delta}$ mice may reflect metabolic changes in the mice rather than a loss of liver transport mechanisms. Indeed, metabolic profiling of the *Ercc1*$^{-/\Delta}$ mice revealed increased serum HDL but decreased LDL and VLDL and increased urinary ketone bodies[125]. These changes mimic caloric restriction [186] and occur as a consequence genetic reprogramming rather than diminished nutrient intake in the *Ercc1*$^{-/\Delta}$

mice (Figure 7 and[113, 125]). The growth hormone/insulin-like growth factor-1 axis is also attenuated in *Ercc1*$^{-/\Delta}$ mice and old WT mice (Figure 7 and[29, 113]). The decrease in IGF-1 may contribute to impaired liver regeneration[187].

Ercc1$^{-/\Delta}$ mice age rapidly as a consequence of an engineered mutation in the gene that encodes one subunit of the DNA repair endonuclease ERCC1-XPF [43], which is required for multiple DNA repair pathways [22, 48]. XFE progeroid syndrome, which the ERCC1-deficient mice model, is characterized by accelerated aging of the hematopoietic, hepatobiliary, endocrine, musculoskeletal and neurological systems[29, 109]. Werner syndrome, caused by mutations in *WRN*, which encodes a DNA repair helicase and exonuclease, is characterized by early onset cancer, cardiovascular disease and osteoporosis[188]. Both *Ercc1*$^{-/\Delta}$ and *Wrn*$^{\Delta hel/\Delta hel}$ mice display early onset of dyslipidemia, steatosis, pseudocapillarization and defenestration in the liver[189]. This demonstrates that DNA repair is critical for protecting against loss of liver homeostasis and function. Importantly, levels of 8-oxo-deoxyguanine, an endogenous oxidative DNA lesion, are greater in old WT mice than young[190-192], consistent with the hypothesis that unrepaired DNA damage may contribute to liver aging even in repair-proficient organisms.

The mice in this study were not exposed to environmental genotoxins. Thus the degenerative changes observed are attributed to the accumulation of oxidative damage arising as a consequence of normal metabolism. The fact that the onset of degenerative changes are accelerated in DNA repair-deficient *Ercc1*$^{-/\Delta}$ mice compared to WT reveals that specifically endogenous DNA damage can drive liver degeneration, likely through driving hepatocyte senescence[193]. In humans, environmental exposures as well as endogenously produced genotoxic by-products undoubtedly contribute to the accumulating burden of DNA damage and thereby age-related liver dysfunction.

It is important to note that many of the age-related endpoints measured were more severely affected in *Ercc1*$^{-/\Delta}$ mice than in WT mice near the end of their respective lifespans. This includes LFTs, fibrosis, steatosis, pseudocapillarization, and anisokaryosis. A unifying explanation for why the liver of 4-5 month-old Ercc1$^{-/\Delta}$ mice looks worse than 2-3 year-old WT mice is that the *Ercc1*$^{-/\Delta}$ mice undergo activation of stress response pathways, similar to that induced by caloric restriction, which are protective, as the result of accumulated, unrepaired DNA damage. (Figure 7 and [29, 113]). Thus the *Ercc1*$^{-/\Delta}$ mice survive longer than expected given their burden of damage and therefore have extreme aging, comparable to that of supercentenarians[158]. Nevertheless, *Ercc1*$^{-/\Delta}$ mice develop the majority of structural and funtional characteristics of old human[149] and mouse liver within a matter of five months, rather than years. The vast majority of these changes occur in adulthood (after 7 weeks of age), making the changes distinct from developmental abnormalities and degenerative in nature. *Ercc1*$^{-/\Delta}$ mice therefore represent an accurate model system for rapidly testing hypotheses about the mechanism underlying age-related liver degeneration and pharmacological interventions aimed at delaying or ameliorating age-associated liver disease

3.0 ENDOGENOUS DNA DAMAGE DRIVES CELLULAR SENESCENCE

Senescence is a cell fate decision in response to DNA damage, chronic oncogenic signaling or short telomeres. Cellular senescence is thought to contribute to aging and the concomitant loss of tissue homeostasis. However, experimental evidence linking senescence and aging, and elucidating the causes of senescence *in vivo* are lacking. Human fibroblasts undergo senescence if challenged with super-physiological doses of genotoxic stress that also damages other cellular macromolecules. We employed a genetic approach to specifically ask if spontaneous nuclear DNA damage promotes cellular senescence. *Ercc1*$^{-/-}$ mouse embryonic fibroblasts (MEFs) are deficient in nucleotide excision repair, interstrand crosslink repair and end-joining of some double-strand breaks. *Ercc1*$^{-/-}$ primary MEFs grown at 20% oxygen exhibited rapid cellular senescence compared to congenic wild-type cells. This was rescued only partially at 3% oxygen and also occurred in ERCC1-deficient mouse tissues. Remarkably, *Ercc1*$^{-/-}$ cells exhibited significant mitochondrial elongation and dysfunction, likely promoting further DNA damage. Our data provides evidence that physiological levels of endogenous DNA damage promote cellular senescence.

3.1 INTRODUCTION

The 21st century has brought a global demographic shift, such that the number of individuals over the age of 60 is increasing rapidly in both developed and non-developed nations. In 1950, there were approximately 205 million persons over the age of 60 worldwide. However, by 2050 that number is predicted to reach 2 billion[1]. Advanced age is the greatest risk factor for numerous chronic degenerative diseases, including cardiovascular disease, arthritis, cataracts, glaucoma, osteoporosis, type 2 diabetes, and neurodegenerative disorders such as Alzheimer's disease and Parkinson's disease. Eighty percent of individuals over the age of 65 have at least one chronic disease and greater than 50% have two or more[194]. In the United States alone, the direct medical costs associated with these chronic diseases is estimated to be $582 billion annually[195]. In order to improve the quality of life for the elderly, and to minimize the economic burden from the medical care of the aged population, it is critical to identify the molecular mechanisms that underlie aging.

Aging is a multifactorial process characterized by the loss of tissue function and the decreased ability to maintain homeostasis. This leads to an impaired ability to respond to stress and a dramatically increased risk of morbidity and mortality[12]. At the cellular level, time-dependent accumulation of damage to macromolecules and organelles is thought to contribute to age-related dysfunction. Currently there is no consensus about the type(s) of damage that are most important in driving aging. Types of damage that have been implicated include damage to proteins, DNA and mitochondria[196-198].

There is a large body of evidence supporting the hypothesis that DNA damage plays a causative role in aging. Mice with inherited defects in DNA repair mechanisms necessary to remove damage from the genome develop accelerated aging syndromes, suggesting that DNA

damage when not repaired can drive aging[13]. This phenomenon is not limited to mice, as humans with inherited mutations in DNA repair genes can also exhibit accelerated aging, or progeroid syndromes[14]. In addition, DNA damage induces cellular senescence, which is thought to contribute to aging.

Senescent cells exhibit a large, flattened morphology, irreversible growth arrest, increased senescence-associated beta-galactosidase (SA-β-gal) activity, increased expression of $p16^{INK4a}$, and persistent nuclear foci containing DNA damage response (DDR) proteins[16, 199-203]. Senescent cells are more frequently found in the tissues of aged humans, primates, and rodents compared to young organisms, and are localized at sites of age-related pathologies, suggesting that senescent cells may contribute to age-associated functional decline[16-19, 204]. However, a direct causal relationship between cellular senescence and aging has yet to be established.

DNA damage activates ATM and ATR, two essential protein kinases involved in the DDR. Subsequently, ATM and ATR phosphorylate and activate downstream kinases, CHK1 and CHK2. These signaling events lead to the phosphorylation of p53 on serine 15, and upregulation of p21 and $p16^{INK4a}$, leading to the onset of cellular senescence[15, 157, 201, 205]. DNA is subject to damage from environmental factors such as plant toxins, benzopyrenes, ultraviolet and ionizing radiation. In addition, nucleoside bases can undergo spontaneous hydrolysis, resulting in apyrimidinic sites, and single-strand breaks[206]. Reactive free radicals, such as hydroxyl radical ($^{\bullet}OH$) produced during aerobic metabolism, can result in damage to the bases and phosphodiester backbone of DNA[207-209]. Cellular senescence is a consequence of genotoxic stress, and studies aiming to elucidate the mechanism(s) of how DNA damage causes cellular senescence have administered ionizing radiation (10-20Gy), doxorubicin (12-800nM),

aphidicolin (200ng/ml), etoposide (900nM), and cisplatin (2.2μM) to trigger senescence[203, 210, 211]. Thus, it is not clear if physiological levels of spontaneous (endogenous) DNA damage are sufficient to drive cellular senescence. Furthermore, all genotoxins, when administered to cells or animals, damage not only DNA but also all other cellular macromolecules including phospholipids, proteins and RNA [212, 213]. The aim of this study was to understand if there is a direct causal relationship between endogenous DNA damage and cellular senescence *in vitro* and *in vivo*.

In order to focus solely on the contribution of endogenous, nuclear DNA damage to senescence and aging, we took a genetic approach and utilized DNA repair-deficient *Ercc1*$^{-/-}$ primary mouse embryonic fibroblasts (MEFs). ERCC1 is one subunit of a structure-specific endonuclease involved in nucleotide excision repair, interstrand crosslink repair and the repair of a subset of DNA double-strand breaks [22, 45, 48]. Mutations that result in a severe reduction of ERCC1-XPF protein levels result in accelerated aging, in humans and mice[14, 29]. We have found that primary *Ercc1*$^{-/-}$ MEFs undergo premature cellular senescence if grown at 20% and 3% oxygen compared to congenic repair-proficient MEFs. In addition, senescent cells were abundant in the liver and spleen of ERCC1-deficient mice. Interestingly, mitochondrial dysfunction and high levels of reactive oxygen species accompanied cellular senescence in *Ercc1*$^{-/-}$ MEFs in response to endogenous DNA damage.

3.2 MATERIALS AND METHODS

Animal Care and Experimentation

All animal studies were conducted in compliance with the US Department of Health and Human Services Guide for the Care and Use of Laboratory Animals, and were approved by the University of Pittsburgh Institutional Animal Care and Use Committee. *Ercc1*$^{-/-}$ and *Ercc1*$^{-/\Delta}$ mice were bred and genotyped as previously described [22, 29].

Generation and culture of primary mouse embryonic fibroblasts (MEFs)

Ercc1$^{-/-}$ primary MEFs were developed from embryonic day 12 to 15 embryos derived from crossing inbred C57BL/6 mice heterozygous for each null allele, as previously described [22]. *Ercc1*$^{-/-}$*p53*$^{-/-}$ double-knockout primary MEFs were created from embryos derived from crossing double-heterozygous mice in an inbred C57BL/6 background. Genomic DNA was isolated from a tissue sample of each embryo with the NucleoSpin DNA extraction system (740741.24, Macherey-Nagel, Bethlehem, PA). Genotyping of the *Ercc1* allele was done by PCR co-amplification of the 3' end of exon 7 from the wild-type allele and the neomycin resistance marker cloned into exon 7 of the targeted allele with primers specific for exon 7, neo, and intron 7 (5'-AGCCGACCTCCTTATGGAAA, 5'-TCGCCTTCTTGACGAGTTCT, and 5'-ACAGATGCTGAGGGCAGACT, respectively). WT (0.25-kb) and mutant (0.4-kb) products were separated by electrophoresis on a 2% agarose gel.

Primary MEFs were cultured in a 1:1 mixture of Dulbecco's modified Eagle's medium and Ham's F10 with 10% fetal bovine serum and antibiotics and incubated at 3% or 20% oxygen. Cell lines simultaneously derived from wild-type (WT) littermate embryos were used as controls in all experiments.

Cell Proliferation Measurement

Proliferation was assessed as previously described [22]. Briefly, WT and mutant MEFs were plated at a density of 0.25 x 10^6 per 6-cm dish. Cells were trypsinized at confluence, counted,

and replated at the same density until mutant cells stopped growing. The total number of cells at each passage was calculated as follows: (no. of cells at previous passage/no. of cells plated) x no. of cells at current passage. The total cell number was plotted as the log cell number.

Immunofluorescence

WT and *Ercc1*$^{-/-}$ MEFs were cultured on glass coverslips until they reached 50% confluence. Cells were fixed with 2% paraformaldehyde in PBS for 15 minutes. Cells were permeabilized with 0.1% Triton X-100 in PBS and the phosphorylated form of γ-H2AX detected with monoclonal anti-γ-H2AX (05-636, Millipore, Billerica, MA) and Alexa 594-conjugated goat anti-mouse IgG (A-11005, Invitrogen, Carlsbad, CA) in PBS with 0.15% glycine and 0.5% bovine serum albumin. γ-H2AX foci were counted with an Olympus BX51 fluorescent microscope.

Immunohistochemistry

Ki67 staining was performed on deparaffinized tissue sections from 20 wk-old WT and *Ercc1*$^{-/\Delta}$ mice. Endogenous peroxidase activity was blocked with 3% hydrogen peroxide for 15 minutes. Tissue sections were subjected to heat induced-epitope retrieval by incubation in sodium citrate buffer (10mM, pH 6.0) for 30 min in a decloaker, followed by 30 min cool-down. Blocking was performed using 5% normal rabbit serum for 20 min at room temperature. The primary antibody for Ki67 (rat anti-mouse Ki67 (TEC-3), M-7249, Dako Cytomation, Carpinteria, CA) was applied for 1 hour at a 1:50 dilution at room temperature. The secondary antibody was applied at a 1:300 dilution for 30 minutes, followed by the label antibody (ABC Elite, Vector Laboratories, Burlingame, CA) for 30 minutes. DAB chromagen (Dako Cytomation, Carpinteria, CA) was applied for 6 minutes, followed by 2 rinse steps in distilled water. Hematoxylin was used as a

counterstain, and slides were dehydrated, cleared and coverslipped. Brightfield images were collected using an Olympus BX51 fluorescent microscope

Senescence-associated (SA) β-Galactosidase

Frozen tissue sections and primary WT and *Ercc1*$^{-/-}$ MEFs were fixed in 0.25% gluteraldehyde and 2% paraformaldehyde for ten minutes at room temperature. Following three rinses in PBS, SA-β-Gal staining was performed as previously described [16, 214]

Apoptosis Measurement

WT and *Ercc1*$^{-/-}$ primary MEFs were stained for apoptosis markers FITC-Annexin V and propidium iodide (556547, BD Biosciences, San Diego, CA) according to manufacturer's instructions. Apoptotic cells were measured on the Cyan LX 9 color high speed flow cytometer (Beckman Coulter, Brea, CA) and quantified using Summit v.4.3 software.

Immunoblotting

Cells were trypsinized, pelleted, and the pellet was dissolved in ice-cold NETT buffer (100mM NaCl, 50mM Tris pH 7.5, 5mM EDTA pH 8.0, 0.5% Triton-X) with Mini-complete protease inhibitor tablet (11836153001, Roche Applied Science, Indianapolis, IN). 50μg of whole cell lysate was boiled in 4X loading buffer [0.25mol/L Tris-HCl (pH 8.5), 8% SDS, 1.6mmol/L EDTA, 0.1mol/L DTT, 0.04% bromophenol blue, 40% glycerol] and separated by SDS-PAGE on a 4-20% Mini-PROTEAN gradient gel (Bio-Rad, Hercules, CA), and transferred to nitrocellulose membrane. Primary antibodies against p16 (clone M-156, Santa Cruz Biotechnology, Santa Cruz, CA), p21 (ab7960, Abcam, Cambridge, MA), cleaved caspase-3 (9661S, Cell Signaling Technology, Danvers, MA), beta-actin (ab13822, Abcam, Cambridge, MA) and tubulin (ab4074, Abcam, Cambridge, MA) were used at a dilution of 1:500. This was followed by a 1:1000 dilution of either AP-conjugated anti-chicken IgG (ab6878, Abcam,

Cambridge, MA), AP-conjugated anti-rabbit IgG (S-373, Promega, Madison, WI), or HRP anti-rabbit IgG (656120, Invitrogen, Carlsbad, CA). Blots were developed and imaged using the Alpha Innotech Red gel imaging system. Densitometry was calculated using the spot density software on the Alpha Innotech Red gel imaging system.

Measurement of reactive oxygen species

H_2-DCFDA (C6827, Invitrogen, Carlsbad, CA) was used to measure general oxidative stress levels in primary WT and *Ercc1*$^{-/-}$ MEFs. 10mM H_2-DCFDA in DMSO was diluted in PBS to a final concentration of 10μM in PBS and added to cells in 10 cm dishes for 20 minutes at 37°C. Following incubation, cells were scraped, pelleted, and resuspended in 1 ml PBS. H_2-DCFDA fluorescence intensity was measured on the Cyan LX 9 color high speed flow cytometer (Beckman Coulter, Brea, CA) and quantified using Summit v.4.3 software.

To measure superoxide anion levels, WT and *Ercc1*$^{-/-}$ MEFs were grown in 10-cm dishes to 80-90% confluency and rinsed with PBS once. MitoSox reagent (M36008, Invitrogen, Carlsbad, CA) was diluted to a 2.5mM stock solution and applied to cells diluted 1:1000 in PBS for a 2.5μM working solution. Cells were incubated for 20 minutes at 37°C and scraped, pelleted and resuspended in 1 ml PBS. MitoSox fluorescence intensity was acquired on the Cyan LX 9 color high speed flow cytometer (Beckman Coulter, Brea, CA) and quantified using Summit v.4.3 software.

JC-1 measurement

Mitochondrial membrane potential was assessed using the cationic carbocyanine dye, JC-1 (T-3168, Invitrogen, Carlsbad, CA). Cells were grown on MatTek glass bottom culture dishes at 3 x 10^4 cells/ml. Cells were washed once in PBS and incubated for 30 minutes at 37°C in serum-free DMEM with 1.0μg/ml JC-1. Following wash with PBS, 20 random stage positions were

captured at a 40X magnificiation using a Nikon Eclipse Ti microscope equipped with a Photometrics CoolSnap HQ2 camera. n=150 cells were analyzed in 3 independent cell lines for WT and *Ercc1*$^{-/-}$ at 3% and 20% O_2 using Nikon Elements image analysis software.

Measuring ATP

Cellular ATP levels were measured using the ATPlite™ Luminescence Assay System (6016941, Perkin Elmer, Waltham, MA) following manufacturer's instructions. WT and *Ercc1*$^{-/-}$ MEFs were grown on 10-cm dishes in either complete MEF media (recipe above) or media with no glucose (replaced with galactose). The following day cells were trypsinized, counted, and 2.0 x 10^4 cells were plated in triplicate in 96-well plates. Cells were immediately lysed and ATP levels measured following manufacturer's instructions.

Electron microscopy

WT and *Ercc1*$^{-/-}$ MEFs were rinsed in PBS and fixed in 2.5% gluteraldehyde in PBS, pH 7.4, for 1 hour at room temperature. Following 3 10-min washes in PBS, cell monolayers are post-fixed in 1% OsO4 with 1% potassium ferricyanide. Monolayers are dehydrated in a graded series of alcohol (30%, 50%, 70%, 90% for 10 min and 100% 3 times for 15 min). Cells are immersed in Polybed812 3 times, each for 1 hour, and on the third rinse in epon beam capsules are inverted over the monolayers and allowed to polymerize at 37°C over night followed by 60°C for 48 hours. Beam capsules and underlying cells are removed from the dishes, sectioned, and imaged using the JEOL JEM 1011 microscope (JEOL Ltd, Peabody, MA).

3.3 RESULTS

3.3.1 DNA repair deficiency accelerates the onset of cellular senescence

To determine if spontaneous, endogenous DNA damage can drive cellular senescence, we measured multiple parameters associated with senescence in early passage WT and DNA repair deficient primary MEFs and followed these parameters with increasing passage number. By passage 6, proliferation of *Ercc1*$^{-/-}$ MEFs was substantially reduced compared to WT MEFs cultured at atmospheric (20% O_2) (Figure 10A). The difference in growth rates continued to increase with further passaging, until the *Ercc1*$^{-/-}$ cells ceased to proliferate further at passage 9. Growing *Ercc1*$^{-/-}$ MEFs at 3% O_2 (normoxia) partially rescued their growth defect (Figure 10A), but did not fully restore proliferation to WT levels. The growth of WT MEFs was also greater at 3% O_2 than 20%O_2, although only marginally.

To decipher if the reduced growth of *Ercc1*$^{-/-}$ MEFs was due to cellular senescence, three markers of senescence were measured: γ-H2AX foci, SA-β-galactosidase (SA-β-gal) activity, and $p16^{INK4a}$ expression. With increasing passage number, there was a significant increase in the fraction of cells with γ-H2AX foci (Figure 10B). Furthermore, if considering the same passage number, there was a significantly greater fraction of WT and *Ercc1*$^{-/-}$ MEFs with γ-H2AX foci in cultures grown at 20% O_2 than 3% O2. At 20% O_2, *Ercc1*$^{-/-}$ MEFs had significantly more γ-H2AX foci. These data support the conclusion that γ-H2AX foci, accumulate with time as a consequence of oxidative DNA damage.

SA-β-gal activity is another hallmark feature of senescent cells. Unlike γ-H2AX foci, a significant increase in SA-β-gal was not detected until passage 7 of WT MEFs and only at 20% O_2 (Figure 10C). Likewise, significantly increased SA-β-gal activity was detected in *Ercc1*$^{-/-}$ MEFs grown at 20% O_2, but not 3%.O_2. However, in the DNA repair deficient cells, there was already a significant increase in SA-β-gal activity at passage 3, and this increased significantly with further passaging. These data are consistent with the γ-H2AX data indicating that fraction of cells undergoing senescence increases over time in culture and that senescence is exacerbated by oxidative stress and failure to repair spontaneous DNA damage.

At passage 3, after only 10-12 days *ex vivo*, the expression of p16^{INK4a}, a third marker of cellular senescence, was approximately 2-fold higher in *Ercc1*$^{-/-}$ MEFs compared to WT MEFs, when cultured at 3% or 20% O_2 (Figure 10D). Taken together, these results demonstrate that DNA repair deficient *Ercc1*$^{-/-}$ primary MEFs undergo cellular senescence much more rapidly than congenic WT cells. Senescence is further accelerated by oxidative stress (20% O_2 relative to 3%O_2), supporting the conclusion that endogenous oxidative DNA damage can drive cellular senescence. Interestingly, SA-β-gal appears to be a less sensitive marker of cellular senescence than either γ-H2AX or p16^{INK4a}. γ-H2AX foci that appear in early passage cells may be caused by DNA damage. Alternatively, γ-H2AX foci or p16^{INK4a} expression that occurs in early passage cells may reflect transient and reversible events, whereas SA-β-gal activity is characteristic of irreversible senescence.

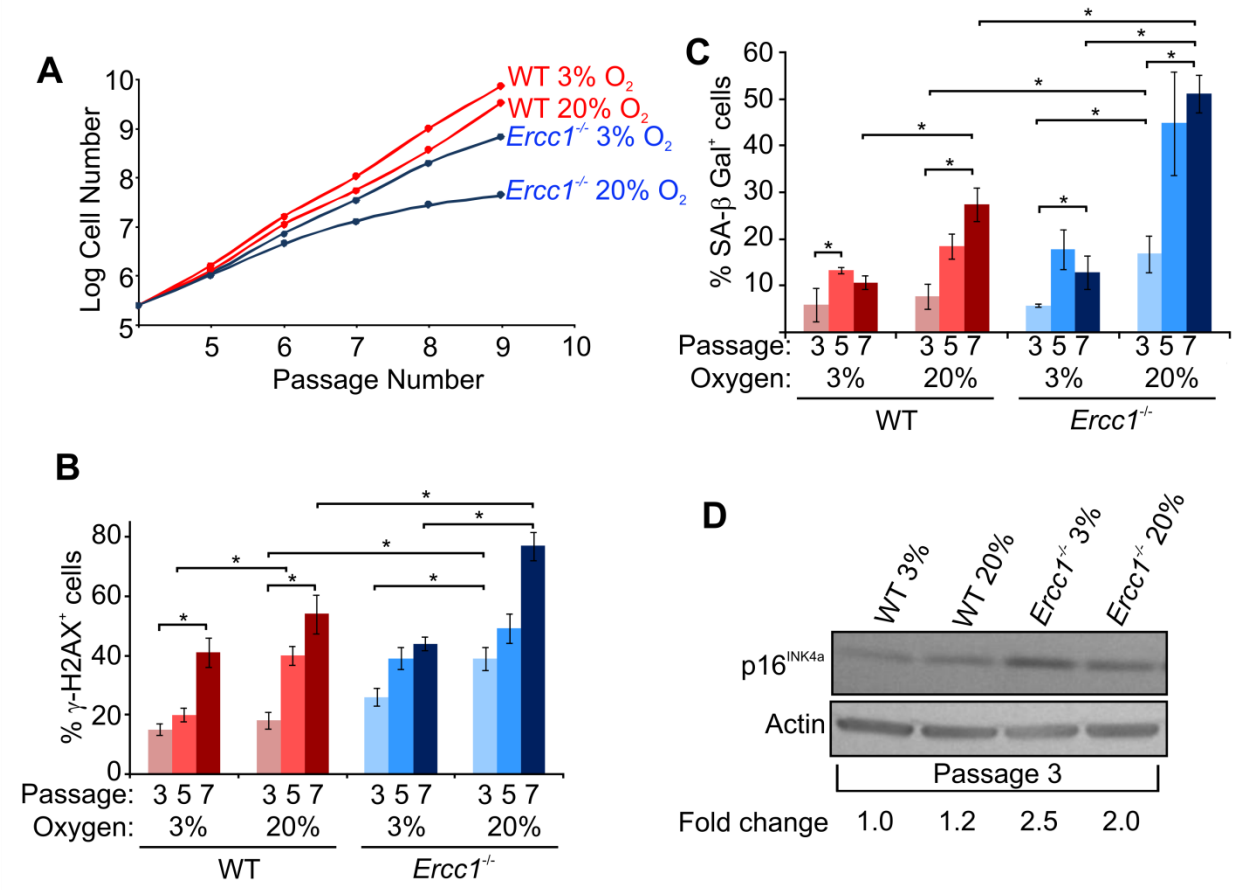

Figure 10. DNA repair deficiency promotes the onset of cellular senescence

(A) Cell proliferation was measured in congenic WT and *Ercc1*$^{-/-}$ primary MEFs from passage 4 through passage 9 in split cultures grown at 3% or 20% O2. Shown is the average of 4 experiments done on independent MEF cell lines. (B) Quantification of γ-H2AX foci in WT and *Ercc1*$^{-/-}$ MEFs at passages 3, 5 and 7 grown at 3% or 20% O_2. Cells were fixed and immunostained for phosphor-H2AX foci. Ten random fields were analyzed for each cell line and percent of c with foci determined. The average of 3 independent cell lines is plotted on the graph. Error bars represent ±S.E.M. Asterisk indicates significance using a two tailed Student's t-test where $p<0.05$. (C) Quantification of SA-β-Gal positive cells in WT and Ercc1-/- MEF cultures at passage 3, 5 and 7 at 3% or 20% O2. Cells were fixed and stained with X-gal. Ten random fields of view were analyzed for each cell line and the percent of 100-300 cells staining positively for SA-β-Gal determined. The average of 3 independent cell lines is plotted on the graph. Error bars represent the S.E.M. Asterisk indicates significance using a two tailed Student's t-test where $p<0.05$. (D) Immunoblot detection of the senescence marker $p16^{INK4a}$ in passage 3 WT and *Ercc1*$^{-/-}$ MEFs cultured at 3% or 20% O_2. β-actin was used as a loading control to calculate the fold-increase in p16 expression relative to WT cells cultured at 3% O2.

3.3.2 *Ercc1*$^{-/-}$ MEFs undergo p53-dependent senescence and not apoptosis

Cellular senescence as a consequence of genotoxic stress occurs through a p53-dependent mechanism a majority of the time[215]. Thus, as further evidence that spontaneous DNA damage was driving cellular senescence in *Ercc1*$^{-/-}$ MEFs, we asked if senescence in these cells is p53-dependent. Indeed, genetic deletion of p53 in an *Ercc1* knockout background completely rescued their proliferation defect (Figure 11A). Interestingly, the growth of *Ercc1*$^{-/-}$*p53*$^{-/-}$ primary MEFs was significantly greater than WT MEFs, suggesting that even the proliferation of repair-proficient cells is limited by oxidative stress.

In response to genotoxic stress, p53 activates the downstream effector p21 resulting in cell cycle withdrawal[216]. p21 expression is >3-fold increased in early passage WT cells grown at 20% O_2 compared to growth at 3% O_2 (Figure 11B). Similarly, there was a 4-fold induction of p21 expression in *Ercc1*$^{-/-}$ MEFs compared to congenic WT cells at passage 3 grown at 3% O_2 and an approximately 2-fold increase at 20% O_2. These results further support the conclusion that endogenous oxidative DNA damage drives cellular senescence in *Ercc1*$^{-/-}$ MEFs, and this process may also occur in DNA repair-proficient WT cells.

To rule out the possibility that proliferation of *Ercc1*$^{-/-}$ cells was also limited by apoptosis, we measured markers of early and late apoptosis. Flow cytometric detection of Annexin-V, a marker of early apoptosis, revealed no significant increase in the number of apoptotic cells in WT cultures with increasing passage number of increased oxidative stress (Figure 11C). Nor was there a significant increase in the DNA repair-deficient *Ercc1*$^{-/-}$ MEFs compared to WT cells. Interestingly, passage 7 *Ercc1*$^{-/-}$ MEFs at 3% O_2 exhibited higher levels of apoptotic Annexin-V/PI+ cells than *Ercc1*$^{-/-}$ MEFs at 20% O_2. As confirmation, we measured expression of cleaved caspase-3, a marker of late apoptosis, in WT and *Ercc1*$^{-/-}$ MEFs at passage

3 and 7 (Figure 11D). There was a modest increase in cleaved caspase-3 in *Ercc1*$^{-/-}$ MEFs at 3% O_2 at passage 7 relative to 20% O_2 and WT cells. But there was significant increase in this marker of apoptosis *Ercc1*$^{-/-}$ MEFs compared to WT cells, with increased oxygen tension, or increased passage number. We conclude that oxidative DNA damage is not driving apoptosis in primary MEFs.

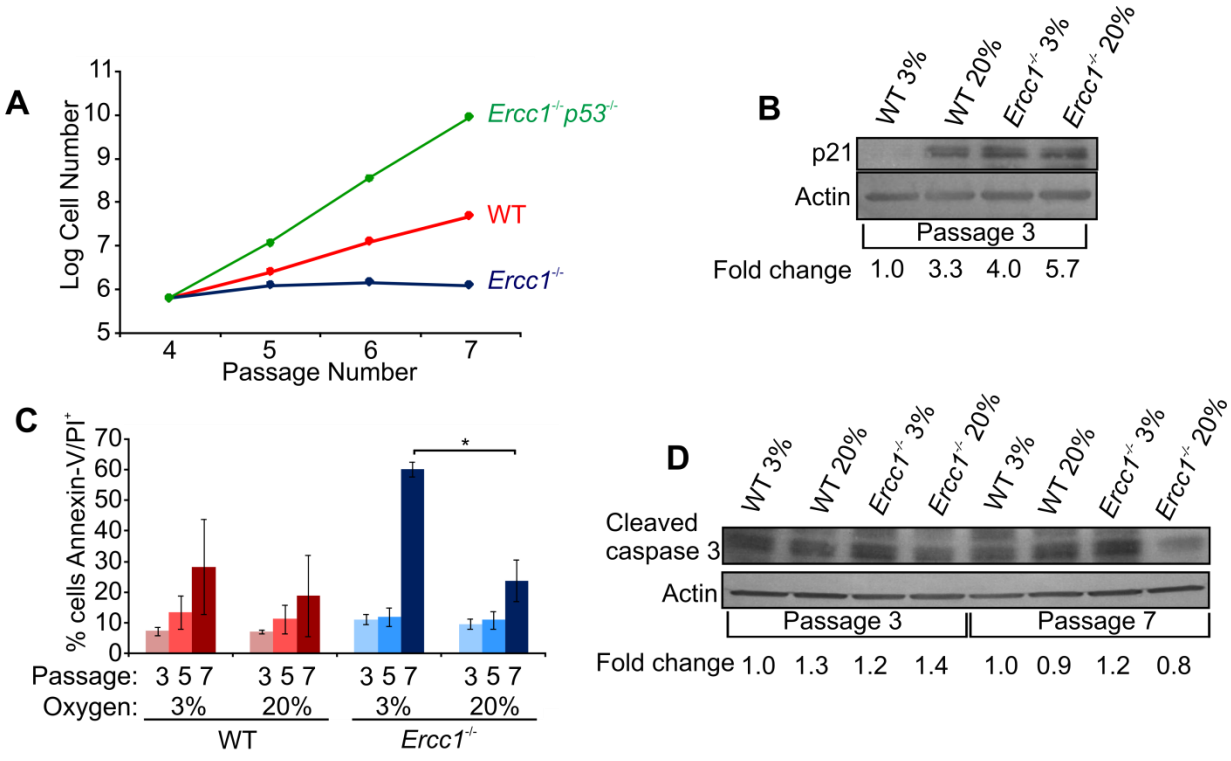

Figure 11. Cell loss in *Ercc1*$^{-/-}$ MEF is due to p53-dependent senescence and not apoptosis

(A) Growth of primary, congenic *Ercc1*$^{-/-}$*p53*$^{-/-}$, *Ercc1*$^{-/-}$, and WT primary MEFs from passage 4 through 7 at 20% O_2. The graph represents the average of three independent cell lines of each genotype. (B) Immunoblot detection of p21, a downstream effector of p53, in whole cell lysates of passage 3 WT and Ercc1-/- primary MEFs cultured at 3% or 20% O_2. β-actin was used as a loading control to calculate the fold-increase in p21 expression relative to WT cells cultured at 3% O_2. (C) Apoptosis was measured by staining *Ercc1*$^{-/-}$ and WT MEFs for Annexin-V and propidium iodide (PI) and analyzing by flow cytometry. The graph represents the percent of cells that were positive for both Annexin-V and PI. The average values obtained from 3 independent cell lines is plotted. Error bars represent the S.E.M. Asterisk indicates significance using a two tailed Student's t-test where $p<0.05$. (D)

Immunoblot detection of the apoptosis marker cleaved caspase-3 in whole cell lysates of passage 3 and passage 7 WT and *Ercc1*$^{-/-}$ primary MEFs cultured at 3% or 20% O_2. β-actin was used as a loading control to calculate the fold-increase in cleaved caspase-3 expression relative to WT cells cultured at 3% O_2.

3.3.3 Cellular senescence occurs *in vivo* in ERCC1-deficient mice

To determine if the premature cellular senescence observed in *Ercc1*$^{-/-}$ MEFs was an artifact caused by *ex vivo* culture conditions, we measured proliferation and SA-β-gal activity in several tissues from ERCC1-deficient mice (*Ercc1*$^{-/\Delta}$). *Ercc1*$^{-/\Delta}$ mice, which model a human progeroid syndrome and age approximately six-fold faster than normal mice, display numerous aging-related degenerative symptoms and pathologies by 20 weeks of age[158, 217]. In both liver and spleen, there were numerous foci of SA-β-gal in 20 week-old *Ercc1*$^{-/\Delta}$ mice, but not WT littermates (Figure 12A). Similarly, in the spleen and large and small intestine, there was much less Ki67 staining, an S-phase antigen and marker of proliferating cells (Figure 12B). These *in vivo* data support the *in vitro* data. There are more senescent cells in the *Ercc1*$^{-/\Delta}$ progeroid mice, supporting the conclusion that endogenous DNA damage, if not repaired, can drive cellular senescence *in vivo*. This data further extends the parallels between *Ercc1*$^{-/\Delta}$ progeroid mice and old WT mice.

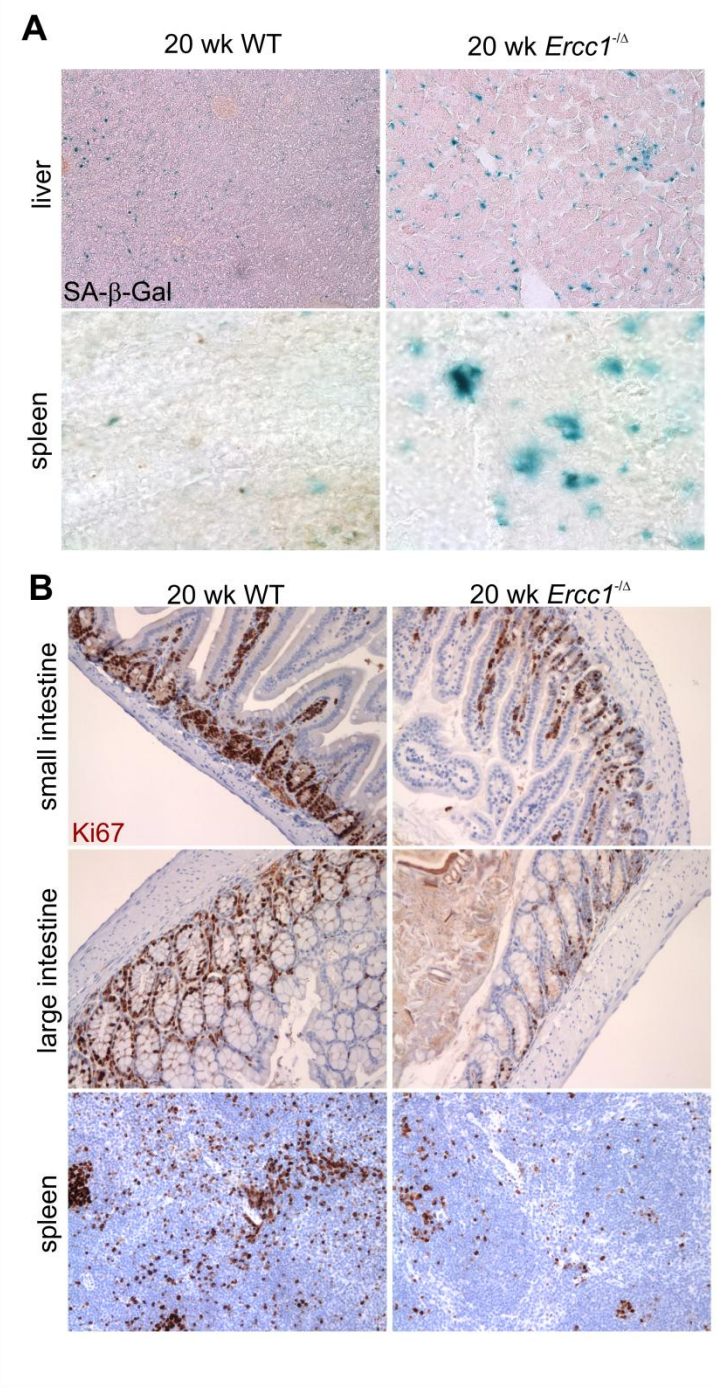

Figure 12. Cellular senescence is observed *in vivo* in ERCC1-deficient mice

(A) SA-β gal histochemical stain on sections of liver, spleen and small intestine from *Ercc1*$^{-/\Delta}$ and age-matched WT mice. Images were captured at 20X magnification. (B) Immunostaining for the proliferation marker Ki67 in sections of small intestine, large intestine and spleen from *Ercc1*$^{-/\Delta}$ and age-matched WT mice. Images were captured at 20X magnification.

3.3.4 *Ercc1*$^{-/-}$ MEFs exhibit changes in mitochondrial structure

ERCC1-XPF deficiency leads to genome-wide transcriptional changes that significantly correlate with transcriptional changes associated with old age[113, 218]. One of the major biological processes that is significantly perturbed in old and progeroid mice is downregulation of genes required for the mitochondrial electron transport chain [29, 204]. Thus, we examined mitochondrial structure and function in *Ercc1*$^{-/-}$ MEFs at multiple passages. Transmission electron microscopy (TEM) images revealed that even as early as passage 3, the mitochondria in *Ercc1*$^{-/-}$ MEFs are elongated compared to those in congenic WT cells (Figure 13A). This is exacerbated if the cells care cultured at 20% O_2. The mitochondrial phenotype worsened with further passaging. By passage 7, the mitochondria in *Ercc1*$^{-/-}$ MEFs were dramatically enlarged in diameter and length, hypodense and diffuse in appearance (Figure 4B). These abnormalities were also seen in WT cells at passage 7 albeit to a much lesser extent.

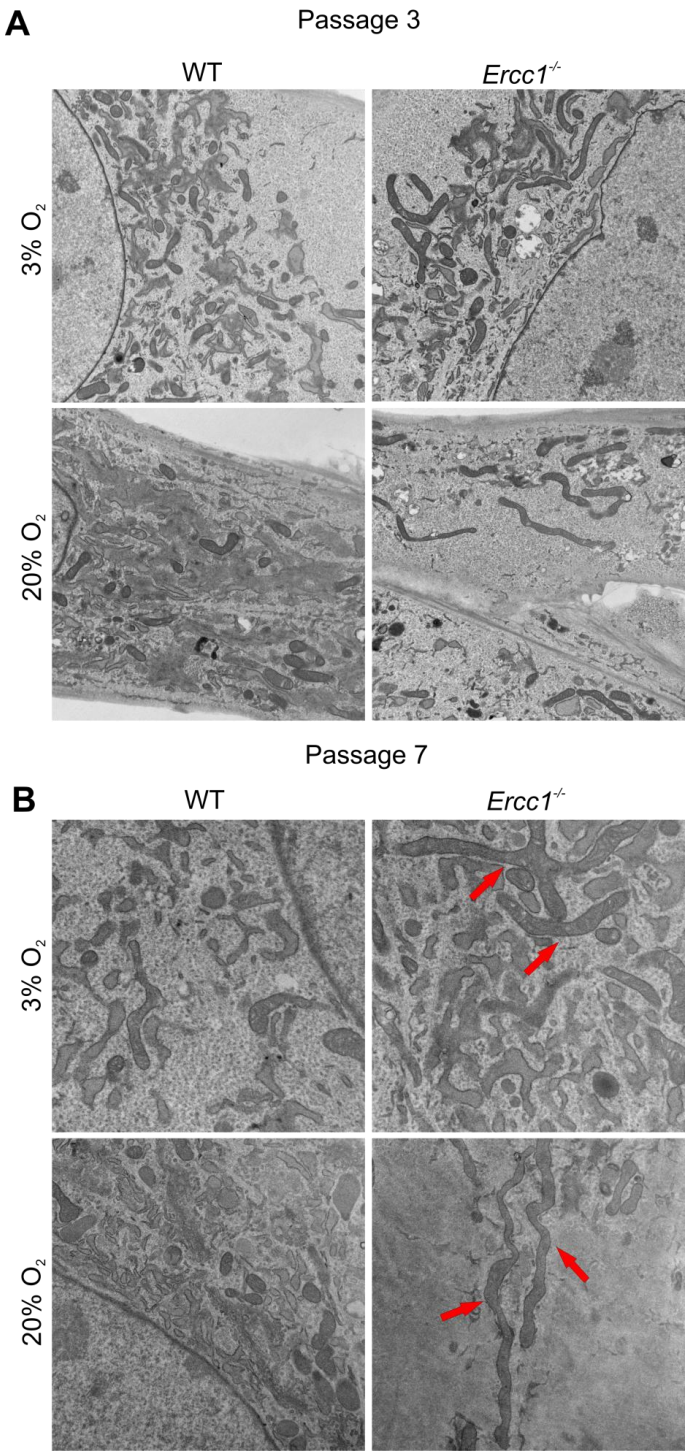

Figure 13. Oxidative stress and DNA repair deficiency promotes structural changes in the mitochondria

(A) Transmission electron micrographs (TEM; 15000X) of passage 3 *Ercc1*$^{-/-}$ MEFs exhibiting elongated mitochondria at both 3% and 20% O_2 compared to WT MEFs (B) Transmission electron micrographs (TEM;

15000X) of passage 7 *Ercc1*$^{-/-}$ MEFs exhibiting elongated mitochondria at both 3% and 20% O_2 compared to WT MEFs. Affected mitochondria are indicated with red arrows.

3.3.5 Mitochondria in *Ercc1*$^{-/-}$ MEFs produce high levels of ROS

H_2-DCFDA is a fluorescent dye used to measure reactive oxygen species [219]. We measured H_2-DCFDA in primary MEFs with increasing passage number to assess when and if mitochondrial dysfunction occurs relative to the onset of cellular senescence. H_2-DCFDA was significantly increased in *Ercc1*$^{-/-}$ MEFs at 20% O_2 compared to WT MEFs at 20% O_2, at passage 5 and 7, but not passage 3 (Figure 14A). No significant increase in H_2-DCFDA signal was detected in WT cells at 20% O_2, or between cells cultured at 3% and 20% O_2.

To specifically quantify mitochondrial-derived superoxide anion, WT and *Ercc1*$^{-/-}$ MEFs were stained with MitoSox[220]. Superoxide anion levels were significantly higher in *Ercc1*$^{-/-}$ MEFs at 3% O_2 compared to WT cells cultured at 3% O_2 at passages 3, 5, and 7 (Figure 14B), indicating that endogenous DNA damage results in high levels of superoxide anion. This demonstrates that the increase in ROS occurs simultaneously with the structural changes in mitochondria observed by TEM. In addition, growing MEFs at 20% O_2, induced significantly more superoxide anion production compared to 3% O_2 atmosphere. This was true and to the same extent in WT and *Ercc1*$^{-/-}$ MEFs. Interestingly, the level of superoxide anion decreased with increasing passage number for cells grown at 20% O_2, supporting the notion that by the time the mitochondria are elongated, they are no longer producing ROS. These data show a particularly strong correlation with conditions that induce cellular senescence (ERCC1-deficiency, 20% O_2), suggesting that mitochondrial superoxide anion precedes and contributes to cellular senescence.

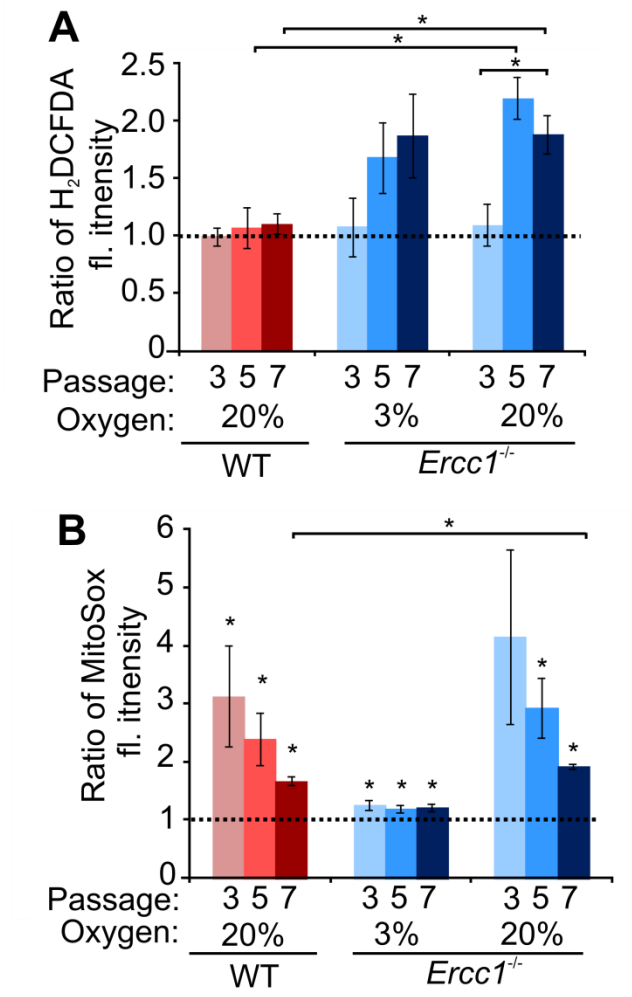

Figure 14. Oxidative stress and DNA repair deficiency promote increased mitochondrial-derived reactive oxygen species

(A) Oxidative stress was measured with H_2-DCFDA by flow cytometry. WT and *Ercc1*$^{-/-}$ MEFs at passage 3, 5, and 7 were stained with H_2-DCFDA and fluorescence intensity was measured by flow cytometry. H_2-DCFDA fluorescence intensity is expressed as a ratio to WT MEFs grown under 3% O_2. The average of 3 independent cell lines is plotted on the graph. Error bars represent ±S.E.M. Asterisk indicates significance using a two tailed Student's t-test where $p<0.05$. (B) Levels of superoxide anion were detected using MitoSox reagent. WT and *Ercc1*$^{-/-}$ MEFs at passage 3, 5, and 7 were stained with MitoSox and fluorescence intensity was measured by flow cytometry. MitoSox fluorescence intensity is expressed as a ratio to WT MEFs grown under 3% O_2 (dotted line). The average of 3 independent cell lines is plotted on the graph. Error bars represent ±S.E.M. Asterisk indicates significance using a two tailed Student's t-test where $p<0.05$.

3.3.6 Impaired mitochondrial function in senescent cells

To further assess mitochondrial integrity and function, we used JC-1, a cationic dye that fluoresces green as a monomer. JC-1 enters the mitochondrial membrane of live cells and aggregates when the membrane potential is high, causing a shift in emission to red. Live cell imaging and quantitative image analysis was used to determine the ratio of JC-1 red aggregates:green monomers in WT and *Ercc1*$^{-/-}$ MEFs. At passage 3, *Ercc1*$^{-/-}$ MEFs had lower mitochondrial membrane potential compared to WT MEFs, when cultured at 3% or 20% O_2 (Figure 15A). This indicates that endogenous DNA damage drives loss of mitochondrial membrane potential. In addition, the mitochondrial membrane potential of was significantly lower in *Ercc1*$^{-/-}$ MEFs grown at 20% O_2 than the same cells cultured at 3% O_2. A time-dependent decrease in mitochondrial membrane potential was observed in WT cells at 20% O_2, and *Ercc1*$^{-/-}$ cells at both 3% and 20% O_2. This suggests that unrepaired nuclear DNA damage caused by ROS can affect mitochondrial function.

Another important measure of mitochondrial function is ATP production. Surprisingly, *Ercc1*$^{-/-}$ MEFs had significantly higher steady-state levels of ATP than WT MEFs (Figure 15B). This was true at passage 4 and 6, when a significant fraction of cells were senescent. Curiously, the steady-state level of ATP increased for both *Ercc1*$^{-/-}$ and WT cells with increased passage number. Interestingly, when the cells were switched from glucose-containing media to one with galactose only, ATP levels dropped. The drop was much more precipitous in *Ercc1*$^{-/-}$ MEFs than WT MEFs. These data indicate that *Ercc1*$^{-/-}$ cells are much more dependent on glycolysis than oxidative phosphorylation for ATP production than are WT cells, which is consistent with their gene expression profile that showed reduced expression of electron transport chain proteins[29]. In addition, the data suggest that as cells senesce, ATP production is increased via glycolysis.

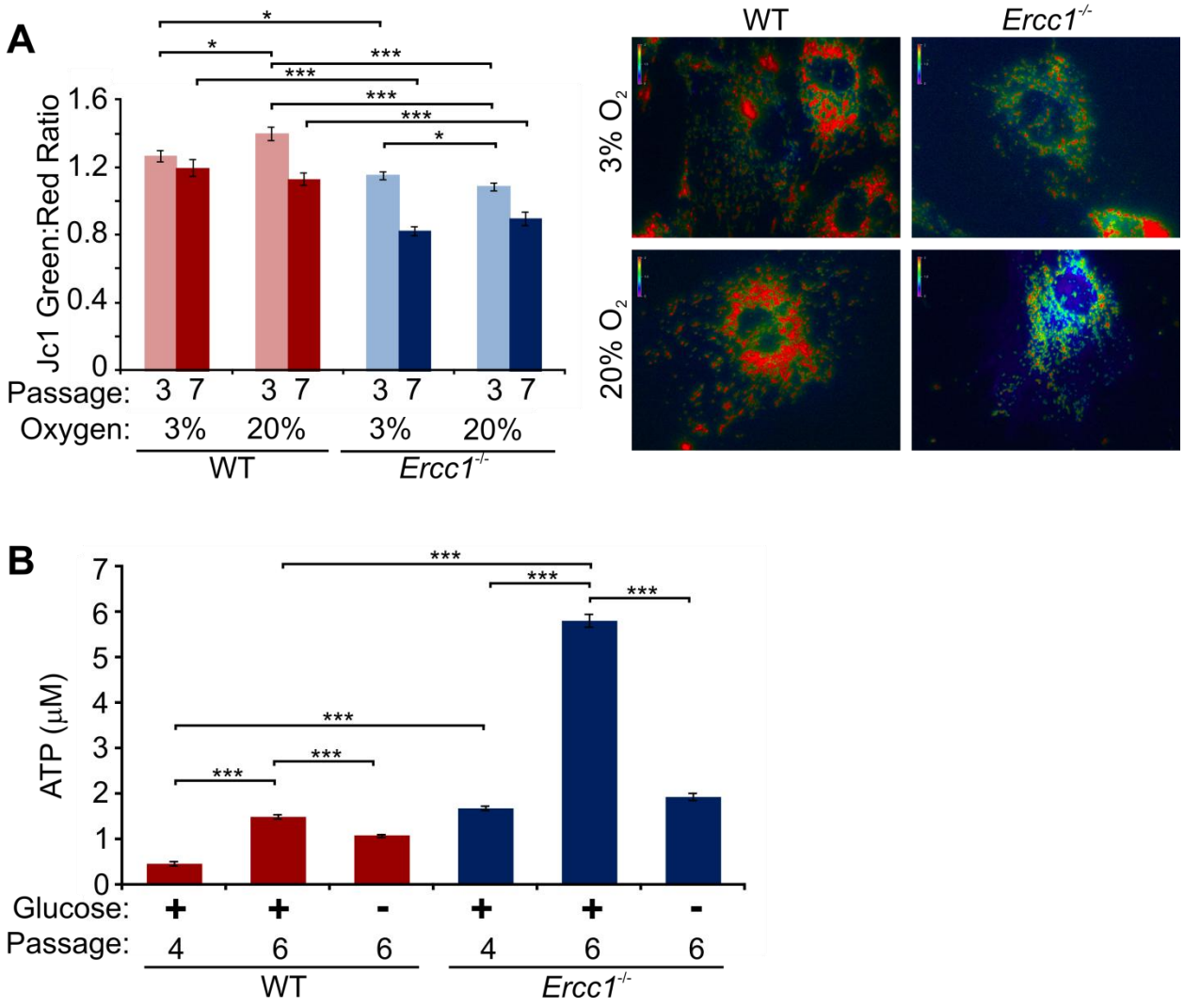

Figure 15. Oxidative stress and DNA repair deficiency promote functional changes in the mitochondria

(A) Mitochondrial membrane potential was measured by live-cell imaging using JC-1. The graph represents the ratio of JC1 red (aggregates): JC1 green (monomers) for n=150 cells in 3 independent cell lines for WT and *Ercc1*$^{-/-}$ at 3% and 20% O_2. Error bars represent ±S.E.M. * indicates significance using a two tailed Student's t-test where $p<0.05$, and *** indicates $p<0.001$. Representative images are shown in the right-hand panels. (B) Steady-state ATP levels were measured in WT and *Ercc1*$^{-/-}$ MEFS at passage 4 and passage 6 at 20% O_2 in either complete media

which contains glucose or glucose-free media in which galactose was the main sugar source. The graph represents the average of 3 independent experiments ±S.E.M. *** indicates significance using a two tailed Student's t-test where $p<0.001$.

3.3.7 Mitochondrial-derived ROS promotes cellular senescence

Table 4 summarizes the senescence-associated and mitochondrial endpoints measured. Remarkably, evidence of mitochondrial dysfunction and increased ROS production is detected prior to markers of cellular senescence in *Ercc1*$^{-/-}$ MEFs. This suggests that mitochondrial dysfunction may be a cause rather than a consequence of cellular senescence. If true, the prediction is that cellular senescence could be prevented by attenuating mitochondrial ROS To test this, *Ercc1*$^{-/-}$MEFs were treated with two free radical scavengers, XJB and Tempol. XJB and Tempol are structurally-related nitroxide radicals that quench cellular free radicals in recycling manner. XJB has an additional gramicidin S moiety that targets XJB specifically to the mitochondrial membrane. Passage 5 *Ercc1*$^{-/-}$ MEFs at 20% O_2 were treated with 2μM of XJB and Tempol for a period of 24 hours and total cell number was measured immediately following treatment. *Ercc1*$^{-/-}$ MEFs exhibited increased proliferation in response to treatment with XJB (Figure 16A), demonstrating that mitochondrially-derived ROS does play a causal role in promoting cellular senescence caused by endogenous DNA damage. In addition to measuring proliferation, we also observed evidence of decreased SA-β-gal activity in passage 5 *Ercc1*$^{-/-}$ MEFs that had undergone 24 hour treatment with XJB (Figure 16B).

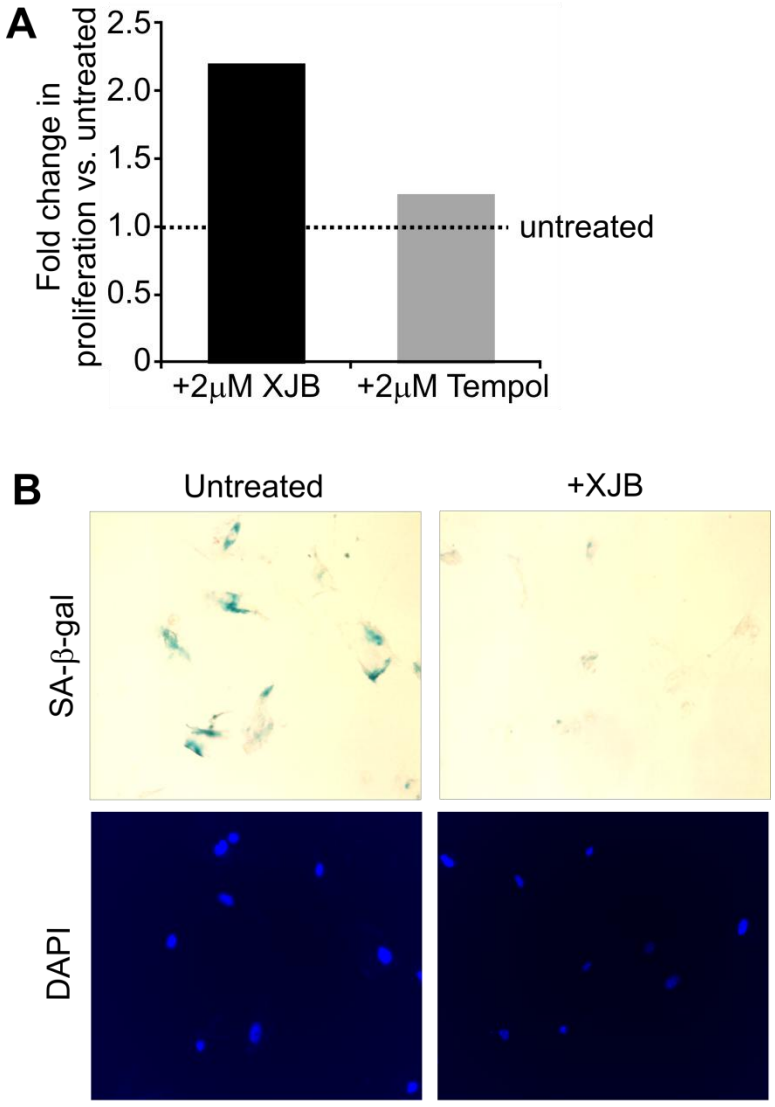

Figure 16. A mitochondrial-targeted free radical scavenger decreases senescence in *Ercc1*$^{-/-}$ MEFs

(A) *Ercc1*$^{-/-}$ MEFs at passage 5 plated at equal density were treated with 2μM XJB, 2μM Tempol or nothing for 24 hours. The number of cells was measured immediately after removal of the drug, and plotted as a ratio compared to untreated *Ercc1*$^{-/-}$ MEFs, indicated by the dotted line set at 1. (B) *Ercc1*$^{-/-}$ MEFs at passage 5 were treated with 2μM XJB or 2μM Tempol for 24 hours were fixed and stained for SA-β-gal immediately. Images are 40X magnification

ENDPOINT	WT 3% O_2			WT 20% O_2			*Ercc1*$^{-/-}$ 3%O_2			*Ercc1*$^{-/-}$ 20%O_2		
Passage	3	5	7	3	5	7	3	5	7	3	5	7
Proliferation	--	--	--	--	--	↓	--	--	↓	--	↓↓	↓↓
SA-β Gal	--	--	--	--	↑	↑	--	--	--	↑	↑	↑↑
γ-H2AX	--	--	↑	--	↑	↑	--	↑	↑	↑	↑	↑↑
p16^{INK4a}	1.0			1.2			2.5			2.0		
MT morphology	--	--	--	--	--	+	+	+	+	+	+	++
H_2-DCFDA	--	--	--	--	--	--	--	↑	--	--	↑	↑
MitoSox	--	--	--	↑	↑	↑	↑	↑	↑	--	↑	↑
Δψm (JC-1)	--		↓	--		↓	↓		↓↓	↓		↓↓

Table 4. Summary of senescence and mitochondrial endpoints in WT and *Ercc1*$^{-/-}$ MEFs

Endpoints of cellular senescence and mitochondrial function in WT and *Ercc1*$^{-/-}$ MEFs cultured at 3% or 20% O_2. Arrows represent increase or decrease at indicated passages (3, 5, or 7). Pink/red shading indicates an increase; green color indicates a decrease. Numeric values for p16^{INK4a} represent fold increase in p16 protein level, determined with normalization to loading control, β-actin.

3.4 DISCUSSION

There is strong evidence that DNA damage robustly induces cellular senescence[203, 210]. Furthermore, there is strong evidence that defects in DNA repair, causing accumulation of DNA damage, accelerates aging of one or more tissues[13, 14]. However it is not known if endogenous DNA damage that occurs spontaneously in cells drives cellular senescence, and if senescent cells contribute to aging. To test this, we asked if DNA repair deficiency was sufficient to drive cellular senescence *in vitro* and *in vivo*. Using primary MEFs, it is possible to compare

congenic cell lines that differ only in their DNA repair capacity and therefore their burden of spontaneous nuclear DNA damage. *Ercc1*$^{-/-}$ MEFs, with undetectable levels of ERCC1-XPF endonuclease were used. Loss of ERCC1-XPF impairs nucleotide excision repair of helix-distorting DNA monoadducts, the repair of DNA interstrand crosslinks, and the repair of a subset of DNA double-strand breaks[22, 45, 48]. Senescence endpoints were measured in untreated WT and *Ercc1*$^{-/-}$ MEFs at multiple passages, to determine if the accumulation of endogenous DNA damage is sufficient to induce cellular senescence. Comparing the same endpoints in cells grown at 20% O_2 as compared to 3% O_2, enabled determination of whether endogenously produced ROS promotes genotoxic stress and senescence.

Based on measurement of numerous markers of cellular senescence, the DNA repair deficient cells spontaneously senesce demonstrably more rapidly than WT cells, indicating that endogenous DNA damage is sufficient to drive cell senescence. WT MEFs at 20% O_2 do not exhibit signs of cellular senescence (SA-β-gal, decreased proliferation) until passage 7. In contrast, *Ercc1*$^{-/-}$ MEFs at 20% O_2 display SA-β-gal, decreased proliferation, γH2AX foci, and increased p16 expression as early as passage 3, and these worsen with increasing time in culture (Figure 1). Accelerated senescence is also seen in cultured fibroblasts from patients with ataxia telangiectasia (AT) and Werner syndrome (WS)[221, 222]. AT and WS are human diseases that result from mutations in ATM kinase, a master regulator of the DNA damage response[223], and WRN helicase, required to resolve replication stress particularly at telomeres[224], respectively. Patients with AT and WS, like patients with reduced expression of ERCC1-XPF, have symptoms of accelerated aging. In human cells, unlike MEFs, cellular senescence is largely driven by replication-dependent telomere shortening[225]. Therefore, our data in MEFs provides novel evidence that endogenous DNA damage can drive cellular senescence.

Senescence markers were detected earlier and to a greater extent if cells are grown at 20% O_2 compared to 3% O_2. p16 expression is modestly increased in passage 3 WT MEFs grown at 20% O_2 compared to cells grown at 3% O_2. SA-β-gal activity and γH2AX foci are increased in WT cells cultured at 20% O_2, by passages 5 and 7, respectively, but not if the same cells are cultured at 3% O_2. Proliferation is reduced by p7 in WT cells grown at 20% O_2 relative to 3%. Similarly, γH2AX foci, SA-β-gal activity and impaired proliferation are detected at an earlier passage in *Ercc1*$^{-/-}$ MEFs cultured at 20% O_2 compared to the same cells grown at 3% O_2. This, coupled with the above, strongly supports the conclusion that endogenously produced ROS, which is exacerbated when cells are grown at a higher oxygen tension, can drive cellular senescence at least in part by causing oxidative DNA damage.

γH2AX is considered a marker of DNA double-strand breaks, replication stress and senescent cells[226, 227]. Interestingly, γH2AX was always detected prior to replicative senescence or SA-β-gal activity. γH2AX foci are significantly increased in passage 7 WT MEFs at 3% O_2 but there is no observed loss of proliferation. γH2AX foci are significantly increased earlier in WT MEFs grown at 20% O_2 (passage 5), but SA-β-gal and proliferation aren't affected until later (passage 7). In *Ercc1*$^{-/-}$ MEFs, γH2AX foci are significantly increased compared to WT cells even at passage 3, for cells grown at 3% or 20% O_2. However, SA-β-gal activity is not increased at passage 3 at 3% O_2 and proliferation is not affected until passage 5 or 7. In both WT and DNA repair deficient cells, γH2AX foci increase with increasing passage number, reaching 50% of WT cells and 80% of *Ercc1*$^{-/-}$ cells with foci by passage 7. These data suggest that the γH2AX foci detected early in culture, particularly in the DNA repair deficient cells, are likely to be double-strand breaks or replication stress due to oxidative DNA lesions. But those that accumulate with increased time in culture, even in WT cells, are more likely to be a phenotype of

senescent cells rather than frank DNA damage. This is consistent with γH2AX being a component of permanent DNA SCARS, which are defined as DNA segments with chromatin alterations reinforcing senescence[203].

Primary WT and *Ercc1*$^{-/-}$ MEFs grown at 20% O_2 have signficantly higher levels of ROS (MitoSox) at passage 5 and p7, compared to the same cells grown at 3% O_2. This demonstrates that growing MEFs at atmospheric oxygen induces endogenous production of ROS. WT MEFs grown at 20% O_2 exhibit signs of mitochondrial dysfunction by passage 7, including structural changes and reduced membrane potential. This demonstrates that standard culture conditions (atmospheric oxygen levels) rapidly induce cellular changes that amplify damage and feed forward to drive MEFs to senescence

DNA repair-deficient *Ercc1*$^{-/-}$ MEFs also exhibit enlarged and dysfunctional mitochondria, but much earlier than WT MEFs, demonstrating a link between a nuclear DNA damage and mitochondrial dysfunction. *Ercc1*$^{-/-}$ MEFs, grown at 3% and 20% O_2, exhibit enlarged and diffuse mitochondria compared to WT cells, as early as passage 3. *Ercc1*$^{-/-}$ MEFs also have higher levels of ROS (H_2-DCFDA and MitoSox) than WT MEFs, beginning at passage 5. Similar findings have been reported in *S. cerevisiae*: DNA repair deficient strains exhibit higher levels of ROS[228]. This invokes a model of a vicious cycle in which genotoxic damage perturbs mitochondrial function, which in turn leads to increased ROS production and consequently more nuclear DNA damage. The fact that this process was accelerated in cells defective in nuclear DNA repair, suggests that loss of mitochondrial function is an active process rather than passive, *i.e.*, occurring via signaling mechanisms between the nucleus and mitochondria, rather than as a consequence of direct mitochondrial damage.

Giant mitochondria have been shown to accumulate in aged or damaged cells in response to inhibition of autophagic pathways[229]. Hence, nuclear DNA damage or activation of the DNA damage response might inhibit autophagy. Fission and fusion regulate the morphology of mitochondria[230]. Thus it is possible that mitochondrial fission-fusion cycles are dysregulated in response to nuclear DNA damage. Mitofusin 1 (*mfn1*), a key regulator of mitochondrial fusion and morphology in mammalian cells[231], is significantly downregulated in liver in *Ercc1*$^{-/-}$ mice[29], illustrating the potential for abnormalities in mitochondrial fission-fusion cycles, but not explaining giant mitochondria.

Taken together, our data provide experimental evidence that physiological levels of endogenous DNA damage can drive cellular senescence. This is not an artifact of an *in vitro* culture system, as replicative senescence was also detected in tissues of ERCC1-deficient mice. Since these mice display accelerated aging of numerous organ systems[14], including the liver[204], these data strengthen the link between cellular senescence and aging. Treatment of *Ercc1*$^{-/-}$ MEFs with a mitochondrial-targeted free radical scavenger delayed cellular senescence in *Ercc1*$^{-/-}$ MEFs. This provides evidence that although the DNA damage studied herein, occurred spontaneously as a consequence of intracellular processes, it is possible to attenuate this DNA damage, which in turn might delay senescence and/or aging-related degenerative changes.

3.5 ACKNOWLEDGEMENTS

Jennifer Stripay (Research assistant in Dr. Paul Robbins lab, Microbiology and Molecular Genetics, University of Pittsburgh) treated *Ercc1*$^{-/-}$ MEFs with XJB and measured SA-β-gal

activity (Figure 16B). Salony Maniar (Center for Biological Imaging, University of Pittsburgh) assisted with live-cell image analysis using JC-1 (Figure 15A).

4.0 OVERALL SUMMARY AND CONCLUSIONS

The overarching goal of my thesis was to address the questions; does a direct causal relationship exist between cellular senescence and aging, and DNA damage and aging? I took a genetic approach to address this experimental question, and studied mice and cells deficient for ERCC1-XPF, a essential DNA repair endonuclease. Mutations that result in severe reduction of ERCC1-XPF protein levels result in accelerated aging, in humans and mice. The advantage of this genetic approach was that it eliminated confounding genetic variables that often plague human studies of aging, as the only difference between inbred mice and congenic (WT and *Ercc1*$^{-/-}$) cell lines was the deficiency of ERCC1-XPF. Therefore, the differences I observed in ERCC1-deficient mice and cells compared to WT mice and cells, could be directly attributed to the absence of this DNA repair enzyme, and the subsequent effects of endogenous DNA damage.

The data presented herein demonstrates that physiological levels of endogenously produced DNA damage are sufficient to drive cellular senescence both *in vitro* and *in vivo*. The first study took an *in vivo* approach and tested if the accelerated aging phenotype observed in ERCC1-deficient mice was similar to normal aging at the molecular, cellular and whole tissue level. This addresses a fundamental question regarding the usefulness of mouse models of progeria in the study of human aging. The liver was the organ I chose to study because the degeneration found in *Ercc1*$^{-/\Delta}$ mouse liver was previously implicated as the life-limiting factor in ERCC1-null mice[118]. It was my goal to quantitatively and qualitatively characterize the

hepatic changes in *Ercc1*$^{-/\Delta}$ mice and directly compare these with the changes that occur with normal aging. The results indicated that the structural and functional changes observed in the liver of progeroid *Ercc1*$^{-/\Delta}$ mice over the course of their 6-month lifespan closely paralleled age-associated changes that occurred in WT mice. Liver of aged WT and 20 week-old *Ercc1*$^{-/\Delta}$ mice both displayed areas of necrosis, foci of hepatocellular degeneration and acute inflammation. However, *Ercc1*$^{-/\Delta}$ mice exhibited more severe loss of hepatic architecture, fibrosis, steatosis, pseudocapillarization, and anisokaryosis than old WT mice. The data also indicated that the liver of *Ercc1*$^{-/\Delta}$ mice had a reduced capacity for regeneration, as demonstrated by impaired hepatocellular proliferation following partial hepatectomy. Importantly, there was a highly significant correlation in genome-wide transcriptional changes between old WT and *Ercc1*$^{-/\Delta}$ mice. Taken together, our data indicates that there are strong functional, regulatory and histopathological parallels between accelerated aging driven by a DNA repair defect and normal aging.

This study on the effect of endogenous DNA damage in the liver raises an important question for future studies on aging; is age-related loss of tissue homeostasis is driven by a cell autonomous or non-autonomous effect? More specifically, is the accelerated liver aging observed in DNA repair deficient *Ercc1*$^{-/\Delta}$ mice the result of accumulated damage in the hepatocytes, or are resident liver stem cells negatively impacted, leading to a loss of regenerative capacity and subsequent tissue dysfunction? One approach to address this question would be to utilize Cre-lox technology to create cell lineage-specific knockouts of *Ercc1*, and observe the effect(s) that result from the loss of functional DNA repair in one specific cell type, such as hepatocytes. Alternatively, parabiosis is another experimental approach to answer this question. In the case of where a young WT mouse is fused to an *Ercc1*$^{-/\Delta}$ mouse, if the aging symptoms are

alleviated, it will indicate that accelerated aging in response to DNA damage is cell non-autonomous, and can be ameliorated by a circulating factor from the young WT mouse.

The second hypothesis addressed in my thesis was that endogenous DNA damage that occurs spontaneously in cells is sufficient to drive cellular senescence. Endogenous DNA damage occurs from normal cellular processes at a high frequency. Endogenous sources of DNA damage can result in single-strand breaks, double-strand breaks, and abasic sites, and can promote mutagenesis similar to exogenous DNA damaging agents[232]. Previous studies determined that high levels of ionizing radiation, doxorubicin, bleomycin, actinomycin D, aphidicolin, cisplatin and hydrogen peroxide can induce cellular senescence[210, 211, 233, 234]. The aim of this study was to determine if physiological levels of endogenous DNA damage could drive senescence. The experiments were carried out using *Ercc1*$^{-/-}$ primary MEFs, which accumulate DNA damage, in the absence of any genotoxic treatment, eliminating off-target effects on other cellular macromolecules. *Ercc1*$^{-/-}$ MEFs spontaneously exhibited markers of cellular senescence, including reduced proliferation, SA-β-gal staining, increased p16^{INK4a}, and increased γ-H2AX foci, earlier than WT MEFs cultured under the same conditions. This result indicated that endogenous DNA damage, if not repaired, accelerates the onset of cellular senescence. An unanticipated finding from this study was that mitochondria in *Ercc1*$^{-/-}$ MEFs were elongated compared to WT MEFs and produced more reactive oxygen species, indicative of uncoupling of the electron transport chain. Treatment of *Ercc1*$^{-/-}$ MEFs with a mitochondrial-targeted free radical scavenger, XJB, rescued senescence. Furthermore, evidence of mitochondrial abnormalities and dysfunction was detected prior to markers of cellular senescence in *Ercc1*$^{-/-}$ MEFs. These data support the conclusion that mitochondrial-derived ROS causes DNA damage that drives cell senescence. Similar mitochondrial and senescence-

associated changes were detected in WT cells albeit at a later time interval than in *Ercc1*$^{-/-}$ MEFs, indicating that DNA repair mechanisms are inadequate to cope with the normal burden of DNA damage and stave off cellular senescence indefinitely. *Ercc1*$^{-/-}$ MEFs represent a useful *in vitro* model system for assaying pharmacologic interventions aimed at delaying or ameliorating premature cellular senescence due to DNA damage. This line of future work is important for the thousands of individuals who undergo chemotherapy, oftentimes with a DNA-damaging chemical. *Ercc1*$^{-/-}$ MEFs are also a useful tool for screening environmental and dietary exposures that promote DNA damage and cellular senescence.

The mitochondrial phenotype observed in *Ercc1*$^{-/-}$ MEFs presents some exciting opportunities for future work. Transmission electron microscopic analysis of *Ercc1*$^{-/-}$ MEFs revealed an accumulation of dysfunctional mitochondria, a percentage of which appeared to be undergoing a specific form of autophagy known as mitophagy. It is known that aging cells are unable to maintain their quality control mechanisms and thus exhibit improper turnover of organelles[235]. It is plausible that insufficient or dysfunctional mitophagy could drive the accumulation of elongated mitochondria. Previous work has shown that giant mitochondria accumulate in aged or damaged cells in response to inhibition of autophagic pathways[229]. Preservation or enhancement of autophagic pathways may be a potential therapeutic target for ameliorating the mitochondrial phenotype observed in *Ercc1*$^{-/-}$ MEFs[236]. The direction of future studies may also focus on processes of mitochondrial fission and fusion in DNA repair-deficient cells and animals. It is likely that mitochondrial fission-fusion cycles are dysregulated in response to nuclear DNA damage, as the result of genome-wide transcriptional responses to damage. The gene expression profile of *Ercc1*$^{-/-}$ mice reveals that there is significant downregulation of mitofusin 1 (*mfn1*) compared to age-matched WT mice[29]. Mitofusin 1 is a

key protein in regulation of mitochondrial fusion and morphology in mammalian cells[231]. Determination of mtDNA replication and mitochondrial biogenesis in *Ercc1*$^{-/-}$ MEFs would be interesting, as reports indicate that DNA damage can induce biogenesis of mitcohondria in an ATM and PGC-1α-dependent pathway[237].

My studies have advanced our knowledge of the cellular response to endogenous DNA damage, both *in vitro* and *in vivo*. The signaling mechanisms that are activated in response to spontaneous DNA damage will provide clues to a more complete mechanism and potential pharmacologic targets for ameliorating or delaying age-related disease and dysfunction.

5.0 APPENDIX

Abbreviation	Definition
ERCC1	Excision repair cross complementation group 1
NER	Nucleotide excision repair
ICL	Interstrand crosslink
DSB	Double-strand break
CPD	Cyclobutane pyrimidine dimer
COFS	Cerebro-oculo-facio-skeletal syndrome
HR	Homologous recombination
NHEJ	Non-homologous end joining
UDS	Unscheduled DNA synthesis
CS	Cockayne syndrome
IR	Ionizing radiation
ATM	Ataxia telangiectasia mutated
ATR	Ataxia telangiectasia and Rad3 related
DDR	DNA damage response
MEFs	Mouse embryonic fibroblasts

Table 5. Abbreviations

Figure 17. Mouse models of DNA repair deficiency: *Ercc1*$^{-/-}$ and *Ercc1*$^{-/\Delta}$

Representative images of *Ercc1*$^{-/-}$ (left; 3 wks of age) and *Ercc1*$^{-/\Delta}$ (right; 18 wks of age) mice.

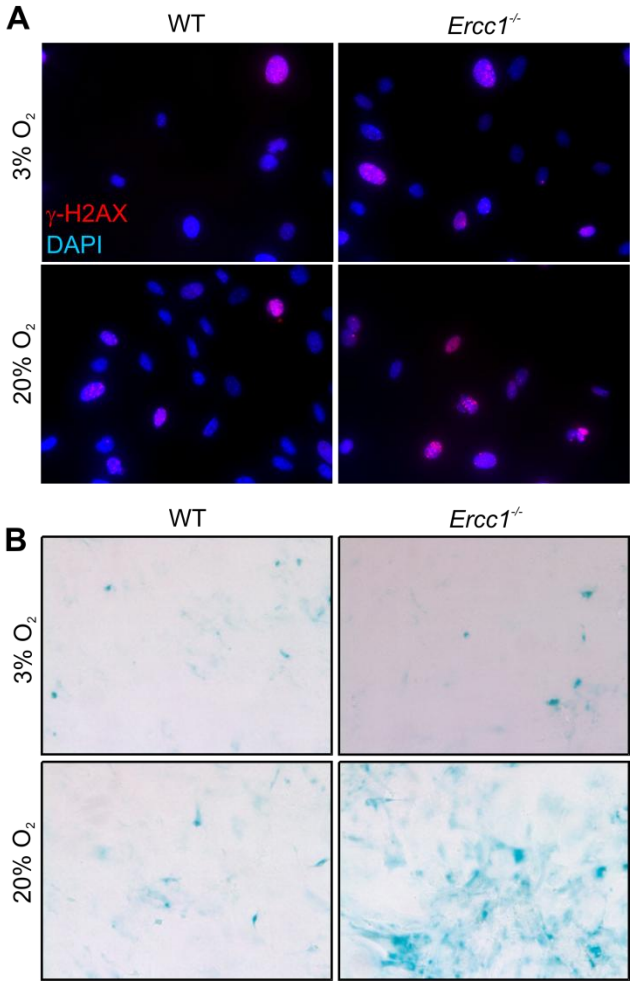

Figure 18. Evidence of premature cellular senescence in *Ercc1*$^{-/-}$ MEFs

(A) Representative γ-H2AX immunofluorescence images of WT and *Ercc1*$^{-/-}$ MEFs at passage 3. Blue color represents DAPI staining in nuclei and red foci represent γ-H2AX. Images were captured at 20X magnification. (B) Representative SA-β-gal images of WT and *Ercc1*$^{-/-}$ MEFs at passage 7. Blue color represents senescent cells. Images were captured at 20X magnification.

BIBLIOGRAPHY

[1] P.D. Department of Economic and Social Affairs, World Population Ageing: 1950-2050, in: U. Nations (Ed.), United Nations, New York, 2001.
[2] M. Heron, D.L. Hoyert, S.L. Murphy, J. Xu, K.D. Kochanek, B. Tejada-Vera, Deaths: final data for 2006, Natl Vital Stat Rep, 57 (2009) 1-134.
[3] N.A. Berger, P. Savvides, S.M. Koroukian, E.F. Kahana, G.T. Deimling, J.H. Rose, K.F. Bowman, R.H. Miller, Cancer in the elderly, Trans Am Clin Climatol Assoc, 117 (2006) 147-155; discussion 155-146.
[4] R.C. Lawrence, D.T. Felson, C.G. Helmick, L.M. Arnold, H. Choi, R.A. Deyo, S. Gabriel, R. Hirsch, M.C. Hochberg, G.G. Hunder, J.M. Jordan, J.N. Katz, H.M. Kremers, F. Wolfe, Estimates of the prevalence of arthritis and other rheumatic conditions in the United States. Part II, Arthritis Rheum, 58 (2008) 26-35.
[5] D.S. Friedman, R.C. Wolfs, B.J. O'Colmain, B.E. Klein, H.R. Taylor, S. West, M.C. Leske, P. Mitchell, N. Congdon, J. Kempen, Prevalence of open-angle glaucoma among adults in the United States, Arch Ophthalmol, 122 (2004) 532-538.
[6] N. Congdon, J.R. Vingerling, B.E. Klein, S. West, D.S. Friedman, J. Kempen, B. O'Colmain, S.Y. Wu, H.R. Taylor, Prevalence of cataract and pseudophakia/aphakia among adults in the United States, Arch Ophthalmol, 122 (2004) 487-494.
[7] R. Burge, B. Dawson-Hughes, D.H. Solomon, J.B. Wong, A. King, A. Tosteson, Incidence and economic burden of osteoporosis-related fractures in the United States, 2005-2025, J Bone Miner Res, 22 (2007) 465-475.
[8] L.J. Melton, 3rd, How many women have osteoporosis now?, J Bone Miner Res, 10 (1995) 175-177.
[9] C. U.S. Department of Health and Human Services, National Diabetes Fact Sheet: national estimates and general information on diabetes and prediabetes in the United States, in, U.S. Department of Health and Human Services, Atlanta, GA, 2011.
[10] L.E. Hebert, P.A. Scherr, J.L. Bienias, D.A. Bennett, D.A. Evans, Alzheimer disease in the US population: prevalence estimates using the 2000 census, Arch Neurol, 60 (2003) 1119-1122.
[11] L.J. Findley, The economic impact of Parkinson's disease, Parkinsonism Relat Disord, 13 Suppl (2007) S8-S12.
[12] T.B. Kirkwood, Understanding the odd science of aging, Cell, 120 (2005) 437-447.
[13] E.C. Friedberg, L.B. Meira, Database of mouse strains carrying targeted mutations in genes affecting biological responses to DNA damage Version 7, DNA Repair (Amst), 5 (2006) 189-209.
[14] S.Q. Gregg, A.R. Robinson, L.J. Niedernhofer, Physiological consequences of defects in ERCC1-XPF DNA repair endonuclease, DNA Repair (Amst), 10 (2011) 781-791.

[15] R.H. te Poele, A.L. Okorokov, L. Jardine, J. Cummings, S.P. Joel, DNA damage is able to induce senescence in tumor cells in vitro and in vivo, Cancer Res, 62 (2002) 1876-1883.
[16] G.P. Dimri, X. Lee, G. Basile, M. Acosta, G. Scott, C. Roskelley, E.E. Medrano, M. Linskens, I. Rubelj, O. Pereira-Smith, et al., A biomarker that identifies senescent human cells in culture and in aging skin in vivo, Proc Natl Acad Sci U S A, 92 (1995) 9363-9367.
[17] U. Herbig, M. Ferreira, L. Condel, D. Carey, J.M. Sedivy, Cellular senescence in aging primates, Science, 311 (2006) 1257.
[18] G. Ding, N. Franki, A.A. Kapasi, K. Reddy, N. Gibbons, P.C. Singhal, Tubular cell senescence and expression of TGF-beta1 and p21(WAF1/CIP1) in tubulointerstitial fibrosis of aging rats, Exp Mol Pathol, 70 (2001) 43-53.
[19] J.P. Coppe, C.K. Patil, F. Rodier, Y. Sun, D.P. Munoz, J. Goldstein, P.S. Nelson, P.Y. Desprez, J. Campisi, Senescence-associated secretory phenotypes reveal cell-nonautonomous functions of oncogenic RAS and the p53 tumor suppressor, PLoS Biol, 6 (2008) 2853-2868.
[20] C. Petit, A. Sancar, Nucleotide excision repair: from E. coli to man, Biochimie, 81 (1999) 15-25.
[21] I. Kuraoka, W.R. Kobertz, R.R. Ariza, M. Biggerstaff, J.M. Essigmann, R.D. Wood, Repair of an interstrand DNA cross-link initiated by ERCC1-XPF repair/recombination nuclease, J Biol Chem, 275 (2000) 26632-26636.
[22] A. Ahmad, A.R. Robinson, A. Duensing, E. van Drunen, H.B. Beverloo, D.B. Weisberg, P. Hasty, J.H. Hoeijmakers, L.J. Niedernhofer, ERCC1-XPF endonuclease facilitates DNA double-strand break repair, Mol Cell Biol, 28 (2008) 5082-5092.
[23] R.G. Sargent, R.L. Rolig, A.E. Kilburn, G.M. Adair, J.H. Wilson, R.S. Nairn, Recombination-dependent deletion formation in mammalian cells deficient in the nucleotide excision repair gene ERCC1, Proc Natl Acad Sci U S A, 94 (1997) 13122-13127.
[24] C. Schlake, K. Ostermann, H. Schmidt, H. Gutz, Analysis of DNA repair pathways of Schizosaccharomyces pombe by means of swi-rad double mutants, Mutat Res, 294 (1993) 59-67.
[25] J.J. Sekelsky, K.S. McKim, G.M. Chin, R.S. Hawley, The Drosophila meiotic recombination gene mei-9 encodes a homologue of the yeast excision repair protein Rad1, Genetics, 141 (1995) 619-627.
[26] D.B. Busch, H. van Vuuren, J. de Wit, A. Collins, M.Z. Zdzienicka, D.L. Mitchell, K.W. Brookman, M. Stefanini, R. Riboni, L.H. Thompson, R.B. Albert, A.J. van Gool, J. Hoeijmakers, Phenotypic heterogeneity in nucleotide excision repair mutants of rodent complementation groups 1 and 4, Mutat Res, 383 (1997) 91-106.
[27] X.D. Zhu, L. Niedernhofer, B. Kuster, M. Mann, J.H. Hoeijmakers, T. de Lange, ERCC1/XPF removes the 3' overhang from uncapped telomeres and represses formation of telomeric DNA-containing double minute chromosomes, Mol Cell, 12 (2003) 1489-1498.
[28] P. Munoz, R. Blanco, J.M. Flores, M.A. Blasco, XPF nuclease-dependent telomere loss and increased DNA damage in mice overexpressing TRF2 result in premature aging and cancer, Nat Genet, 37 (2005) 1063-1071.
[29] L.J. Niedernhofer, G.A. Garinis, A. Raams, A.S. Lalai, A.R. Robinson, E. Appeldoorn, H. Odijk, R. Oostendorp, A. Ahmad, W. van Leeuwen, A.F. Theil, W. Vermeulen, G.T. van der Horst, P. Meinecke, W.J. Kleijer, J. Vijg, N.G. Jaspers, J.H. Hoeijmakers, A new progeroid syndrome reveals that genotoxic stress suppresses the somatotroph axis, Nature, 444 (2006) 1038-1043.
[30] N.G. Jaspers, A. Raams, M.C. Silengo, N. Wijgers, L.J. Niedernhofer, A.R. Robinson, G. Giglia-Mari, D. Hoogstraten, W.J. Kleijer, J.H. Hoeijmakers, W. Vermeulen, First reported

patient with human ERCC1 deficiency has cerebro-oculo-facio-skeletal syndrome with a mild defect in nucleotide excision repair and severe developmental failure, Am J Hum Genet, 80 (2007) 457-466.
[31] W.L. de Laat, N.G. Jaspers, J.H. Hoeijmakers, Molecular mechanism of nucleotide excision repair, Genes Dev, 13 (1999) 768-785.
[32] A.M. Sijbers, P.J. van der Spek, H. Odijk, J. van den Berg, M. van Duin, A. Westerveld, N.G. Jaspers, D. Bootsma, J.H. Hoeijmakers, Mutational analysis of the human nucleotide excision repair gene ERCC1, Nucleic Acids Res, 24 (1996) 3370-3380.
[33] A. Tapias, J. Auriol, D. Forget, J.H. Enzlin, O.D. Scharer, F. Coin, B. Coulombe, J.M. Egly, Ordered conformational changes in damaged DNA induced by nucleotide excision repair factors, J Biol Chem, 279 (2004) 19074-19083.
[34] A.J. Bardwell, L. Bardwell, A.E. Tomkinson, E.C. Friedberg, Specific cleavage of model recombination and repair intermediates by the yeast Rad1-Rad10 DNA endonuclease, Science, 265 (1994) 2082-2085.
[35] C.H. Park, T. Bessho, T. Matsunaga, A. Sancar, Purification and characterization of the XPF-ERCC1 complex of human DNA repair excision nuclease, J Biol Chem, 270 (1995) 22657-22660.
[36] J.H. Enzlin, O.D. Scharer, The active site of the DNA repair endonuclease XPF-ERCC1 forms a highly conserved nuclease motif, EMBO J, 21 (2002) 2045-2053.
[37] O.V. Tsodikov, D. Ivanov, B. Orelli, L. Staresincic, I. Shoshani, R. Oberman, O.D. Scharer, G. Wagner, T. Ellenberger, Structural basis for the recruitment of ERCC1-XPF to nucleotide excision repair complexes by XPA, EMBO J, 26 (2007) 4768-4776.
[38] L. Li, S.J. Elledge, C.A. Peterson, E.S. Bales, R.J. Legerski, Specific association between the human DNA repair proteins XPA and ERCC1, Proc Natl Acad Sci U S A, 91 (1994) 5012-5016.
[39] O.V. Tsodikov, J.H. Enzlin, O.D. Scharer, T. Ellenberger, Crystal structure and DNA binding functions of ERCC1, a subunit of the DNA structure-specific endonuclease XPF-ERCC1, Proc Natl Acad Sci U S A, 102 (2005) 11236-11241.
[40] K. Tripsianes, G. Folkers, E. Ab, D. Das, H. Odijk, N.G. Jaspers, J.H. Hoeijmakers, R. Kaptein, R. Boelens, The structure of the human ERCC1/XPF interaction domains reveals a complementary role for the two proteins in nucleotide excision repair, Structure, 13 (2005) 1849-1858.
[41] K.H. Kraemer, D.D. Levy, C.N. Parris, E.M. Gozukara, S. Moriwaki, S. Adelberg, M.M. Seidman, Xeroderma pigmentosum and related disorders: examining the linkage between defective DNA repair and cancer, J Invest Dermatol, 103 (1994) 96S-101S.
[42] L.V. Mayne, A.R. Lehmann, Failure of RNA synthesis to recover after UV irradiation: an early defect in cells from individuals with Cockayne's syndrome and xeroderma pigmentosum, Cancer Res, 42 (1982) 1473-1478.
[43] G. Weeda, I. Donker, J. de Wit, H. Morreau, R. Janssens, C.J. Vissers, A. Nigg, H. van Steeg, D. Bootsma, J.H. Hoeijmakers, Disruption of mouse ERCC1 results in a novel repair syndrome with growth failure, nuclear abnormalities and senescence, Curr Biol, 7 (1997) 427-439.
[44] T. Itoh, S. Linn, T. Ono, M. Yamaizumi, Reinvestigation of the classification of five cell strains of xeroderma pigmentosum group E with reclassification of three of them, J Invest Dermatol, 114 (2000) 1022-1029.

[45] A.M. Sijbers, W.L. de Laat, R.R. Ariza, M. Biggerstaff, Y.F. Wei, J.G. Moggs, K.C. Carter, B.K. Shell, E. Evans, M.C. de Jong, S. Rademakers, J. de Rooij, N.G. Jaspers, J.H. Hoeijmakers, R.D. Wood, Xeroderma pigmentosum group F caused by a defect in a structure-specific DNA repair endonuclease, Cell, 86 (1996) 811-822.
[46] C.A. Hoy, L.H. Thompson, C.L. Mooney, E.P. Salazar, Defective DNA cross-link removal in Chinese hamster cell mutants hypersensitive to bifunctional alkylating agents, Cancer Res, 45 (1985) 1737-1743.
[47] I.U. De Silva, P.J. McHugh, P.H. Clingen, J.A. Hartley, Defining the roles of nucleotide excision repair and recombination in the repair of DNA interstrand cross-links in mammalian cells, Mol Cell Biol, 20 (2000) 7980-7990.
[48] L.J. Niedernhofer, H. Odijk, M. Budzowska, E. van Drunen, A. Maas, A.F. Theil, J. de Wit, N.G. Jaspers, H.B. Beverloo, J.H. Hoeijmakers, R. Kanaar, The structure-specific endonuclease Ercc1-Xpf is required to resolve DNA interstrand cross-link-induced double-strand breaks, Mol Cell Biol, 24 (2004) 5776-5787.
[49] J. McWhir, J. Selfridge, D.J. Harrison, S. Squires, D.W. Melton, Mice with DNA repair gene (ERCC-1) deficiency have elevated levels of p53, liver nuclear abnormalities and die before weaning, Nat Genet, 5 (1993) 217-224.
[50] A. de Vries, C.T. van Oostrom, F.M. Hofhuis, P.M. Dortant, R.J. Berg, F.R. de Gruijl, P.W. Wester, C.F. van Kreijl, P.J. Capel, H. van Steeg, et al., Increased susceptibility to ultraviolet-B and carcinogens of mice lacking the DNA excision repair gene XPA, Nature, 377 (1995) 169-173.
[51] H. Nakane, S. Takeuchi, S. Yuba, M. Saijo, Y. Nakatsu, H. Murai, Y. Nakatsuru, T. Ishikawa, S. Hirota, Y. Kitamura, et al., High incidence of ultraviolet-B-or chemical-carcinogen-induced skin tumours in mice lacking the xeroderma pigmentosum group A gene, Nature, 377 (1995) 165-168.
[52] M. Tian, R. Shinkura, N. Shinkura, F.W. Alt, Growth retardation, early death, and DNA repair defects in mice deficient for the nucleotide excision repair enzyme XPF, Mol Cell Biol, 24 (2004) 1200-1205.
[53] M. Raschle, P. Knipscheer, M. Enoiu, T. Angelov, J. Sun, J.D. Griffith, T.E. Ellenberger, O.D. Scharer, J.C. Walter, Mechanism of replication-coupled DNA interstrand crosslink repair, Cell, 134 (2008) 969-980.
[54] N. Bhagwat, A.L. Olsen, A.T. Wang, K. Hanada, P. Stuckert, R. Kanaar, A. D'Andrea, L.J. Niedernhofer, P.J. McHugh, XPF-ERCC1 participates in the Fanconi anemia pathway of cross-link repair, Mol Cell Biol, 29 (2009) 6427-6437.
[55] P. Knipscheer, M. Raschle, A. Smogorzewska, M. Enoiu, T.V. Ho, O.D. Scharer, S.J. Elledge, J.C. Walter, The Fanconi anemia pathway promotes replication-dependent DNA interstrand cross-link repair, Science, 326 (2009) 1698-1701.
[56] I.M. Munoz, K. Hain, A.C. Declais, M. Gardiner, G.W. Toh, L. Sanchez-Pulido, J.M. Heuckmann, R. Toth, T. Macartney, B. Eppink, R. Kanaar, C.P. Ponting, D.M. Lilley, J. Rouse, Coordination of structure-specific nucleases by human SLX4/BTBD12 is required for DNA repair, Mol Cell, 35 (2009) 116-127.
[57] S. Fekairi, S. Scaglione, C. Chahwan, E.R. Taylor, A. Tissier, S. Coulon, M.Q. Dong, C. Ruse, J.R. Yates, 3rd, P. Russell, R.P. Fuchs, C.H. McGowan, P.H. Gaillard, Human SLX4 is a Holliday junction resolvase subunit that binds multiple DNA repair/recombination endonucleases, Cell, 138 (2009) 78-89.

[58] J.M. Svendsen, A. Smogorzewska, M.E. Sowa, B.C. O'Connell, S.P. Gygi, S.J. Elledge, J.W. Harper, Mammalian BTBD12/SLX4 assembles a Holliday junction resolvase and is required for DNA repair, Cell, 138 (2009) 63-77.
[59] S.L. Andersen, D.T. Bergstralh, K.P. Kohl, J.R. LaRocque, C.B. Moore, J. Sekelsky, Drosophila MUS312 and the vertebrate ortholog BTBD12 interact with DNA structure-specific endonucleases in DNA repair and recombination, Mol Cell, 35 (2009) 128-135.
[60] A.D. Auerbach, Fanconi anemia and its diagnosis, Mutat Res, 668 (2009) 4-10.
[61] G.P. Crossan, L. van der Weyden, I.V. Rosado, F. Langevin, P.H. Gaillard, R.E. McIntyre, F. Gallagher, M.I. Kettunen, D.Y. Lewis, K. Brindle, M.J. Arends, D.J. Adams, K.J. Patel, Disruption of mouse Slx4, a regulator of structure-specific nucleases, phenocopies Fanconi anemia, Nat Genet, 43 (2011) 147-152.
[62] Y. Kim, F.P. Lach, R. Desetty, H. Hanenberg, A.D. Auerbach, A. Smogorzewska, Mutations of the SLX4 gene in Fanconi anemia, Nat Genet, 43 (2011) 142-146.
[63] C. Stoepker, K. Hain, B. Schuster, Y. Hilhorst-Hofstee, M.A. Rooimans, J. Steltenpool, A.B. Oostra, K. Eirich, E.T. Korthof, A.W. Nieuwint, N.G. Jaspers, T. Bettecken, H. Joenje, D. Schindler, J. Rouse, J.P. de Winter, SLX4, a coordinator of structure-specific endonucleases, is mutated in a new Fanconi anemia subtype, Nat Genet, 43 (2011) 138-141.
[64] E. Hefner, S.B. Preuss, A.B. Britt, Arabidopsis mutants sensitive to gamma radiation include the homologue of the human repair gene ERCC1, J Exp Bot, 54 (2003) 669-680.
[65] B.S. Baker, A.T. Carpenter, P. Ripoll, The Utilization during Mitotic Cell Division of Loci Controlling Meiotic Recombination and Disjunction in DROSOPHILA MELANOGASTER, Genetics, 90 (1978) 531-578.
[66] J. Fishman-Lobell, J.E. Haber, Removal of nonhomologous DNA ends in double-strand break recombination: the role of the yeast ultraviolet repair gene RAD1, Science, 258 (1992) 480-484.
[67] E.L. Ivanov, J.E. Haber, RAD1 and RAD10, but not other excision repair genes, are required for double-strand break-induced recombination in Saccharomyces cerevisiae, Mol Cell Biol, 15 (1995) 2245-2251.
[68] H.L. Klein, Different types of recombination events are controlled by the RAD1 and RAD52 genes of Saccharomyces cerevisiae, Genetics, 120 (1988) 367-377.
[69] R.H. Schiestl, S. Prakash, RAD10, an excision repair gene of Saccharomyces cerevisiae, is involved in the RAD1 pathway of mitotic recombination, Mol Cell Biol, 10 (1990) 2485-2491.
[70] F. Prado, A. Aguilera, Role of reciprocal exchange, one-ended invasion crossover and single-strand annealing on inverted and direct repeat recombination in yeast: different requirements for the RAD1, RAD10, and RAD52 genes, Genetics, 139 (1995) 109-123.
[71] F. Paques, J.E. Haber, Two pathways for removal of nonhomologous DNA ends during double-strand break repair in Saccharomyces cerevisiae, Mol Cell Biol, 17 (1997) 6765-6771.
[72] J.L. Ma, E.M. Kim, J.E. Haber, S.E. Lee, Yeast Mre11 and Rad1 proteins define a Ku-independent mechanism to repair double-strand breaks lacking overlapping end sequences, Mol Cell Biol, 23 (2003) 8820-8828.
[73] R.G. Sargent, J.L. Meservy, B.D. Perkins, A.E. Kilburn, Z. Intody, G.M. Adair, R.S. Nairn, J.H. Wilson, Role of the nucleotide excision repair gene ERCC1 in formation of recombination-dependent rearrangements in mammalian cells, Nucleic Acids Res, 28 (2000) 3771-3778.
[74] G.M. Adair, R.L. Rolig, D. Moore-Faver, M. Zabelshansky, J.H. Wilson, R.S. Nairn, Role of ERCC1 in removal of long non-homologous tails during targeted homologous recombination, EMBO J, 19 (2000) 5552-5561.

[75] L.J. Niedernhofer, J. Essers, G. Weeda, B. Beverloo, J. de Wit, M. Muijtjens, H. Odijk, J.H. Hoeijmakers, R. Kanaar, The structure-specific endonuclease Ercc1-Xpf is required for targeted gene replacement in embryonic stem cells, EMBO J, 20 (2001) 6540-6549.
[76] A.Z. Al-Minawi, N. Saleh-Gohari, T. Helleday, The ERCC1/XPF endonuclease is required for efficient single-strand annealing and gene conversion in mammalian cells, Nucleic Acids Res, 36 (2008) 1-9.
[77] H. Satoh, K. Hiyama, M. Takeda, Y. Awaya, K. Watanabe, Y. Ihara, H. Maeda, S. Ishioka, M. Yamakido, Telomere shortening in peripheral blood cells was related with aging but not with white blood cell count, Jpn J Hum Genet, 41 (1996) 413-417.
[78] R.T. Hagelstrom, K.B. Blagoev, L.J. Niedernhofer, E.H. Goodwin, S.M. Bailey, Hyper telomere recombination accelerates replicative senescence and may promote premature aging, Proc Natl Acad Sci U S A, 107 (2010) 15768-15773.
[79] Y. Wu, T.R. Mitchell, X.D. Zhu, Human XPF controls TRF2 and telomere length maintenance through distinctive mechanisms, Mech Ageing Dev, 129 (2008) 602-610.
[80] K.H. Kraemer, M.M. Lee, J. Scotto, Xeroderma pigmentosum. Cutaneous, ocular, and neurologic abnormalities in 830 published cases, Arch Dermatol, 123 (1987) 241-250.
[81] A. Ahmad, J.H. Enzlin, N.R. Bhagwat, N. Wijgers, A. Raams, E. Appledoorn, A.F. Theil, J.H. JH, W. Vermeulen, J.J. NG, O.D. Scharer, L.J. Niedernhofer, Mislocalization of XPF-ERCC1 nuclease contributes to reduced DNA repair in XP-F patients, PLoS Genet, 6 e1000871.
[82] S. Arase, T. Kozuka, K. Tanaka, M. Ikenaga, H. Takebe, A sixth complementation group in xeroderma pigmentosum, Mutat Res, 59 (1979) 143-146.
[83] B. Zelle, F. Berends, P.H. Lohman, Repair of damage by ultraviolet radiation in xeroderma pigmentosum cell strains of complementation groups E and F, Mutat Res, 73 (1980) 157-169.
[84] C. Nishigori, K. Ishizaki, H. Takebe, S. Imamura, M. Hayakawa, A case of xeroderma pigmentosum group F with late onset of clinical symptoms, Arch Dermatol, 122 (1986) 510-511.
[85] K. Yamamura, M. Ichihashi, T. Hiramoto, M. Ogoshi, K. Nishioka, Y. Fujiwara, Clinical and photobiological characteristics of xeroderma pigmentosum complementation group F: a review of cases from Japan, Br J Dermatol, 121 (1989) 471-480.
[86] P.G. Norris, J.L. Hawk, J.A. Avery, F. Giannelli, Xeroderma pigmentosum complementation group F in a non-Japanese patient, J Am Acad Dermatol, 18 (1988) 1185-1188.
[87] Y. Fujiwara, Y. Uehara, M. Ichihashi, K. Nishioka, Xeroderma pigmentosum complementation group F: more assignments and repair characteristics, Photochem Photobiol, 41 (1985) 629-634.
[88] S. Kondo, A. Mamada, C. Miyamoto, C.H. Keong, Y. Satoh, Y. Fujiwara, Late onset of skin cancers in 2 xeroderma pigmentosum group F siblings and a review of 30 Japanese xeroderma pigmentosum patients in groups D, E and F, Photodermatol, 6 (1989) 89-95.
[89] H.W. Thielmann, O. Popanda, L. Edler, E.G. Jung, Clinical symptoms and DNA repair characteristics of xeroderma pigmentosum patients from Germany, Cancer Res, 51 (1991) 3456-3470.
[90] S. Moriwaki, C. Nishigori, S. Imamura, T. Yagi, C. Takahashi, N. Fujimoto, H. Takebe, A case of xeroderma pigmentosum complementation group F with neurological abnormalities, Br J Dermatol, 128 (1993) 91-94.
[91] M. Berneburg, P.H. Clingen, S.A. Harcourt, J.E. Lowe, E.M. Taylor, M.H. Green, J. Krutmann, C.F. Arlett, A.R. Lehmann, The cancer-free phenotype in trichothiodystrophy is unrelated to its repair defect, Cancer Res, 60 (2000) 431-438.

[92] Y. Matsumura, C. Nishigori, T. Yagi, S. Imamura, H. Takebe, Characterization of molecular defects in xeroderma pigmentosum group F in relation to its clinically mild symptoms, Hum Mol Genet, 7 (1998) 969-974.
[93] K.W. Brookman, J.E. Lamerdin, M.P. Thelen, M. Hwang, J.T. Reardon, A. Sancar, Z.Q. Zhou, C.A. Walter, C.N. Parris, L.H. Thompson, ERCC4 (XPF) encodes a human nucleotide excision repair protein with eukaryotic recombination homologs, Mol Cell Biol, 16 (1996) 6553-6562.
[94] A.M. Sijbers, P.C. van Voorst Vader, J.W. Snoek, A. Raams, N.G. Jaspers, W.J. Kleijer, Homozygous R788W point mutation in the XPF gene of a patient with xeroderma pigmentosum and late-onset neurologic disease, J Invest Dermatol, 110 (1998) 832-836.
[95] A. Westerveld, J.H. Hoeijmakers, M. van Duin, J. de Wit, H. Odijk, A. Pastink, R.D. Wood, D. Bootsma, Molecular cloning of a human DNA repair gene, Nature, 310 (1984) 425-429.
[96] R.B. Lowry, R. MacLean, D.M. McLean, B. Tischler, Cataracts, microcephaly, kyphosis, and limited joint movement in two siblings: a new syndrome, J Pediatr, 79 (1971) 282-284.
[97] S.D. Pena, M.H. Shokeir, Autosomal recessive cerebro-oculo-facio-skeletal (COFS) syndrome, Clin Genet, 5 (1974) 285-293.
[98] J.M. Graham, Jr., K. Anyane-Yeboa, A. Raams, E. Appeldoorn, W.J. Kleijer, V.H. Garritsen, D. Busch, T.G. Edersheim, N.G. Jaspers, Cerebro-oculo-facio-skeletal syndrome with a nucleotide excision-repair defect and a mutated XPD gene, with prenatal diagnosis in a triplet pregnancy, Am J Hum Genet, 69 (2001) 291-300.
[99] T. Nouspikel, P. Lalle, S.A. Leadon, P.K. Cooper, S.G. Clarkson, A common mutational pattern in Cockayne syndrome patients from xeroderma pigmentosum group G: implications for a second XPG function, Proc Natl Acad Sci U S A, 94 (1997) 3116-3121.
[100] L.B. Meira, J.M. Graham, Jr., C.R. Greenberg, D.B. Busch, A.T. Doughty, D.W. Ziffer, D.M. Coleman, I. Savre-Train, E.C. Friedberg, Manitoba aboriginal kindred with original cerebro-oculo- facio-skeletal syndrome has a mutation in the Cockayne syndrome group B (CSB) gene, Am J Hum Genet, 66 (2000) 1221-1228.
[101] W.L. de Laat, A.M. Sijbers, H. Odijk, N.G. Jaspers, J.H. Hoeijmakers, Mapping of interaction domains between human repair proteins ERCC1 and XPF, Nucleic Acids Res, 26 (1998) 4146-4152.
[102] B.C. Hamel, A. Raams, A.R. Schuitema-Dijkstra, P. Simons, I. van der Burgt, N.G. Jaspers, W.J. Kleijer, Xeroderma pigmentosum--Cockayne syndrome complex: a further case, J Med Genet, 33 (1996) 607-610.
[103] D.I. Zafeiriou, F. Thorel, A. Andreou, W.J. Kleijer, A. Raams, V.H. Garritsen, N. Gombakis, N.G. Jaspers, S.G. Clarkson, Xeroderma pigmentosum group G with severe neurological involvement and features of Cockayne syndrome in infancy, Pediatr Res, 49 (2001) 407-412.
[104] F. Thorel, A. Constantinou, I. Dunand-Sauthier, T. Nouspikel, P. Lalle, A. Raams, N.G. Jaspers, W. Vermeulen, M.K. Shivji, R.D. Wood, S.G. Clarkson, Definition of a short region of XPG necessary for TFIIH interaction and stable recruitment to sites of UV damage, Mol Cell Biol, 24 (2004) 10670-10680.
[105] N. Le May, D. Mota-Fernandes, R. Velez-Cruz, I. Iltis, D. Biard, J.M. Egly, NER factors are recruited to active promoters and facilitate chromatin modification for transcription in the absence of exogenous genotoxic attack, Mol Cell, 38 (2010) 54-66.
[106] R. Hirschhorn, In vivo reversion to normal of inherited mutations in humans, J Med Genet, 40 (2003) 721-728.

[107] P.T. Bosma, S.J. van Eert, N.G. Jaspers, G. Stoter, K. Nooter, Functional cloning of drug resistance genes from retroviral cDNA libraries, Biochem Biophys Res Commun, 309 (2003) 605-611.
[108] N.A. Ellis, S. Ciocci, J. German, Back mutation can produce phenotype reversion in Bloom syndrome somatic cells, Hum Genet, 108 (2001) 167-173.
[109] J.M. Prasher, A.S. Lalai, C. Heijmans-Antonissen, R.E. Ploemacher, J.H. Hoeijmakers, I.P. Touw, L.J. Niedernhofer, Reduced hematopoietic reserves in DNA interstrand crosslink repair-deficient Ercc1-/- mice, EMBO J, 24 (2005) 861-871.
[110] K. Parmar, A. D'Andrea, L.J. Niedernhofer, Mouse models of Fanconi anemia, Mutat Res, 668 (2009) 133-140.
[111] F. Nunez, M.D. Chipchase, A.R. Clarke, D.W. Melton, Nucleotide excision repair gene (ERCC1) deficiency causes G(2) arrest in hepatocytes and a reduction in liver binucleation: the role of p53 and p21, FASEB J, 14 (2000) 1073-1082.
[112] M.D. Chipchase, M. O'Neill, D.W. Melton, Characterization of premature liver polyploidy in DNA repair (Ercc1)-deficient mice, Hepatology, 38 (2003) 958-966.
[113] B. Schumacher, I. van der Pluijm, M.J. Moorhouse, T. Kosteas, A.R. Robinson, Y. Suh, T.M. Breit, H. van Steeg, L.J. Niedernhofer, W. van Ijcken, A. Bartke, S.R. Spindler, J.H. Hoeijmakers, G.T. van der Horst, G.A. Garinis, Delayed and accelerated aging share common longevity assurance mechanisms, PLoS Genet, 4 (2008) e1000161.
[114] L.B. Caruso, Silliman, R.A., Geriatric Medicine, in: A.S. Fauci, Braunwald, E., Kasper, D.L., Hauser, S.L., Longo, D.L., Jameson, J.L., Loscalzo, J. (Ed.) Harrison's Principles of Internal Medicine, 17th ed., McGraw Hill, New York, 2006.
[115] A.G. Winter, K. Samuel, K.T. Hsia, D.W. Melton, The repair and recombination enzyme ERCC1 is not required for immunoglobulin class switching, DNA Repair (Amst), 2 (2003) 561-569.
[116] C.E. Schrader, J. Vardo, E. Linehan, M.Z. Twarog, L.J. Niedernhofer, J.H. Hoeijmakers, J. Stavnezer, Deletion of the nucleotide excision repair gene Ercc1 reduces immunoglobulin class switching and alters mutations near switch recombination junctions, J Exp Med, 200 (2004) 321-330.
[117] A. Kotnis, L. Du, C. Liu, S.W. Popov, Q. Pan-Hammarstrom, Non-homologous end joining in class switch recombination: the beginning of the end, Philos Trans R Soc Lond B Biol Sci, 364 (2009) 653-665.
[118] J. Selfridge, K.T. Hsia, N.J. Redhead, D.W. Melton, Correction of liver dysfunction in DNA repair-deficient mice with an ERCC1 transgene, Nucleic Acids Res, 29 (2001) 4541-4550.
[119] N.J. Lawrence, J.J. Sacco, D.G. Brownstein, T.H. Gillingwater, D.W. Melton, A neurological phenotype in mice with DNA repair gene Ercc1 deficiency, DNA Repair (Amst), 7 (2008) 281-291.
[120] T.G. Gorgels, I. van der Pluijm, R.M. Brandt, G.A. Garinis, H. van Steeg, G. van den Aardweg, G.H. Jansen, J.M. Ruijter, A.A. Bergen, D. van Norren, J.H. Hoeijmakers, G.T. van der Horst, Retinal degeneration and ionizing radiation hypersensitivity in a mouse model for Cockayne syndrome, Mol Cell Biol, 27 (2007) 1433-1441.
[121] K.T. Hsia, M.R. Millar, S. King, J. Selfridge, N.J. Redhead, D.W. Melton, P.T. Saunders, DNA repair gene Ercc1 is essential for normal spermatogenesis and oogenesis and for functional integrity of germ cell DNA in the mouse, Development, 130 (2003) 369-378.

[122] C. Paul, J.E. Povey, N.J. Lawrence, J. Selfridge, D.W. Melton, P.T. Saunders, Deletion of genes implicated in protecting the integrity of male germ cells has differential effects on the incidence of DNA breaks and germ cell loss, PLoS One, 2 (2007) e989.
[123] M.E. Dolle, R.A. Busuttil, A.M. Garcia, S. Wijnhoven, E. van Drunen, L.J. Niedernhofer, G. van der Horst, J.H. Hoeijmakers, H. van Steeg, J. Vijg, Increased genomic instability is not a prerequisite for shortened lifespan in DNA repair deficient mice, Mutat Res, 596 (2006) 22-35.
[124] M.C. de Waard, I. van der Pluijm, N. Zuiderveen Borgesius, L.H. Comley, E.D. Haasdijk, Y. Rijksen, Y. Ridwan, G. Zondag, J.H. Hoeijmakers, Y. Elgersma, T.H. Gillingwater, D. Jaarsma, Age-related motor neuron degeneration in DNA repair-deficient Ercc1 mice, Acta Neuropathol, 120 (2010) 461-475.
[125] E. Nevedomskaya, A. Meissner, S. Goraler, M. de Waard, Y. Ridwan, G. Zondag, I. van der Pluijm, A.M. Deelder, O.A. Mayboroda, Metabolic profiling of accelerated aging ERCC1 d/- mice, J Proteome Res, 9 (2010) 3680-3687.
[126] X.L. Li, S.R. Shen, S. Wang, H.H. Ouyang, G.C. Li, Restoration of T cell-specific V(D)J recombination in DNA-PKcs(-/-) mice by ionizing radiation: The effects on survival, development, and tumorigenesis, Sheng Wu Hua Xue Yu Sheng Wu Wu Li Xue Bao (Shanghai), 34 (2002) 149-157.
[127] E. Sonoda, M.S. Sasaki, C. Morrison, Y. Yamaguchi-Iwai, M. Takata, S. Takeda, Sister chromatid exchanges are mediated by homologous recombination in vertebrate cells, Mol Cell Biol, 19 (1999) 5166-5169.
[128] M. McVey, S.E. Lee, MMEJ repair of double-strand breaks (director's cut): deleted sequences and alternative endings, Trends Genet, 24 (2008) 529-538.
[129] N. Vo, H.Y. Seo, A. Robinson, G. Sowa, D. Bentley, L. Taylor, R. Studer, A. Usas, J. Huard, S. Alber, S.C. Watkins, J. Lee, P. Coehlo, D. Wang, M. Loppini, P.D. Robbins, L.J. Niedernhofer, J. Kang, Accelerated aging of intervertebral discs in a mouse model of progeria, J Orthop Res, 28 (2010) 1600-1607.
[130] P.J. Roughley, Biology of intervertebral disc aging and degeneration: involvement of the extracellular matrix, Spine (Phila Pa 1976), 29 (2004) 2691-2699.
[131] P.J. Roughley, M. Alini, J. Antoniou, The role of proteoglycans in aging, degeneration and repair of the intervertebral disc, Biochem Soc Trans, 30 (2002) 869-874.
[132] F. Tronche, E. Casanova, M. Turiault, I. Sahly, C. Kellendonk, When reverse genetics meets physiology: the use of site-specific recombinases in mice, FEBS Lett, 529 (2002) 116-121.
[133] J. Doig, C. Anderson, N.J. Lawrence, J. Selfridge, D.G. Brownstein, D.W. Melton, Mice with skin-specific DNA repair gene (Ercc1) inactivation are hypersensitive to ultraviolet irradiation-induced skin cancer and show more rapid actinic progression, Oncogene, 25 (2006) 6229-6238.
[134] J. Selfridge, L. Song, D.G. Brownstein, D.W. Melton, Mice with DNA repair gene Ercc1 deficiency in a neural crest lineage are a model for late-onset Hirschsprung disease, DNA Repair (Amst), 9 (2010) 653-660.
[135] N.J. Lawrence, L. Song, J. Doig, A.M. Ritchie, D.G. Brownstein, D.W. Melton, Topical thymidine dinucleotide application protects against UVB-induced skin cancer in mice with DNA repair gene (Ercc1)-deficient skin, DNA Repair (Amst), 8 (2009) 664-671.
[136] A. Smogorzewska, B. van Steensel, A. Bianchi, S. Oelmann, M.R. Schaefer, G. Schnapp, T. de Lange, Control of human telomere length by TRF1 and TRF2, Mol Cell Biol, 20 (2000) 1659-1668.

[137] P. Munoz, R. Blanco, G. de Carcer, S. Schoeftner, R. Benetti, J.M. Flores, M. Malumbres, M.A. Blasco, TRF1 controls telomere length and mitotic fidelity in epithelial homeostasis, Mol Cell Biol, 29 (2009) 1608-1625.
[138] L. Fan, J.O. Fuss, Q.J. Cheng, A.S. Arvai, M. Hammel, V.A. Roberts, P.K. Cooper, J.A. Tainer, XPD helicase structures and activities: insights into the cancer and aging phenotypes from XPD mutations, Cell, 133 (2008) 789-800.
[139] J. Xu, Kochanek, K.D., Murphy, S.L., Tejada-Vera, B., Deaths: Final Data for 2007, in: U.S.D.o.H.a.H. Services (Ed.), Hyattsville, MD, 2010.
[140] J.A. del Olmo, M.A. Serra, F. Rodriguez, A. Escudero, S. Gilabert, J.M. Rodrigo, Incidence and risk factors for hepatocellular carcinoma in 967 patients with cirrhosis, J Cancer Res Clin Oncol, 124 (1998) 560-564.
[141] J. Frith, D. Jones, J.L. Newton, Chronic liver disease in an ageing population, Age Ageing, 38 (2009) 11-18.
[142] H.A. Wynne, L.H. Cope, E. Mutch, M.D. Rawlins, K.W. Woodhouse, O.F. James, The effect of age upon liver volume and apparent liver blood flow in healthy man, Hepatology, 9 (1989) 297-301.
[143] H. Popper, Aging and the liver, Prog Liver Dis, 8 (1986) 659-683.
[144] G.K. Michalopoulos, Liver regeneration, J Cell Physiol, 213 (2007) 286-300.
[145] N.L. Bucher, M.N. Swaffield, J.F. Ditroia, The Influence of Age Upon the Incorporation of Thymidine-2-C14 into the DNA of Regenerating Rat Liver, Cancer Res, 24 (1964) 509-512.
[146] W. Andrew, An electron microscope study of age changes in the liver of the mouse, Am J Anat, 110 (1962) 1-18.
[147] D.L. Schmucker, H. Sachs, Quantifying dense bodies and lipofuscin during aging: a morphologist's perspective, Arch Gerontol Geriatr, 34 (2002) 249-261.
[148] T. Jung, N. Bader, T. Grune, Lipofuscin: formation, distribution, and metabolic consequences, Ann N Y Acad Sci, 1119 (2007) 97-111.
[149] A.J. McLean, V.C. Cogger, G.C. Chong, A. Warren, A.M. Markus, J.E. Dahlstrom, D.G. Le Couteur, Age-related pseudocapillarization of the human liver, J Pathol, 200 (2003) 112-117.
[150] N. Kagansky, S. Levy, D. Keter, E. Rimon, Z. Taiba, Z. Fridman, D. Berger, H. Knobler, S. Malnick, Non-alcoholic fatty liver disease--a common and benign finding in octogenarian patients, Liver Int, 24 (2004) 588-594.
[151] L.A. Adams, P. Angulo, Recent concepts in non-alcoholic fatty liver disease, Diabet Med, 22 (2005) 1129-1133.
[152] A. Warren, P. Bertolino, V.C. Cogger, A.J. McLean, R. Fraser, D.G. Le Couteur, Hepatic pseudocapillarization in aged mice, Exp Gerontol, 40 (2005) 807-812.
[153] M. Hoare, T. Das, G. Alexander, Ageing, telomeres, senescence, and liver injury, J Hepatol, 53 (2010) 950-961.
[154] Y. Ito, K.K. Sorensen, N.W. Bethea, D. Svistounov, M.K. McCuskey, B.H. Smedsrod, R.S. McCuskey, Age-related changes in the hepatic microcirculation in mice, Exp Gerontol, 42 (2007) 789-797.
[155] K. Ohtsubo, T.A. Nomaguchi, A flow cytofluorometric study on age-dependent ploidy class changes in mouse hepatocyte nuclei, Mech Ageing Dev, 36 (1986) 125-131.
[156] C. Pieri, C. Giuli, M. Del Moro, L. Piantanelli, Electron-microscopic morphometric analysis of mouse liver. II. Effect of ageing and thymus transplantation in old animals, Mech Ageing Dev, 13 (1980) 275-283.

[157] P. Hasty, J. Campisi, J. Hoeijmakers, H. van Steeg, J. Vijg, Aging and genome maintenance: lessons from the mouse?, Science, 299 (2003) 1355-1359.
[158] M.E.T. Dolle, Kuiper, R.V., Roodbergen, M., Robinson, J., de Vlugt, S., Wijnhoven, S.W.P., Beems, R.B., de la Fonteyne, L., de With, P., van der Pluijm, I., Niedernhofer, L.J., Hasty, P., Vijg, J., Hoeijmakers, J.H.J., Harry van Steeg, Broad segmental progeroid changes in short-lived Ercc1-/Δ7 mice, Pathobiology of Aging and Age-related diseases, 1 (2011) 7219.
[159] P.O. Seglen, Preparation of isolated rat liver cells, Methods Cell Biol, 13 (1976) 29-83.
[160] K.E. Wack, M.A. Ross, V. Zegarra, L.R. Sysko, S.C. Watkins, D.B. Stolz, Sinusoidal ultrastructure evaluated during the revascularization of regenerating rat liver, Hepatology, 33 (2001) 363-378.
[161] C. Mitchell, H. Willenbring, A reproducible and well-tolerated method for 2/3 partial hepatectomy in mice, Nat Protoc, 3 (2008) 1167-1170.
[162] A. Warren, V.C. Cogger, R. Fraser, L.D. Deleve, R.S. McCuskey, D.G. Le Couteur, The effects of old age on hepatic stellate cells, Curr Gerontol Geriatr Res, 2011 (2011) 439835.
[163] S.N. Hilmer, V.C. Cogger, D.G. Le Couteur, Basal activity of Kupffer cells increases with old age, J Gerontol A Biol Sci Med Sci, 62 (2007) 973-978.
[164] D.G. Le Couteur, A. Warren, V.C. Cogger, B. Smedsrod, K.K. Sorensen, R. De Cabo, R. Fraser, R.S. McCuskey, Old age and the hepatic sinusoid, Anat Rec (Hoboken), 291 (2008) 672-683.
[165] D.G. Le Couteur, V.C. Cogger, A.M. Markus, P.J. Harvey, Z.L. Yin, A.D. Ansselin, A.J. McLean, Pseudocapillarization and associated energy limitation in the aged rat liver, Hepatology, 33 (2001) 537-543.
[166] D.G. Le Couteur, V.C. Cogger, R.S. McCuskey, D.E.C. R, B. Smedsrod, K.K. Sorensen, A. Warren, R. Fraser, Age-related changes in the liver sinusoidal endothelium: a mechanism for dyslipidemia, Ann N Y Acad Sci, 1114 (2007) 79-87.
[167] S.N. Hilmer, V.C. Cogger, R. Fraser, A.J. McLean, D. Sullivan, D.G. Le Couteur, Age-related changes in the hepatic sinusoidal endothelium impede lipoprotein transfer in the rat, Hepatology, 42 (2005) 1349-1354.
[168] N. Fausto, J.S. Campbell, K.J. Riehle, Liver regeneration, Hepatology, 43 (2006) S45-53.
[169] D.L. Schmucker, Age-related changes in liver structure and function: Implications for disease ?, Exp Gerontol, 40 (2005) 650-659.
[170] K. Kitani, Liver and aging, Gastroenterol Jpn, 27 (1992) 276-285.
[171] R. Vranckx, L. Savu, N. Lambert, G.V. de Conchard, R. Grosse, M.S. Mourey, B. Corman, Plasma proteins as biomarkers of the aging process, Am J Physiol, 268 (1995) R536-548.
[172] D.A. Alcorta, Y. Xiong, D. Phelps, G. Hannon, D. Beach, J.C. Barrett, Involvement of the cyclin-dependent kinase inhibitor p16 (INK4a) in replicative senescence of normal human fibroblasts, Proc Natl Acad Sci U S A, 93 (1996) 13742-13747.
[173] F. Rodier, J. Campisi, Four faces of cellular senescence, J Cell Biol, 192 (2011) 547-556.
[174] S.W. Sherwood, D. Rush, J.L. Ellsworth, R.T. Schimke, Defining cellular senescence in IMR-90 cells: a flow cytometric analysis, Proc Natl Acad Sci U S A, 85 (1988) 9086-9090.
[175] A.S. Moraes, A.M. Guaraldo, M.L. Mello, Chromatin supraorganization and extensibility in mouse hepatocytes with development and aging, Cytometry A, 71 (2007) 28-37.
[176] I. Ben-Porath, R.A. Weinberg, The signals and pathways activating cellular senescence, Int J Biochem Cell Biol, 37 (2005) 961-976.
[177] T. Watanabe, H. Shimada, Y. Tanaka, Human hepatocytes and aging: a cytophotometrical analysis in 35 sudden-death cases, Virchows Arch B Cell Pathol, 27 (1978) 307-316.

[178] J. Busquets, X. Xiol, J. Figueras, E. Jaurrieta, J. Torras, E. Ramos, A. Rafecas, J. Fabregat, C. Lama, L. Ibanez, L. Llado, J.M. Ramon, The impact of donor age on liver transplantation: influence of donor age on early liver function and on subsequent patient and graft survival, Transplantation, 71 (2001) 1765-1771.
[179] J.H. Hoofnagle, M. Lombardero, R.K. Zetterman, J. Lake, M. Porayko, J. Everhart, S.H. Belle, K.M. Detre, Donor age and outcome of liver transplantation, Hepatology, 24 (1996) 89-96.
[180] A.G. Maloney, D.L. Schmucker, D.S. Vessey, R.K. Wang, The effects of aging on the hepatic microsomal mixed-function oxidase system of male and female monkeys, Hepatology, 6 (1986) 282-287.
[181] M.A. Sutter, W.G. Wood, L.S. Williamson, R. Strong, K. Pickham, A. Richardson, Comparison of the hepatic mixed function oxidase system of young, adult, and old non-human primates (Macaca nemestrina), Biochem Pharmacol, 34 (1985) 2983-2987.
[182] G.R. Stuart, Y. Oda, J.G. de Boer, B.W. Glickman, Mutation frequency and specificity with age in liver, bladder and brain of lacI transgenic mice, Genetics, 154 (2000) 1291-1300.
[183] X. Wang, E. Quail, N.J. Hung, Y. Tan, H. Ye, R.H. Costa, Increased levels of forkhead box M1B transcription factor in transgenic mouse hepatocytes prevent age-related proliferation defects in regenerating liver, Proc Natl Acad Sci U S A, 98 (2001) 11468-11473.
[184] X. Wang, K. Krupczak-Hollis, Y. Tan, M.B. Dennewitz, G.R. Adami, R.H. Costa, Increased hepatic Forkhead Box M1B (FoxM1B) levels in old-aged mice stimulated liver regeneration through diminished p27Kip1 protein levels and increased Cdc25B expression, J Biol Chem, 277 (2002) 44310-44316.
[185] K. Furrer, A. Rickenbacher, Y. Tian, W. Jochum, A.G. Bittermann, A. Kach, B. Humar, R. Graf, W. Moritz, P.A. Clavien, Serotonin reverts age-related capillarization and failure of regeneration in the liver through a VEGF-dependent pathway, Proc Natl Acad Sci U S A, 108 (2011) 2945-2950.
[186] C. Cruzen, R.J. Colman, Effects of caloric restriction on cardiovascular aging in non-human primates and humans, Clin Geriatr Med, 25 (2009) 733-743, ix-x.
[187] K. Krupczak-Hollis, X. Wang, M.B. Dennewitz, R.H. Costa, Growth hormone stimulates proliferation of old-aged regenerating liver through forkhead box m1b, Hepatology, 38 (2003) 1552-1562.
[188] M. Muftuoglu, J. Oshima, C. von Kobbe, W.H. Cheng, D.F. Leistritz, V.A. Bohr, The clinical characteristics of Werner syndrome: molecular and biochemical diagnosis, Hum Genet, 124 (2008) 369-377.
[189] A. Labbe, C. Garand, V.C. Cogger, E.R. Paquet, M. Desbiens, D.G. Le Couteur, M. Lebel, Resveratrol improves insulin resistance hyperglycemia and hepatosteatosis but not hypertriglyceridemia, inflammation, and life span in a mouse model for Werner syndrome, J Gerontol A Biol Sci Med Sci, 66 (2010) 264-278.
[190] L. Mikkelsen, K. Bialkowski, L. Risom, M. Lohr, S. Loft, P. Moller, Aging and defense against generation of 8-oxo-7,8-dihydro-2'-deoxyguanosine in DNA, Free Radic Biol Med, 47 (2009) 608-615.
[191] R.K. Zahn, G. Zahn-Daimler, S. Ax, G. Reifferscheid, P. Waldmann, H. Fujisawa, M. Hosokawa, DNA damage susceptibility and repair in correlation to calendric age and longevity, Mech Ageing Dev, 119 (2000) 101-112.

[192] N.E. Lopez-Diazguerrero, A. Luna-Lopez, M.C. Gutierrez-Ruiz, A. Zentella, M. Konigsberg, Susceptibility of DNA to oxidative stressors in young and aging mice, Life Sci, 77 (2005) 2840-2854.
[193] F. Rodier, J.P. Coppe, C.K. Patil, W.A. Hoeijmakers, D.P. Munoz, S.R. Raza, A. Freund, E. Campeau, A.R. Davalos, J. Campisi, Persistent DNA damage signalling triggers senescence-associated inflammatory cytokine secretion, Nat Cell Biol, 11 (2009) 973-979.
[194] N.C.o. Aging, Healthy Aging: Fact Sheet, in: N.C.o. Aging (Ed.) www.ncoa.org, Washington, D.C., 2011.
[195] C. Hoffman, and Rice, D.P. , Chronic Care in America: A 21st century challenge, San Francisco, CA, 1996.
[196] E.R. Stadtman, Protein oxidation and aging, Science, 257 (1992) 1220-1224.
[197] K.K. Singh, Mitochondria damage checkpoint, aging, and cancer, Ann N Y Acad Sci, 1067 (2006) 182-190.
[198] J.H. Hoeijmakers, DNA damage, aging, and cancer, N Engl J Med, 361 (2009) 1475-1485.
[199] A.J. Brenner, M.R. Stampfer, C.M. Aldaz, Increased p16 expression with first senescence arrest in human mammary epithelial cells and extended growth capacity with p16 inactivation, Oncogene, 17 (1998) 199-205.
[200] J.P. Coppe, F. Rodier, C.K. Patil, A. Freund, P.Y. Desprez, J. Campisi, The tumor suppressor and aging biomarker p16INK4a induces cellular senescence without the associated inflammatory secretory phenotype, J Biol Chem, (2011).
[201] F. d'Adda di Fagagna, P.M. Reaper, L. Clay-Farrace, H. Fiegler, P. Carr, T. Von Zglinicki, G. Saretzki, N.P. Carter, S.P. Jackson, A DNA damage checkpoint response in telomere-initiated senescence, Nature, 426 (2003) 194-198.
[202] L. Hayflick, The Limited in Vitro Lifetime of Human Diploid Cell Strains, Exp Cell Res, 37 (1965) 614-636.
[203] F. Rodier, D.P. Munoz, R. Teachenor, V. Chu, O. Le, D. Bhaumik, J.P. Coppe, E. Campeau, C.M. Beausejour, S.H. Kim, A.R. Davalos, J. Campisi, DNA-SCARS: distinct nuclear structures that sustain damage-induced senescence growth arrest and inflammatory cytokine secretion, J Cell Sci, 124 (2011) 68-81.
[204] S.Q. Gregg, V. Gutierrez, A.R. Robinson, T. Woodell, A. Nakao, M.A. Ross, G.K. Michalopoulos, L. Rigatti, C.E. Rothermel, I. Kamileri, G. Garinis, D.B. Stolz, L.J. Niedernhofer, A mouse model of accelerated liver aging due to a defect in DNA repair, Hepatology, (2011).
[205] R. Di Micco, M. Fumagalli, A. Cicalese, S. Piccinin, P. Gasparini, C. Luise, C. Schurra, M. Garre, P.G. Nuciforo, A. Bensimon, R. Maestro, P.G. Pelicci, F. d'Adda di Fagagna, Oncogene-induced senescence is a DNA damage response triggered by DNA hyper-replication, Nature, 444 (2006) 638-642.
[206] L.J. Marnett, J.P. Plastaras, Endogenous DNA damage and mutation, Trends Genet, 17 (2001) 214-221.
[207] B. Demple, L. Harrison, Repair of oxidative damage to DNA: enzymology and biology, Annu Rev Biochem, 63 (1994) 915-948.
[208] D.E. Barnes, T. Lindahl, Repair and genetic consequences of endogenous DNA base damage in mammalian cells, Annu Rev Genet, 38 (2004) 445-476.
[209] T. Lindahl, R.D. Wood, Quality control by DNA repair, Science, 286 (1999) 1897-1905.

[210] A. Papadopoulou, D. Kletsas, Human lung fibroblasts prematurely senescent after exposure to ionizing radiation enhance the growth of malignant lung epithelial cells in vitro and in vivo, Int J Oncol, 39 (2011) 989-999.
[211] B.D. Chang, E.V. Broude, M. Dokmanovic, H. Zhu, A. Ruth, Y. Xuan, E.S. Kandel, E. Lausch, K. Christov, I.B. Roninson, A senescence-like phenotype distinguishes tumor cells that undergo terminal proliferation arrest after exposure to anticancer agents, Cancer Res, 59 (1999) 3761-3767.
[212] W.T. Roubal, A.L. Tappel, Damage to proteins, enzymes, and amino acids by peroxidizing lipids, Arch Biochem Biophys, 113 (1966) 5-8.
[213] B.N. Ames, M.K. Shigenaga, T.M. Hagen, Oxidants, antioxidants, and the degenerative diseases of aging, Proc Natl Acad Sci U S A, 90 (1993) 7915-7922.
[214] F. Debacq-Chainiaux, J.D. Erusalimsky, J. Campisi, O. Toussaint, Protocols to detect senescence-associated beta-galactosidase (SA-betagal) activity, a biomarker of senescent cells in culture and in vivo, Nat Protoc, 4 (2009) 1798-1806.
[215] K. Itahana, G. Dimri, J. Campisi, Regulation of cellular senescence by p53, Eur J Biochem, 268 (2001) 2784-2791.
[216] J.P. Brown, W. Wei, J.M. Sedivy, Bypass of senescence after disruption of p21CIP1/WAF1 gene in normal diploid human fibroblasts, Science, 277 (1997) 831-834.
[217] S.Q. Gregg, A.R. Robinson, L.J. Niedernhofer, Physiological consequences of defects in ERCC1-XPF DNA repair endonuclease, DNA Repair (Amst), (2011).
[218] S.Q. Gregg, V. Gutierrez, A.R. Robinson, T. Woodell, A. Nakao, M.A. Ross, G.K. Michalopoulos, L. Rigatti, C.E. Rothermel, I. Kamileri, G. Garinis, D.B. Stolz, L.J. Niedernhofer, A mouse model of accelerated liver aging due to a defect in DNA repair, Hepatology.
[219] E. Eruslanov, S. Kusmartsev, Identification of ROS using oxidized DCFDA and flow-cytometry, Methods Mol Biol, 594 57-72.
[220] P. Mukhopadhyay, M. Rajesh, K. Yoshihiro, G. Hasko, P. Pacher, Simple quantitative detection of mitochondrial superoxide production in live cells, Biochem Biophys Res Commun, 358 (2007) 203-208.
[221] G.M. Martin, C.A. Sprague, C.J. Epstein, Replicative life-span of cultivated human cells. Effects of donor's age, tissue, and genotype, Lab Invest, 23 (1970) 86-92.
[222] A. Tchirkov, P.M. Lansdorp, Role of oxidative stress in telomere shortening in cultured fibroblasts from normal individuals and patients with ataxia-telangiectasia, Hum Mol Genet, 12 (2003) 227-232.
[223] S. Matsuoka, B.A. Ballif, A. Smogorzewska, E.R. McDonald, 3rd, K.E. Hurov, J. Luo, C.E. Bakalarski, Z. Zhao, N. Solimini, Y. Lerenthal, Y. Shiloh, S.P. Gygi, S.J. Elledge, ATM and ATR substrate analysis reveals extensive protein networks responsive to DNA damage, Science, 316 (2007) 1160-1166.
[224] W.H. Cheng, M. Muftuoglu, V.A. Bohr, Werner syndrome protein: functions in the response to DNA damage and replication stress in S-phase, Exp Gerontol, 42 (2007) 871-878.
[225] J. Campisi, The biology of replicative senescence, Eur J Cancer, 33 (1997) 703-709.
[226] C. Wang, D. Jurk, M. Maddick, G. Nelson, C. Martin-Ruiz, T. von Zglinicki, DNA damage response and cellular senescence in tissues of aging mice, Aging Cell, 8 (2009) 311-323.
[227] E.P. Rogakou, C. Boon, C. Redon, W.M. Bonner, Megabase chromatin domains involved in DNA double-strand breaks in vivo, J Cell Biol, 146 (1999) 905-916.

[228] L.A. Rowe, N. Degtyareva, P.W. Doetsch, DNA damage-induced reactive oxygen species (ROS) stress response in Saccharomyces cerevisiae, Free Radic Biol Med, 45 (2008) 1167-1177.
[229] M. Navratil, A. Terman, E.A. Arriaga, Giant mitochondria do not fuse and exchange their contents with normal mitochondria, Exp Cell Res, 314 (2008) 164-172.
[230] C.S. Palmer, L.D. Osellame, D. Stojanovski, M.T. Ryan, The regulation of mitochondrial morphology: intricate mechanisms and dynamic machinery, Cell Signal, 23 1534-1545.
[231] A. Santel, S. Frank, B. Gaume, M. Herrler, R.J. Youle, M.T. Fuller, Mitofusin-1 protein is a generally expressed mediator of mitochondrial fusion in mammalian cells, J Cell Sci, 116 (2003) 2763-2774.
[232] A.L. Jackson, L.A. Loeb, The contribution of endogenous sources of DNA damage to the multiple mutations in cancer, Mutat Res, 477 (2001) 7-21.
[233] F. Rodier, D.P. Munoz, R. Teachenor, V. Chu, O. Le, D. Bhaumik, J.P. Coppe, E. Campeau, C.M. Beausejour, S.H. Kim, A.R. Davalos, J. Campisi, DNA-SCARS: distinct nuclear structures that sustain damage-induced senescence growth arrest and inflammatory cytokine secretion, J Cell Sci, 124 68-81.
[234] S.J. Robles, P.W. Buehler, A. Negrusz, G.R. Adami, Permanent cell cycle arrest in asynchronously proliferating normal human fibroblasts treated with doxorubicin or etoposide but not camptothecin, Biochem Pharmacol, 58 (1999) 675-685.
[235] V.M. Hubbard, R. Valdor, F. Macian, A.M. Cuervo, Selective autophagy in the maintenance of cellular homeostasis in aging organisms, Biogerontology.
[236] H. Koga, S. Kaushik, A.M. Cuervo, Protein homeostasis and aging: The importance of exquisite quality control, Ageing Res Rev, 10 205-215.
[237] X. Fu, S. Wan, Y.L. Lyu, L.F. Liu, H. Qi, Etoposide induces ATM-dependent mitochondrial biogenesis through AMPK activation, PLoS One, 3 (2008) e2009.